SANDIA REPORT

SAND2007-7931
Unlimited Release
Printed December 2007

Electromagnetic Radiation (EMR) Coupling to Complex Systems:

Aperture Coupling into Canonical Cavities in Reverberant and Anechoic Environments and Model Validation

Matthew B. Higgins and Dawna R. Charley

Prepared by Sandia National Laboratories
Albuquerque, New Mexico 87185, and Livermore, California 94550

Sandia is a multiprogram laboratory operated by Sandia Corporation,
a Lockheed Martin Company, for the United States Department of Energy's
National Nuclear Security Administration under Contract DE-AC04-94AL85000.

Issued by Sandia National Laboratories, operated for the United States Department of Energy by Sandia Corporation.

SAND2007-7931
Unlimited Release
Printed December 2007

Electromagnetic Radiation (EMR) Coupling to Complex Systems:

Aperture Coupling into Canonical Cavities in Reverberant and Anechoic Environments and Model Validation

Matthew B. Higgins and Dawna R. Charley
Electromagnetic Qualification and Engineering Dept. 1653

Sandia National Laboratories
POB 5800
Albuquerque, NM 87185-1152

Abstract

Mode-stirred chamber and anechoic chamber measurements were made on two sets of canonical test objects (cylindrical and rectangular) with varying numbers of thin slot apertures. The shielding effectiveness was compared to determine the level of correction needed to compensate the mode-stirred data to levels commensurate with anechoic data from the same test object.

Page Intentional left Blank

Table of Contents

Page Intentional left Blank

List of Figures

List of Tables

Page Intentional left Blank

1.0 Introduction

Electromagnetic Radiation (EMR) leakage into nuclear weapon systems can cause upset of time- and/or mission-critical functions, damage critical electronics, or affect electro-explosive devices. The objective of the Electromagnetic Radiation (EMR) Cable Coupling project is to characterize electromagnetic leakage into cables and metallic cavities. The ultimate goal of this project is to provide a means of predicting pin-level excitations (voltages or currents) of components within a complex system (weapon) when the exterior of the system is exposed to EMR environments over a very broad range of frequencies. This predictive capability can been used as a tool to define/refine requirements, assess systems in revised environments, optimize new designs, design changes or major upgrades, assist in rapid turnaround of prototype designs and troubleshooting, and assist in component- and system-level certification.

The current qualification of components to EMR environments requires an extensive and expensive testing program. For a typical weapon the transfer function from exterior to interior fields must be measured; the coupling of interior fields onto interior cables and components must be measured; and the interior components must be subjected to interior threat-level fields to ensure no degradation of performance. The first section of finding the transfer function, if performed in an anechoic environment, where all 4π steradian angles of a sphere encompassing the weapon would have to be measured at each frequency of interest, would take on the order of 10 to 12 months of continuous testing with angle spacing of five degrees. On the other hand, if this testing was performed in a mode-stirred chamber, then the test time would be on the order of one day. The cost savings are immense. The drawback of the mode-stirred chamber is that the gain of the apertures (or EMR leakage points) is removed in the resultant transfer function and is thus skewed.

The electromagnetic response of single slot and multiple slot apertures in canonical shaped test objects was investigated to understand how a mode-stirred chamber skews the data from an anechoic chamber. This part of the project is a step toward the predictive capabilities of being able to model the transfer function of exterior to interior fields on complex systems (weapons). The comparison of the measured data to existing analytical models developed to compensate the mode-stirred chamber data will be shown. This comparison is an important step to enable more robust predictive models to be developed.

The current uncertainties in the big picture coupling model can be separated in terms of the three parts of the coupling process: exterior scattering, aperture-cavity coupling (shielding effectiveness), and the cable penetration and wiring propagation problem (giving pin-level excitations of the interior components). The current uncertainty in the exterior scattering problem is in the 1-2 dB range. The uncertainty in the aperture coupling problem will be determined using data collected over the past year, but are expected to be in the 5-10 dB range. With the data collected to date, further experimentation (both exploratory and directed by analysts/modelers), and appropriate modeling time, the uncertainties could be reduced to the 1-2 dB range. The uncertainty in the cable penetration and wiring propagation problem is currently unknown. Thus one future goal of the C6 EMR project is to assess the accuracies of the cable and connector coupling predictions and hopefully show that accuracies in the 1-2 dB range can be accomplished.

This year's work concentrated on enabling the prediction of coupling into metallic cavities by evaluating the uncertainties in shielding effectiveness due to slot gain corrections that are not well characterized yet. This was accomplished by quantifying the differences in shielding effectiveness responses of test objects in a mode-stirred chamber (MSC) and an anechoic chamber. The test objects consist of a set of cylinders and rectangular boxes with varying number of slot apertures. Each test object has had its shielding effectiveness measured in the mode-stirred chamber and the anechoic chambers.

Because the mode-stirred chamber averages out any gain of the test object ports of entry, a correction to the MSC response is needed to obtain an estimate of the free space response (as found by the anechoic chamber) of the test object. The electromagnetic leakage into the interior of the canonical test objects occurs through one to eight 2.54 cm (1 inch) long slots around the circumference of the cylinders and in a linear array across one side of the rectangular box. The slots had a height of 20 mils and a depth (wall thickness) of 0.25 inches.

Two objectives of this year’s experiments presented in this report are: 1) evaluate the relative effect of multiple apertures on coupling; and 2) determine the effects of internal losses of the test cavities on the aperture coupling mechanism. The first objective was accomplished using data described in Sections 3.2 and 3.3. The second objective was accomplished by using data described in Section 3.4.

Chapter 2 will discuss the models developed to predict the differences between mode-stirred chamber data and anechoic data. Section 3.1 will discuss the measurement techniques for the mode-stirred chamber and the anechoic chamber. Sections 3.2 and 3.3 will discuss the coupling from slot apertures into lossless cavities and compare the data from the mode-stirred chamber with a slot-gain correction factor applied to the anechoic chamber data. Section 3.4 will discuss similar comparisons into lossy cavities. Chapter 4 will discuss the summary of findings and conclusions from this test series.

2.0 Analytic Model Corrections

Three analytic models were considered for correcting the mode-stirred chamber data to a level commensurate with that of the anechoic data. The three models will be referred to as the intentional emitter, the unintentional emitter, and the Sandia correction factors. The first two models were found in a literature search in the IEEE EMC Journal [1,2]. The last model was developed by Larry Warne and Roy Jorgenson of organization 1652 at Sandia National Laboratories.

The correction factors found in the EMC Journal are represented as directivity, *D*, while the Sandia correction is represented as gain, *G*. The gain of an antenna is simply the directivity of that antenna multiplied by the antenna radiation efficiency. For the case of the slot aperture coupling it is assumed that antenna radiation efficiency is unity, so that gain is equal to directivity.

2.1 Intentional Emitter Correction Factor

The theoretical basis for the directivity of an emitter of a given electrical size is spherical wave theory, which has been well developed for spherical near-field antenna measurements [3]. For an intentional, high-gain emitter (antenna) that can be enclosed within a minimum sphere of radius *a*, the maximum directivity, D_m, is approximately

$$D_m \approx \begin{cases} 3, & ka \le 1 \\ (ka)^2 + 2ka, & ka > 1, \end{cases} \tag{2.1}$$

where k = 2π/λ and λ is the free-space wavelength. When (2.1) is used to estimate the directivity of an unintentional emitter [1], it provides only an upper bound. However, for large *ka* (when the dimensions of the antenna are electrically large, i.e. frequency increases such that the dimension *a* is many wavelengths) it exceeds the actual directivity so much that it is not very accurate.

2.2 Unintentional Emitter Correction Factor

For unintentional emitters, a statistical treatment of directivity was found to be more useful. The same spherical mode theory is used, but it is assumed that the spherical mode coefficients are independent random variables.

The result in [2] is appropriate for sampling over a full sphere, however for a planar cut (such as the anechoic data) the number of independent samples N, is reduced to

$$N_c = 2(2ka + 1) \tag{2.2}$$

Then, the ratio of the expected value of the maximum directivity, $D_{m,c}$ is

$$D_{m,c} \approx \begin{cases} 2.45, & ka \le 1 \\ 0.577 + \ln(N_c) + \dfrac{1}{2N_c}, & ka > 1. \end{cases} \tag{2.3}$$

The result for small *ka* (1) is based on electric and magnetic dipole theory.

2.3 Sandia Correction Factor

According to Larry Warne and Roy Jorgensen of Sandia National Laboratories, a single slot linear aperture has a gain, or for an antenna radiation efficiency equal to one, maximum directivity

$$G = D_{m,S} = \frac{4\mathrm{L}}{\lambda} \tag{2.4}$$

where L is the slot length and is the wavelength. The question here is: how is this result modified by the presence of multiple apertures?

At high frequencies half of the cylindrical test object is in shadow when excited by a plane wave (i.e., in the anechoic chamber). Also for plane wave incidence there is a cos variation in the short circuit current. The short circuit current is what drives the slot, it is a mathematical tool to calculate the coupling. The mode-stirred chamber excitation involves the total circumference s = 2 a of the cylinder. At high frequencies the phasing is randomized by the stirrer rotation. If there were no gain (directivity) issue we would expect that four times the excitation is present in the mode-stirred chamber experiment versus the plane wave experiment (averaging (cos)^2 over the half-circumference we find effectively only s/4 length excitation). However because more than one slot aperture is excited simultaneously by the plane wave the effective array length, L_{eff}, is greater than the actual length, L. As a first cut it is unreasonable to take the effective array length equal to the effective excitation length L_{eff}~s/4. Certainly we have L_{eff}<s/2.

Dividing by the factor of four discussed above we thus have a gain correction

$$D_{m,S} = \frac{\mathrm{L}_{\mathrm{eff}}}{\lambda} \tag{2.5}$$

If there are N equal apertures then s=NL and thus

$$\frac{\mathrm{NL}}{4\lambda} \approx D_{m,S} < \frac{\mathrm{NL}}{2\lambda} \tag{2.6}$$

or if there are eight slots (N = 8)

$$\frac{2\mathrm{L}}{\lambda} \approx D_{m,S} < \frac{4\mathrm{L}}{\lambda} \tag{2.7}$$

To estimate the effect of the slots in a free space environment, the measured mode-stirred chamber data must be compensated by the slot gain (directivity). Since some of the test objects have multiple slots simultaneously driven by multiple random field polarizations, the compensation in dB lies somewhere between

$$10\log_{10}\left(\frac{2\mathrm{L}}{\lambda}\right) \le D_{m,S}(dB) \le 10\log_{10}\left(\frac{4\mathrm{L}}{\lambda}\right) \tag{2.8}$$

The mode-stirred chamber data for the eight slotted cylinder was compensated using the 10log(2L/) formulation (the lower bound of the Sandia correction factor) where the slot length L = 5.08cm (2 inches). The mode-stirred chamber data for the remainder of the test objects uses the single slot Sandia correction factor of 10log(4L/).

2.4 Gain Correction Comparison for a 2 inch slot

The corrections from the three formulations for a 2 inch long thin slot are shown in Figure 2-1. The correction from the intentional emitter (in red) becomes very large as frequency increases, as discussed in Section 2.1 and has a "DC" offset. The correction for the unintentional emitter has a less aggressive slope than the Sandia correction, but has a "DC" offset. It was determined that the intentional emitter correction was too large of a correction for all of the cases and is not included in most of the data comparison sections.

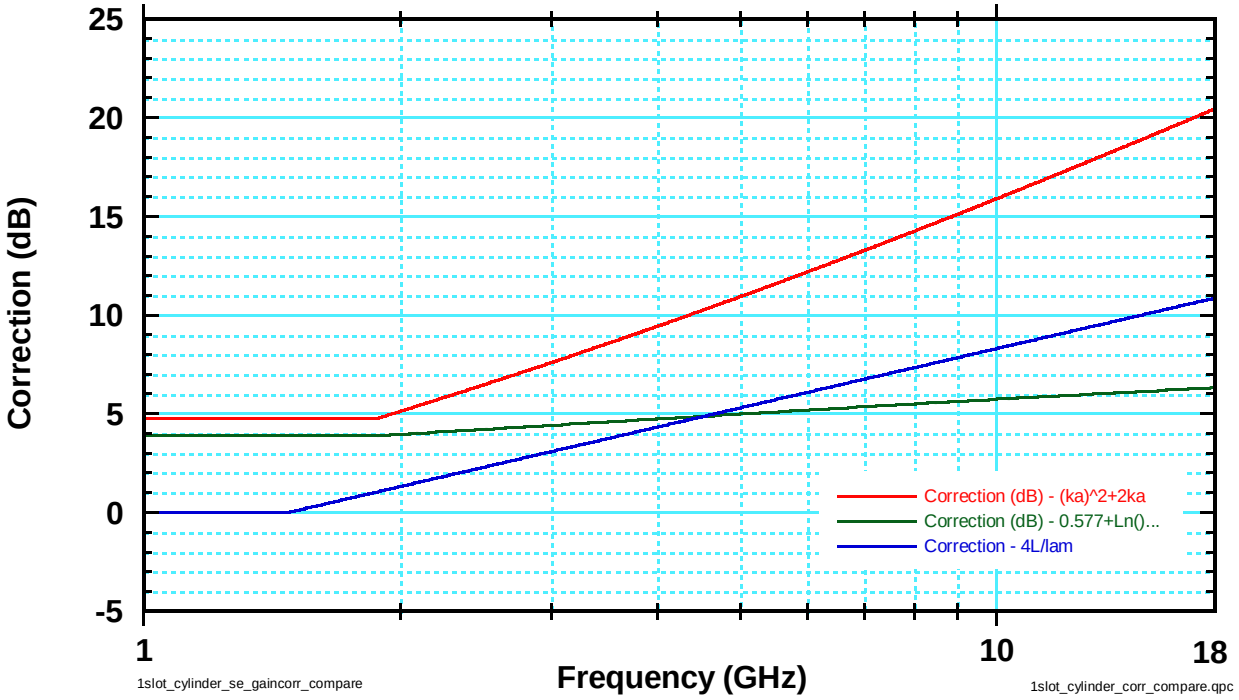

Figure 2-1 Comparison of three correction factors for a 2 inch long slot.

Page Intentional left Blank

3.0 Slot Coupling Tests

Two coupling responses can be seen in the data. The slot response is similar in shape to that of a dipole and the response of the internal cavity modes, which can be quite large for lossless, high Q cavities. Q (or Quality factor) is a term for the amount of average stored electric and magnetic energy divided by the power loss of the cavity. At cavity resonance, the average stored electric energy is equal to the average stored magnetic energy, thus the Q is equal to

$$Q = \frac{2\omega W_e}{P_l} \tag{3.1}$$

where ω is 2π times frequency, W_e is the average stored electric energy, and P_l is the power loss of the cavity. The Q of a cavity can also be calculated from a measurement of the cavity's resonant peaks.

$$Q = \frac{1}{BW} = \frac{\omega_0}{2\Delta\omega} \tag{3.2}$$

where BW is the half-power fractional bandwidth, ω_0 is the resonant frequency, and $\Delta\omega$ is the delta frequency.

Two test object geometries were measured for slot coupling: a cylindrical cavity and a rectangular cavity. The interior dimensions of the cylindrical cavity are an eight inch diameter and a 24 inch length. The slots were positioned circumferentially around the cylinder at the midpoint in height (12 inches). The interior dimensions of the rectangular cavity are 24 inches wide by 15 inches deep by 8.5 inches tall. The slots were positioned on the 24 inch by 8.5 inch face in a linear array 4.25 inches from the bottom. Drawings of the test objects are shown in Appendix A.

Section 3.1 will discuss the experimental setups and a brief description of the Mode-Stirred Chamber and the Anechoic Chamber. Section 3.2 will discuss the high Q cylindrical cavity slot coupling, beginning with a single slot and going to the eight slot setup. The results will be shown and discussed and the various slot corrections will be examined. Section 3.3 will discuss the high Q rectangular cavity slot coupling, again beginning with a single slot and going to the four slot case. The results will be discussed similarly to the cylindrical cavities. Section 3.4 will discuss the low Q cylindrical and rectangular cavities for a single slot.

3.1 Experimental Setups

Two test environments were used to characterize the coupling of slot apertures into cavities: a reverberant (mode-stirred) environment and an anechoic environment. Shielding effectiveness describes how well a test object shields against externally applied EMR. Shielding effectiveness was measured by placing the test object in a test chamber and exposing it to EMR. During the mode-stirred chamber portion of the test, *identical* antennas were placed in both the mode-stirred

chamber and inside the test object. Using the ratio of the EM sensor output power $\left(P^{sensor}\right)$ outside and inside the object, the shielding effectiveness as a function of frequency is calculated as shown in (3.3). Shielding effectiveness data for all tests will be represented as dB of shielding, where large negative numbers indicated very good shielding.

$$SE\,(dB) = 10\log\left(\frac{P_{inside}^{sensor}}{P_{outside}^{sensor}}\right) \tag{3.3}$$

The free space or plane wave illumination testing was done in the anechoic chamber. Here the sensors used to determine the electric field inside and outside the missile are different requiring a calculation of the electric fields prior to calculating the shielding effectiveness. The SE (dB) value is calculated using field strengths as shown in (3.4).

$$SE\,(dB) = 20\log\left(\frac{Efield_{inside}}{Efield_{outside}}\right) \tag{3.4}$$

Shielding effectiveness varies linearly with applied field unless arcing occurs. Given this property, the field strength used to illuminate the test object need not be a specific value so long as it is sufficient to provide a measurable signal.

3.1.1 Mode-Stirred Chamber

A block diagram of the measurement setup is shown in Figure 3-2. The field in the mode-stirred chamber was measured using monopole sensors from 220 MHz to 18 GHz. A model of the sensor response to a given incident field is programmed into the software controlling the measurements. To minimize mismatch error[1] due to the sensors and test object not being 50 ohms, the spectrum analyzer and power meters have 10dB attenuators in line. The 10dB pad near the mismatched load minimizes the standing waves on the transmission line between the pad and spectrum analyzer thus reducing the measurement uncertainties. To acquire data, the instruments used to measure the chamber fields and the test object output were triggered at the same time. The stirrer was rotated at a rate of 30 RPM and for each rotation, the power meters sample (4 locations) the chamber field strength 1000 times. These field measurements were averaged for each of the four sensors and the average of the four sensors was then averaged to obtain a field strength. To acquire data in the mode-stirred chamber, the spectrum analyzer was set in a 'zero span' mode with a time interval of 2 seconds (corresponding to the time the stirrer takes to complete one rotation at 30 rpm). The computer adjusts the analyzer to obtain an on-screen response and 601 points are measured. This data was averaged to obtain a mean value for the response of the DUT to the incident electric field.

[1] The mismatch uncertainty bound $= 20\log\left(1 + \left|\pm\rho_1\rho_2\right|\right)$ in power measurements where ρ_1 and ρ_2 are the source and load reflection coefficients.

Test objects in the mode-stirred chamber require characterization at only one orientation due to RF exposure from many angles of incidence and polarizations. The mode-stirred chamber provides a varying Continuous Wave (CW) EMR that has a chi-squared (χ^2)statistical distribution with two degrees of freedom throughout the chamber volume. Due to the high Q (reverberant) nature of a mode-stirred chamber it takes Q cycles to ring up and Q cycles to ring down with a pulse input.

To determine the repeatability of the measurements, a scan was done where each frequency point was measured five times before moving to the next frequency point. From this data the best case repeatability of the mode-stirred chamber is measured. The results of this scan are shown in Figure 3-1. From a close-up view of this data it appears that the mode-stirred chamber facility repeatability is $\leq \pm 2.5\%$. This uncertainty figure includes the repeatability of the Gigatronics 8542 power meter, Gigatronics 80304 power head and the HP8563E spectrum analyzer.

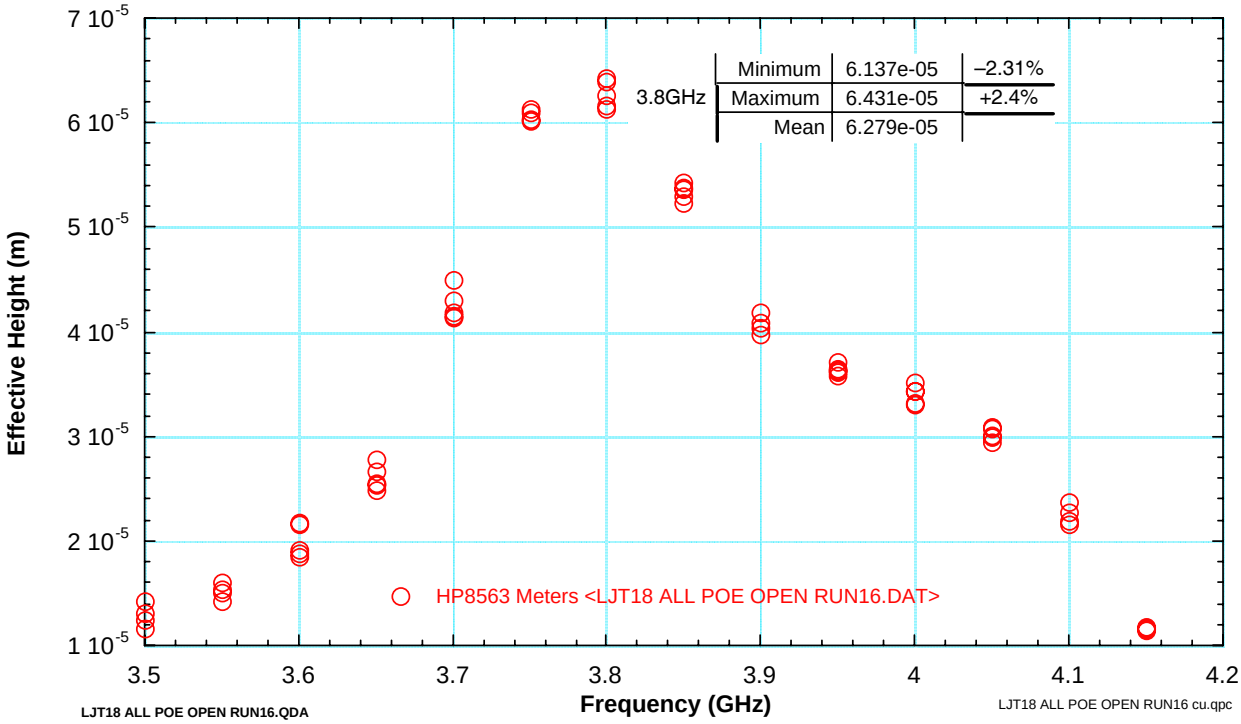

Figure 3-1 Mode stirred chamber repeatability.

In addition to the repeatability issue, the specified accuracy of the spectrum analyzer must also be accounted for. The HP 8763 spectrum analyzer has an absolute amplitude accuracy shown in Table 3-1 and the uncertainties associated with the power meters are shown in Table 3-2. Compared to the spectrum analyzer the power meter measurements have negligible error.

Table 3-1 HP 8563E accuracy

Frequency Band (GHz)	Accuracy (±dB) (relative, typical relative, absolute[2], typical absolute)
30E-9 – 2.9	1.25/0.8/1.8/1.0
2.9 – 6.46	1.5/1.0/2.4/1.5
6.46 – 13.2	2.2/1.5/2.9/2.0
13.2 – 18	2.5/1.5/4.0/2.5

Table 3-2 Gigatronics power sensor uncertainties

Frequency Band (GHz)	RSS[3] Uncertainty (±dB)
0.1 – 1	0.071
1 – 2	0.075
2 – 4	0.083
4 – 6	0.087
6 – 8	0.089
8 – 12.4	0.109
12.4 – 18	0.121

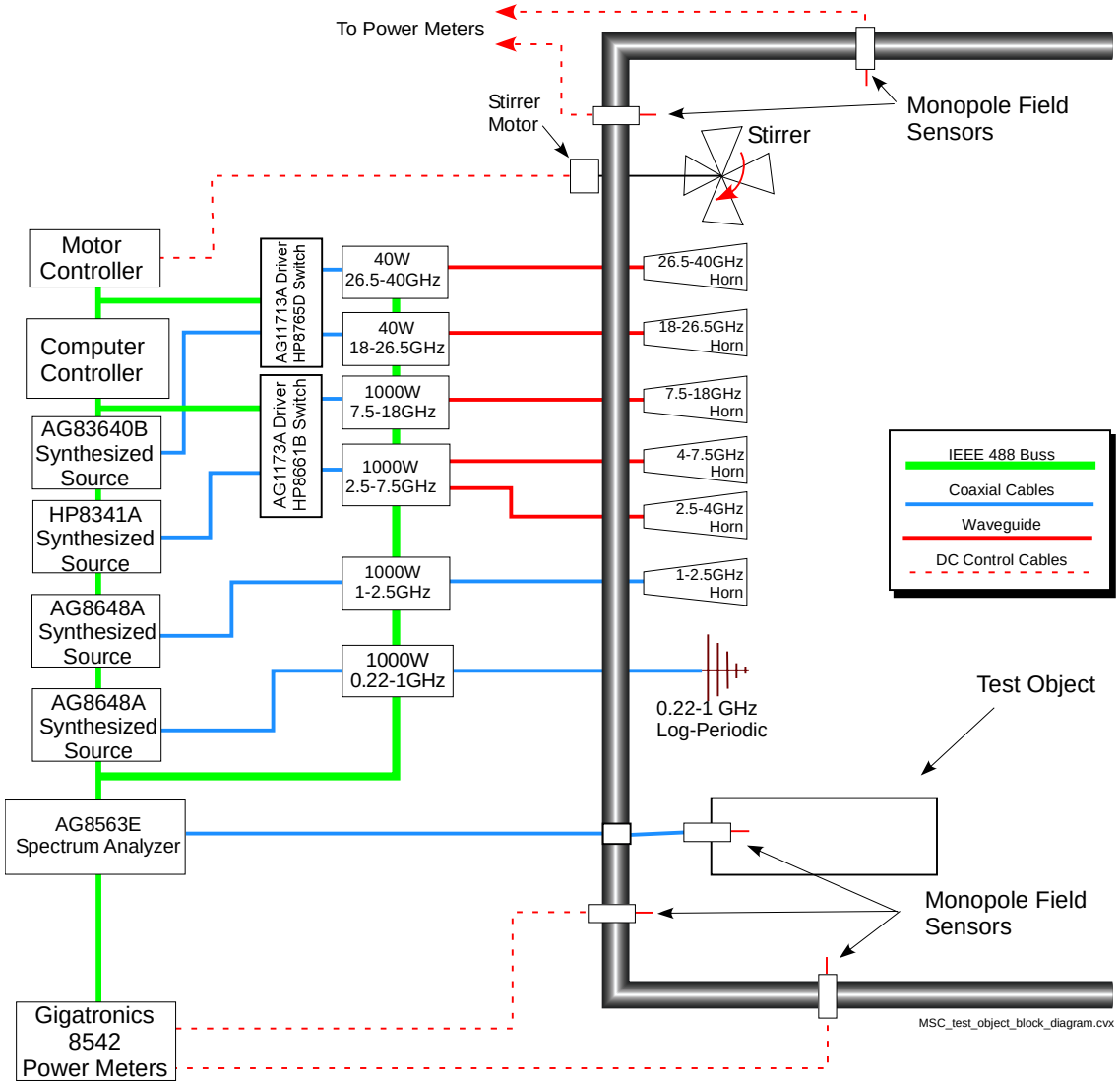

[2] Absolute flatness values referenced to 300MHz CAL OUT.
[3] Square root of the sum of individual uncertainties squared

Figure 3-2 Shielding effectiveness measurement experimental setup in Mode-Stirred Chamber.

3.1.2 Anechoic Chamber

The anechoic chamber provides a simulated free-space environment where reflections from walls and support structures have been reduced. The metallic walls of this shielded enclosure are covered with pyramidal absorbers made of radar absorbing material. A horn antenna radiates a spherical wave front from its aperture into the chamber. Test objects are placed toward the center of the chamber in the quiet zone for the chamber, where the reflections from walls are at the minimum. For frequencies 1-18 GHz the test object is sufficiently far away from the antenna (~5.3 m) that the spherical wave is approximately planer over the dimensions of the test object. At this distance the test object is said to be in the far field of the antenna. These pseudo-plane waves are very close to plane waves in free space. The amplitude of the electric field component of the pseudo-plane wave is calculated using the Friis transmission formula

$$W_t = \frac{P_t G_t}{4\pi d^2} \tag{3.5}$$

and

$$W_t = \frac{1}{2}\mathrm{Re}\left(E_t \times H_t^*\right) \tag{3.6}$$

or for a plane wave

$$W_t = \frac{1}{2}\frac{E_t^2}{Z_0} = \frac{E_{t,RMS}^2}{Z_0} \tag{3.7}$$

where $Z_0 = 120\pi\ \Omega$.

Therefore, the E-field magnitude is

$$E_{t,RMS} = \sqrt{Z_0 \frac{P_t G_t}{4\pi d^2}} = \sqrt{\frac{30 P_t G_t}{d^2}} \tag{3.8}$$

where G_t is the broadside gain of the transmitting horn antenna (shown in Figure 3-3), d is the distance from the antenna to test object, and P_t is the net transmitted power. A block diagram of the Anechoic chamber measurement setup is shown in Figure 3-4.

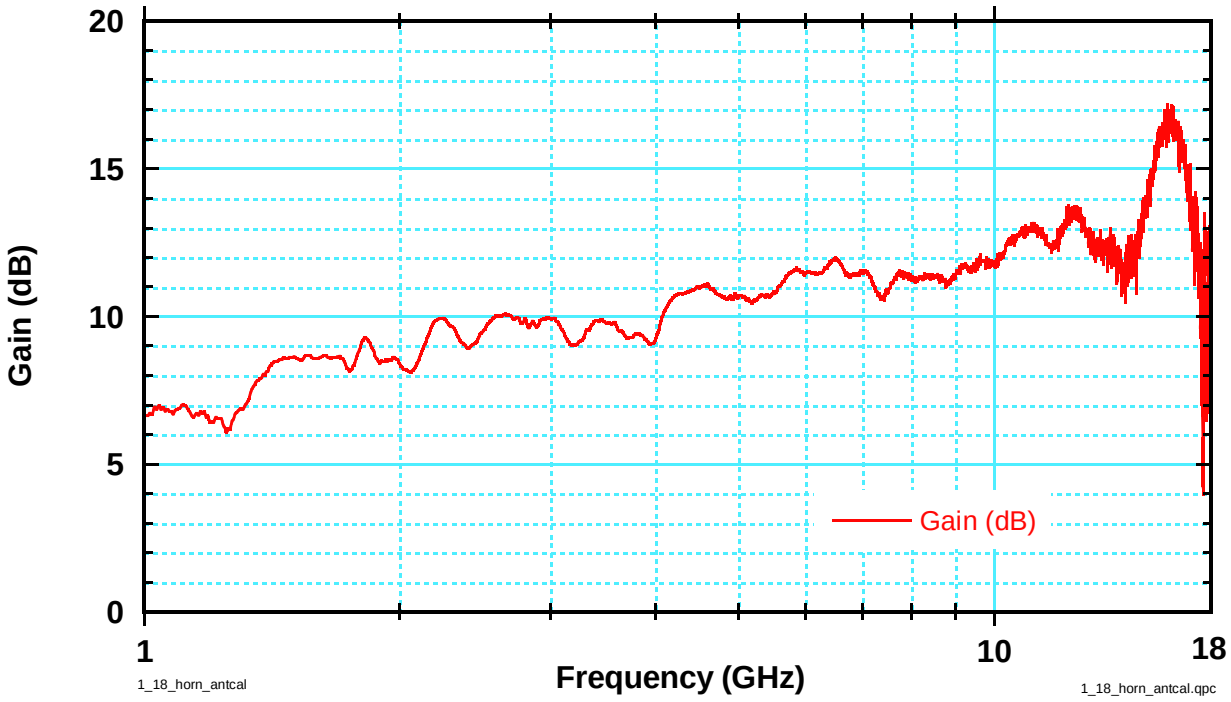

Figure 3-3 Gain (in dB) of transmitting horn antenna used in Anechoic Chamber.

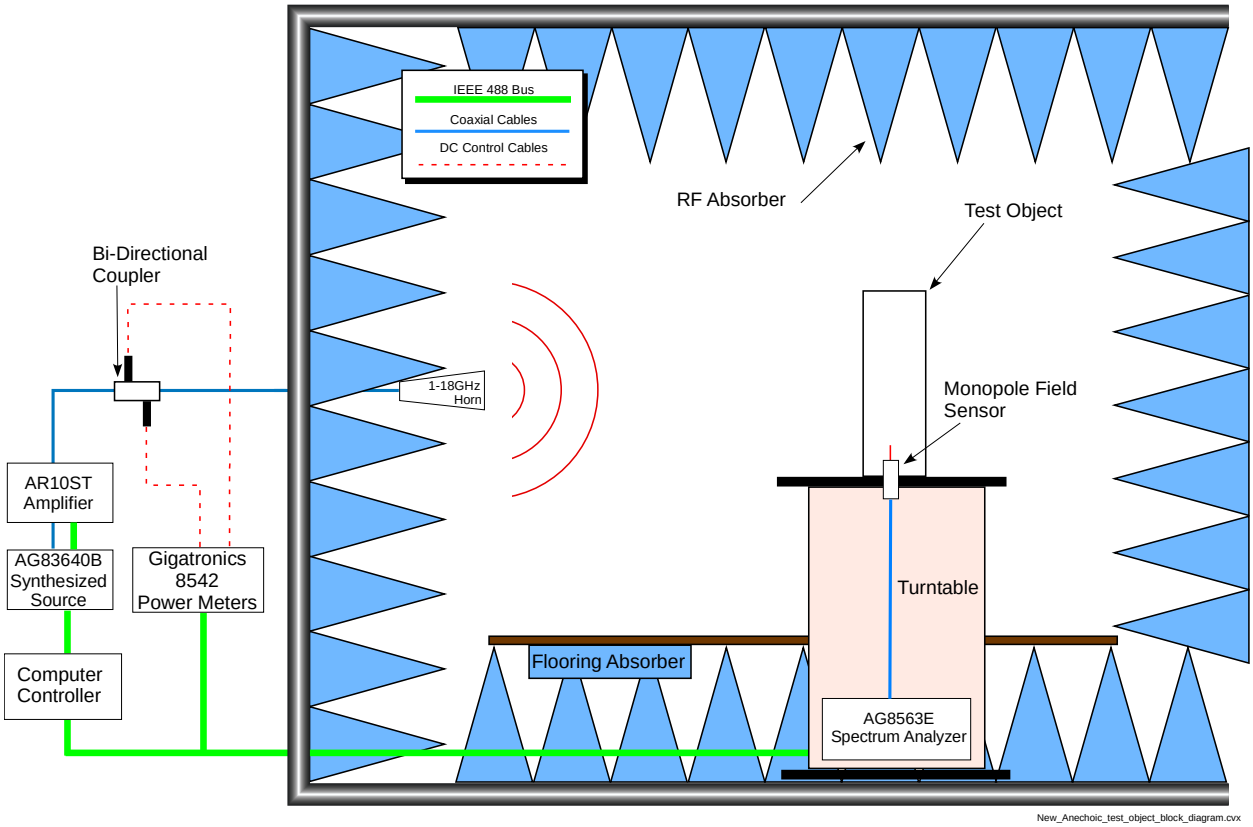

Figure 3-4 Shielding effectiveness measurement experimental setup for azimuthal scan excitation in Anechoic Chamber.

3.2 Cylindrical Test Object Shielding Effectiveness Measurements – Lossless (High Q)

The cylindrical test object series of measurements was performed on four cylinders: a single slot cylinder; a two slot cylinder with the slots diametrically opposed; a eight slotted cylinder with the slots arranged symmetrically on the outer wall around the axis of revolution; and a zero slotted cylinder (or blank cylinder) which was used as a noise floor measurement. A brief summary of the data is presented in Section 3.2.1, with a brief summary of modal responses in cylindrical cavities. The results of the experiment are presented in increasing number of slots, beginning with the single slot case. The blank cylinder results are shown with each case to demonstrate the limitations of the data.

3.2.1 Measurement Results - Overview

The cylindrical test objects were made of aluminum with interior dimensions of eight inch diameter and 24 inch length. A drawing of the cylindrical test object is shown in Figure 3-5. A 4.3mm monopole probe was used to measure the perpendicular electric field at the inside surface of the bottom plate. The probe was placed one inch off center as shown in Figure 3-5.

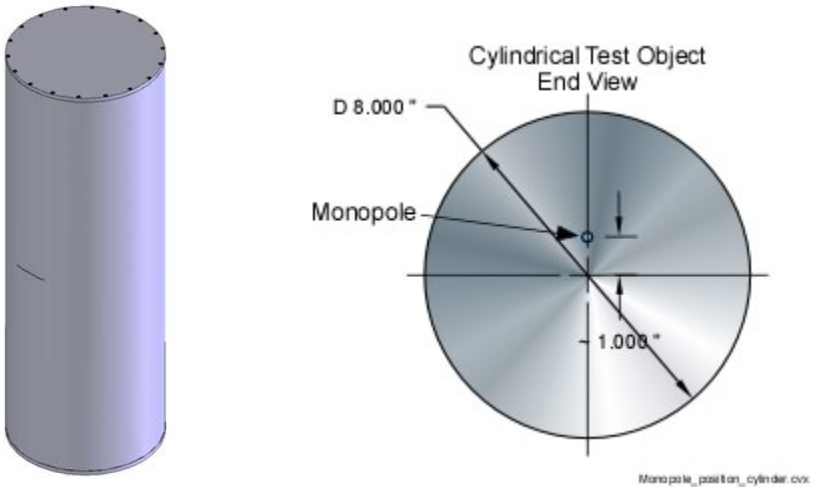

Figure 3-5 Cylindrical test object and monopole placement.

Modes are the configuration of fields inside a cavity. Transverse electromagnetic (TEM) modes cannot exist in a geometry with only a single conductor (boundary conditions are not met). Only structures with multiple conductors such as a coaxial line or a parallel plate capacitor can support TEM modes. For the cylindrical geometry shown above only Transverse Magnetic to z direction $(TM)^z$ and Transverse Electric to z direction $(TE)^z$ modes can exist. Each mode has a frequency where a particular mode is cutoff, i.e. below that frequency the mode cannot exist. The equations governing the cutoff frequencies are shown in (3.9) and (3.10). The letters m, n, and p represent the mode number and p corresponds to the z direction. The first 20 TM^z and TE^z modes are shown in increasing order in Table 3-3 and Table 3-4, respectively. The location of the monopole probe shown in Figure 3-5 allows for detection of the TM^z modes, but not the TE^z modes. Table 3-3 also shows the frequencies of the observed TM^z modes seen in the measured data of the single slotted cylinder.

$$\left(f_r\right)_{mnp}^{TM^z} = \frac{1}{2\pi\sqrt{\mu\varepsilon}}\sqrt{\left(\frac{\chi_{mn}}{a}\right)^2 + \left(\frac{p\pi}{h}\right)^2} \qquad \begin{matrix} m = 0,1,2,3,... \\ n = 1,2,3,... \\ p = 0,1,2,3,... \end{matrix} \tag{3.9}$$

where χ_{mn} is the nth zero of the Bessel function, J_m, of the first kind of order m. [4]

Table 3-3 First 20 TM_z modes of cylindrical test object

m	**n**	**p**	**$(f_r)_{mnp}$ TM_z (GHz)**	**f (GHz) observed**
0	1	0	1.129	1.1286
0	1	1	1.156	1.1557
0	1	2	1.232	1.2312
0	1	3	1.349	1.3478 (very small)
0	1	4	1.498	1.4964
0	1	5	1.670	None observed
1	1	0	1.799	1.7983
1	1	1	1.816	1.8153
0	1	6	1.858	1.8565
1	1	2	1.865	1.8637
1	1	3	1.945	1.9435
1	1	4	2.051	2.0497
0	1	7	2.059	2.0559
1	1	5	2.179	2.1767 (very small)
0	1	8	2.268	2.2658
1	1	6	2.327	2.3246
2	1	0	2.412	2.4108
2	1	1	2.424	2.4314 (very small)
2	1	2	2.461	2.4595
0	1	9	2.485	2.4879 (very small)

$$\left(f_r\right)_{mnp}^{TE^z} = \frac{1}{2\pi\sqrt{\mu\varepsilon}}\sqrt{\left(\frac{\chi'_{mn}}{a}\right)^2 + \left(\frac{p\pi}{h}\right)^2} \qquad \begin{matrix} m = 0,1,2,3,... \\ n = 1,2,3,... \\ p = 1,2,3,... \end{matrix} \tag{3.10}$$

where χ'_{mn} is the nth zero of the derivative of the Bessel function, J_m, of the first kind of order m [4].

Table 3-4 First 20 TE_z modes of cylindrical test object

m	n	p	$(f_r)_{mnp}$ TE_z (GHz)
1	1	1	0.899
1	1	2	0.995
1	1	3	1.137
1	1	4	1.310
2	1	1	1.455
1	1	5	1.503
2	1	2	1.516
2	1	3	1.613
1	1	6	1.710
2	1	4	1.739
0	1	1	1.816
0	1	2	1.866
2	1	5	1.889
1	1	7	1.926
0	1	3	1.945
3	1	1	1.988
3	1	2	2.033
0	1	4	2.051
2	1	6	2.058
3	1	3	2.106

The data shown in Figure 3-6 are the uncorrected results of all four cylindrical test objects measured in the mode-stirred chamber. The very sharp spikes are the TM^z modes of the cavity discussed previously. The red curve is the blank cylinder and represents the noise floor of the mode-stirred chamber measurements. There is no problem with noise in the mode-stirred chamber data for this measurement series.

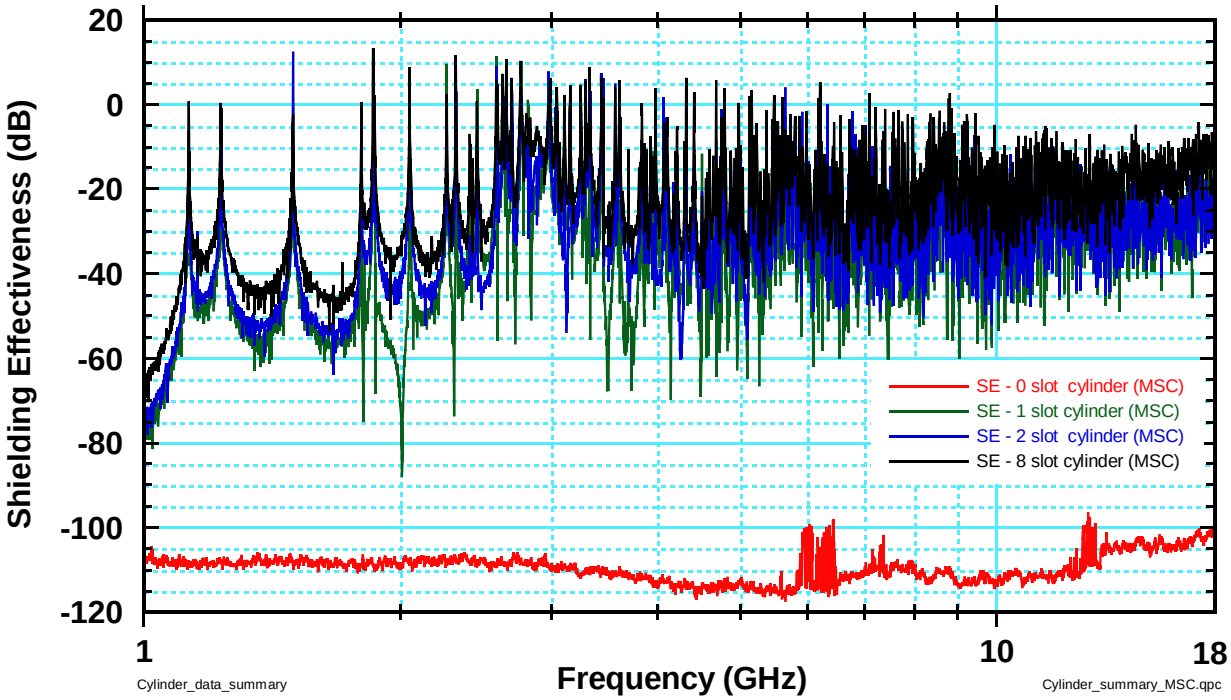

Figure 3-6 Comparison of shielding effectiveness of cylindrical test objects in the mode-stirred chamber.

The data shown in Figure 3-7 are the normalized results of a single azimuthal scan of the single slot cylindrical test object measured in the anechoic chamber. The x-axis is azimuthal position, where 90 degrees is broadside with the slot, the y-axis is frequency on a logarithmic scale, and the color indicates the relative signal amplitude, normalized to the maximum. The reason for performing the azimuthal scans around the test object instead of a single broadside measurement is because the main beam of the slot does not stay centered at 90 degrees for the entire frequency band of interest. It can be seen in Figure 3-7 at ~6 GHz, 12 GHz, and other frequencies. Figure 3-8 shows the data in Figure 3-7 at four discrete frequencies, each in a polar plot. Essentially the antenna pattern for the single slot cylinder at approximately 3, 6, 9, and 12 GHz are shown in Figure 3-8. At 3 GHz the beam is centered at 90 degrees, around the single slot of the cylinder (overlaid in the graph). At 6 GHz the beam has split into two lobes and has a null in at 90 degrees. The plots at 9 and 12 GHz also show the pattern shifting from a single main lobe to multiple lobes.

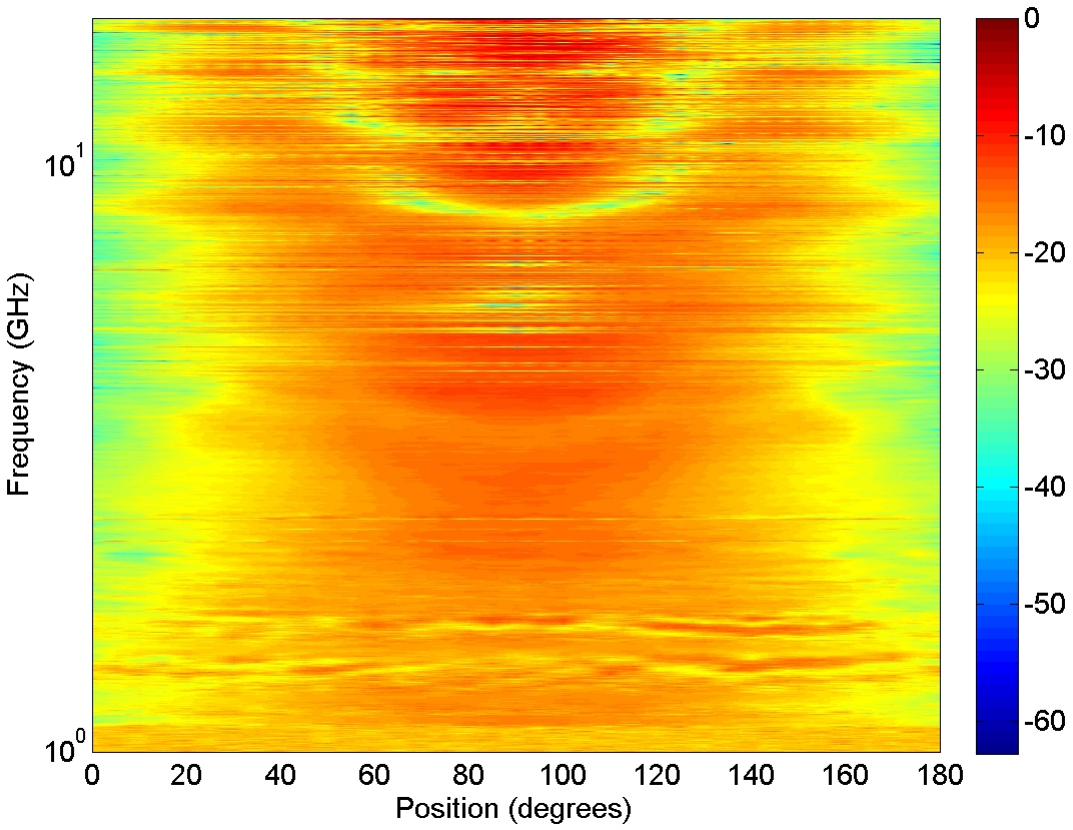

Figure 3-7 Normalized results of a single azimuthal scan of the single slot cylindrical test object measured in the anechoic chamber.

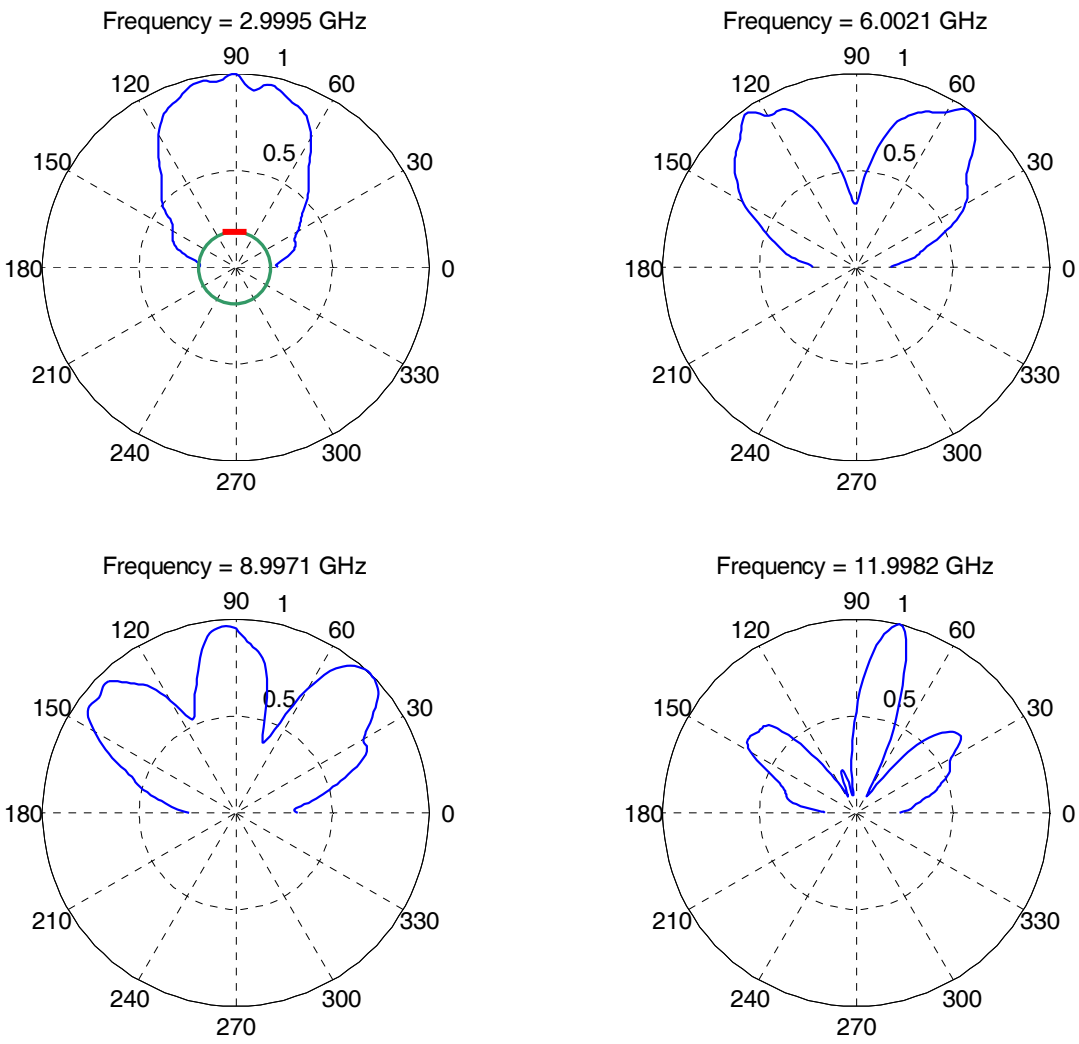

Figure 3-8 Polar plots of antenna pattern of the single slot cylindrical test object at ~3, 6, 9, and 12 GHz.

The data shown in Figure 3-9 are the results of all four cylindrical test objects measured in the anechoic chamber. Each curve is the maximum amplitude of each position of the azimuthal scan at each frequency. Again, the very sharp spikes are the TM^z modes of the cavity discussed previously. The red curve is the blank cylinder and represents the noise floor of the anechoic measurements. There is no problem with noise in the anechoic data above 1.1 GHz for this measurement series. Below 1.1 GHz, the data must be considered suspect, since both the single and two slotted cylinder data is at the same level as the noise floor.

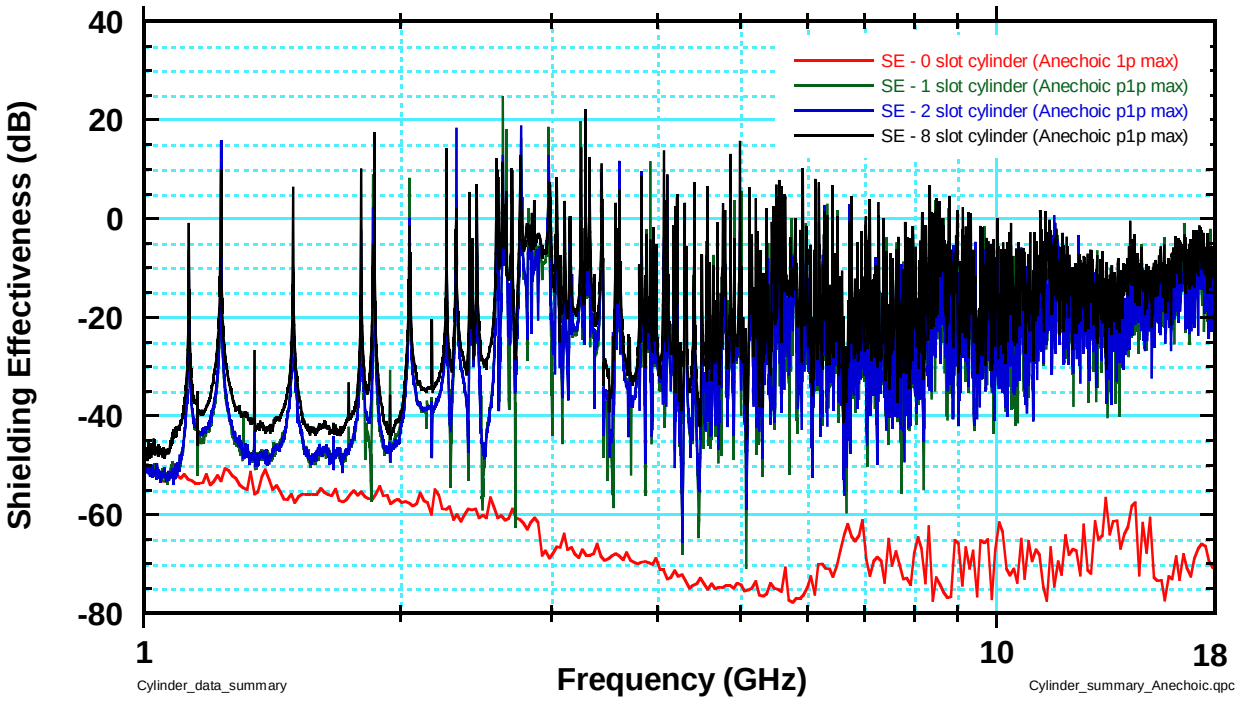

Figure 3-9 Comparison of shielding effectiveness of cylindrical test objects in the Anechoic Chamber.

3.2.2 Single Slot

The results from the single slot cylinder measurements are shown in Figure 3-10. The amplitude of the response in the anechoic chamber is larger than that of the response from the mode-stirred chamber, as expected.

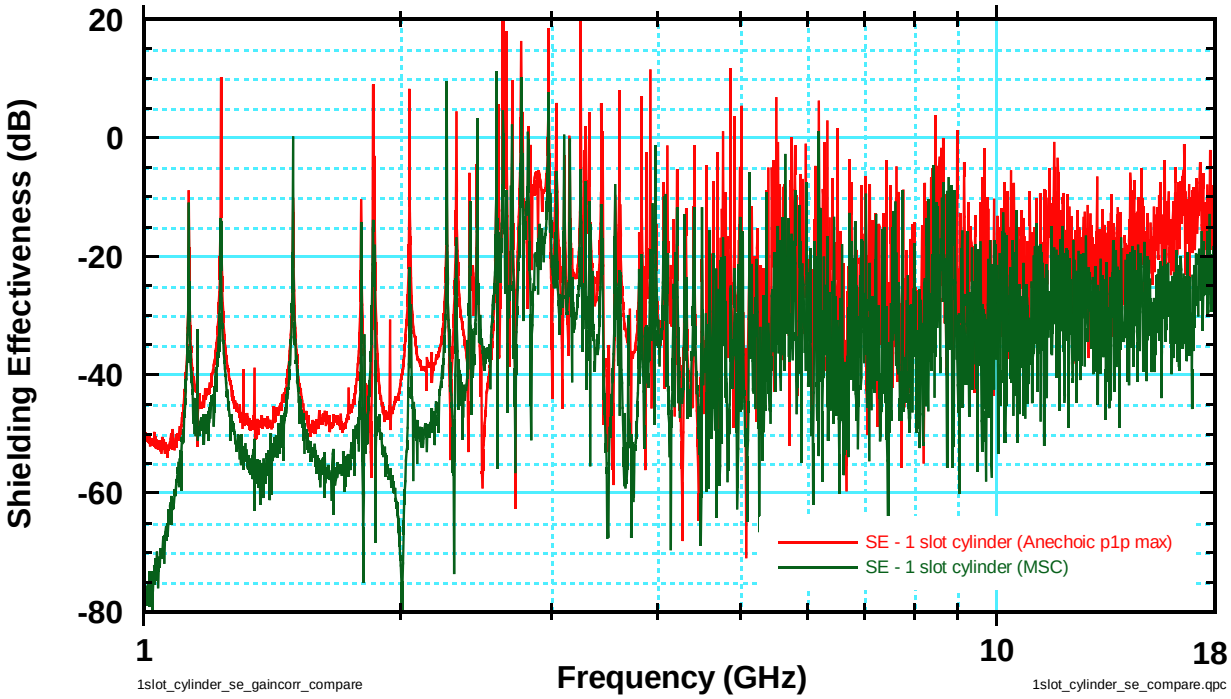

Figure 3-10 Shielding effectiveness of single slotted cylindrical test object in the mode-stirred chamber and anechoic chamber.

Based upon the need for both a low frequency and high frequency correction, the correction for an unintentional emitter was used. The corrected mode-stirred chamber data and anechoic data are compared in Figure 3-11. It is difficult to see how well the correction is working over the entire frequency band from the comparison of the data. A smoothing function (or moving average box car filter) was used to see the overall trend of the curves by essentially removing the high Q features of the cavity modes. Figure 3-12 compares the smoothed corrected mode-stirred chamber data with the anechoic data. There seems to be an approximately constant deviation of the two curves. If we add 4 dB to the corrected mode-stirred chamber data, the curves appear to overlap for the majority of the frequency band, as seen in Figure 3-13 and smoothed in Figure 3-14.

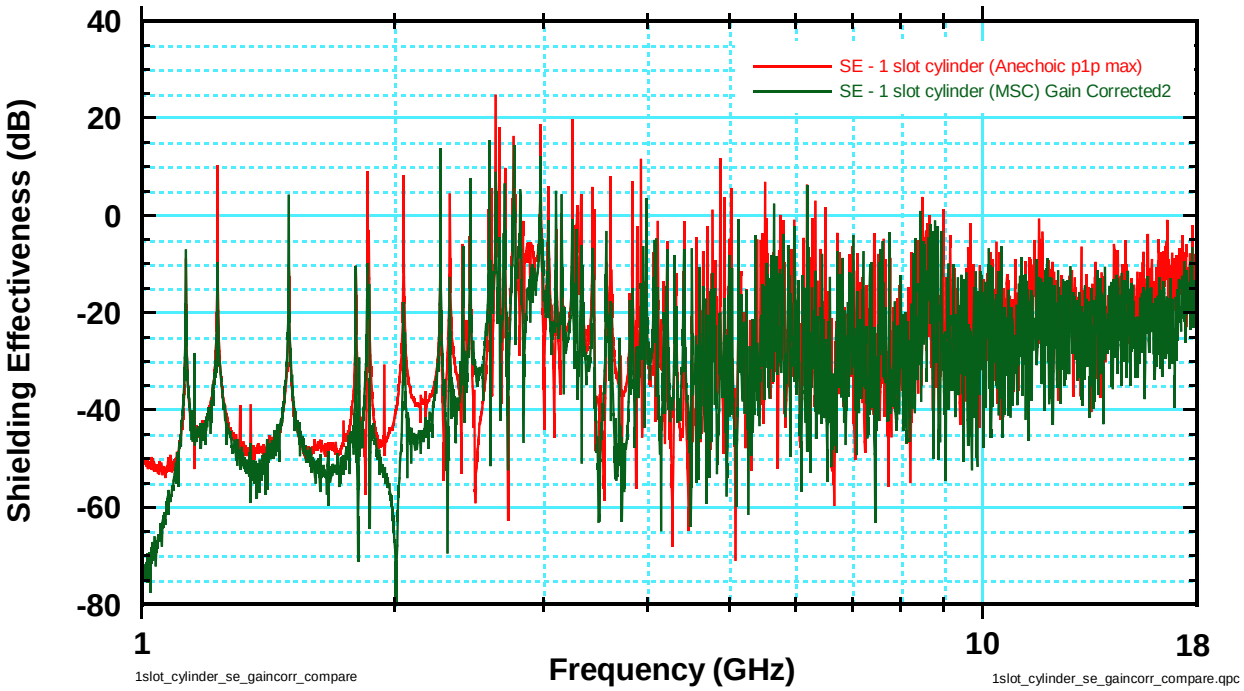

Figure 3-11 Comparison of shielding effectiveness of single slotted cylindrical test object with unintentional emitter correction used for mode-stirred chamber data.

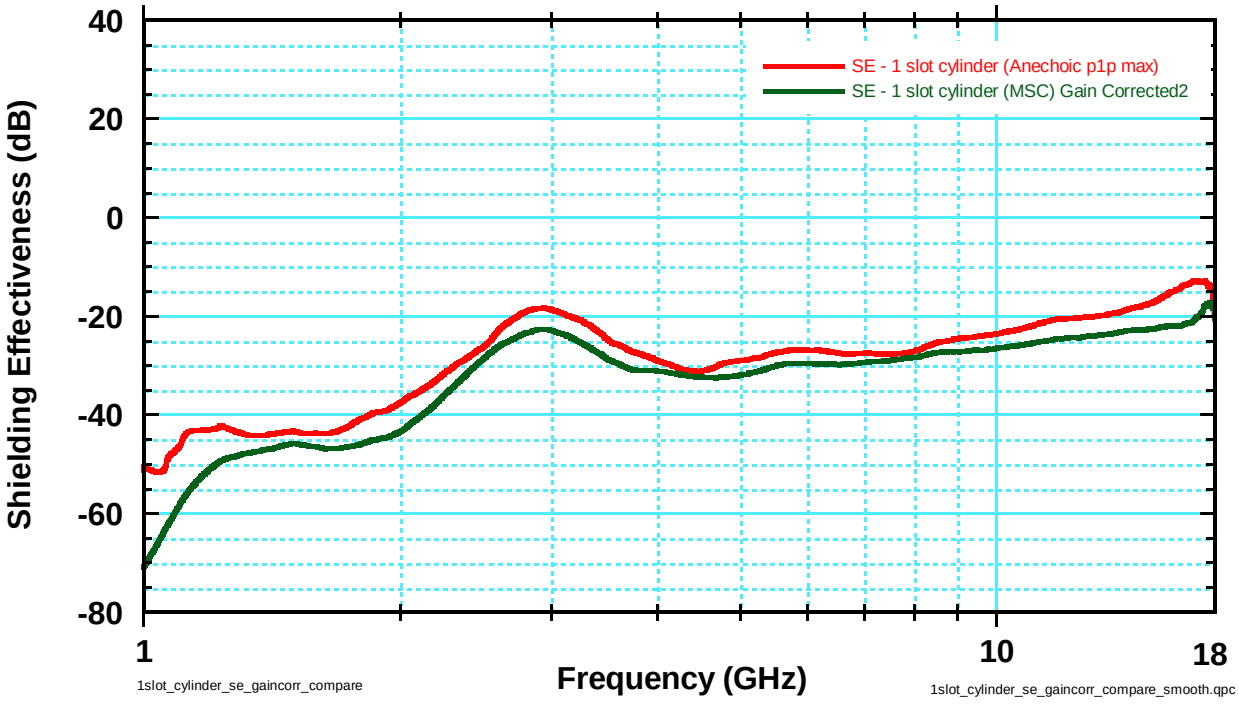

Figure 3-12 Smoothed comparison of shielding effectiveness of single slotted cylindrical test object with unintentional emitter correction used for mode-stirred chamber data.

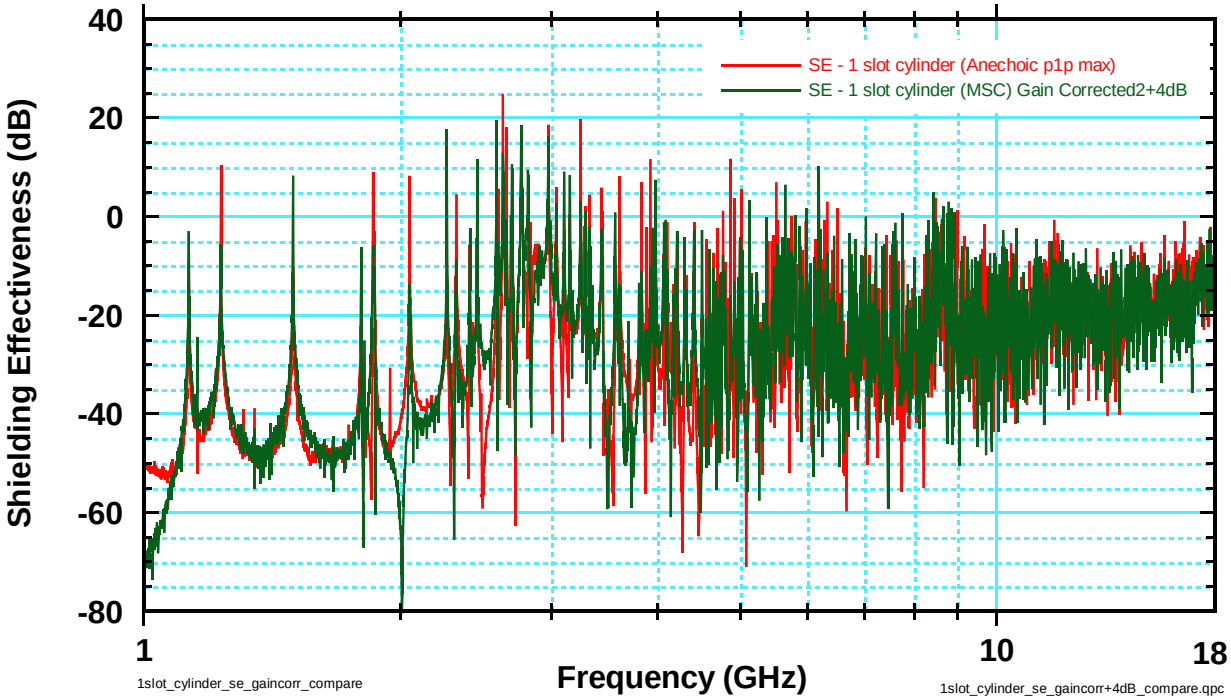

Figure 3-13 Comparison of shielding effectiveness of single slotted cylindrical test object with unintentional emitter correction plus 4 dB used for mode-stirred chamber data.

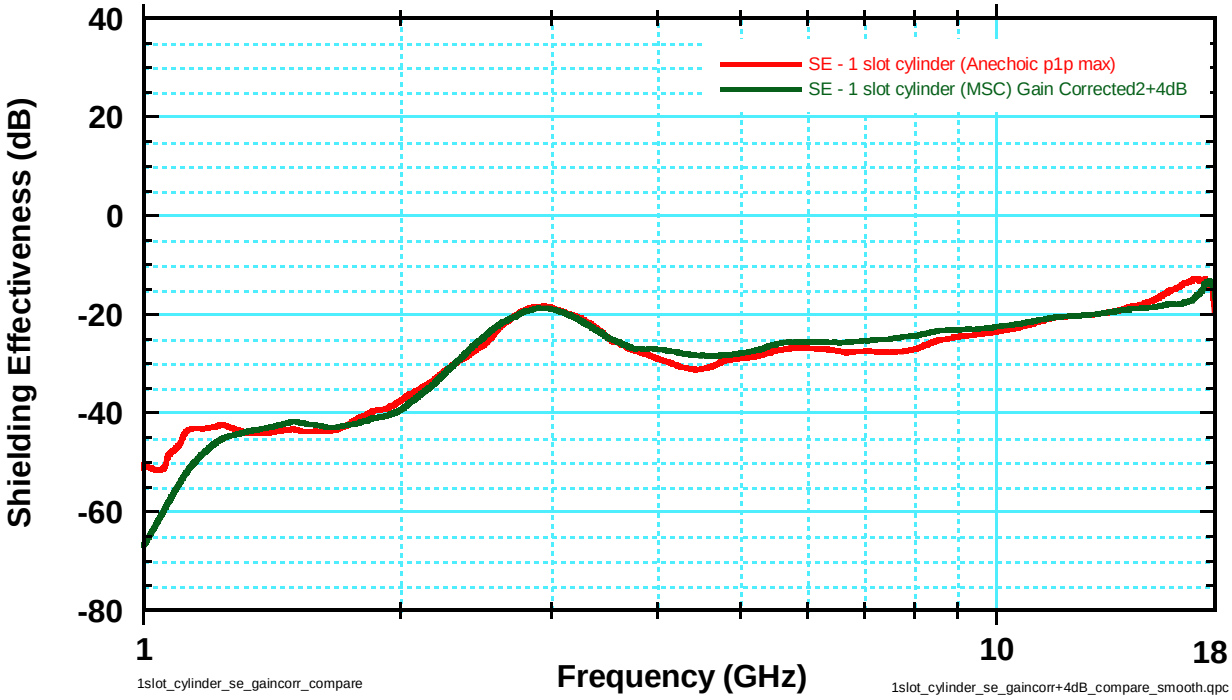

Figure 3-14 Smoothed comparison of shielding effectiveness of single slotted cylindrical test object with unintentional emitter correction plus 4 dB used for mode-stirred chamber data.

3.2.3 Two Slot

The results from the two slot cylinder measurements are shown in Figure 3-15. Again, the amplitude of the response in the anechoic chamber is larger than that of the response from the mode-stirred chamber, as expected.

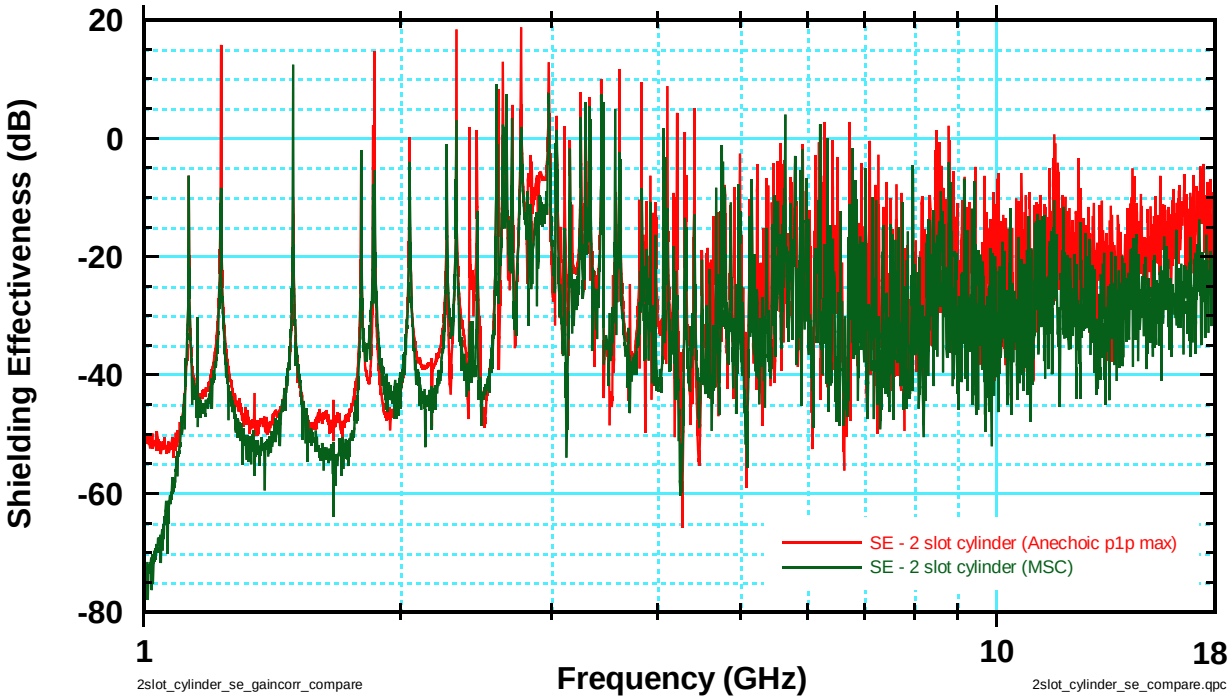

Figure 3-15 Shielding effectiveness of cylindrical test object with two slots in the mode-stirred chamber and anechoic chamber.

Based upon the need for both a low frequency and high frequency correction, the correction for an unintentional emitter was used. The corrected mode-stirred chamber data and anechoic data are compared in Figure 3-16. Figure 3-17 compares the smoothed corrected mode-stirred chamber data with the anechoic data. The low frequency corrected curves appear to match well in the raw data, but the smoothed curves show over correction. The correction at 18 GHz appears not to be sufficiently large enough. Figure 3-18 and Figure 3-19 compare the anechoic data with the mode-stirred chamber data corrected with the Sandia correction ($4L/\lambda$). Although the raw low frequency data is not corrected with the Sandia correction, the smoothed curves at low frequency match quite well. Overall, from the smoothed curve comparison the Sandia correction matches the anechoic data well, except a slight under correction at slot resonance (3 GHz).

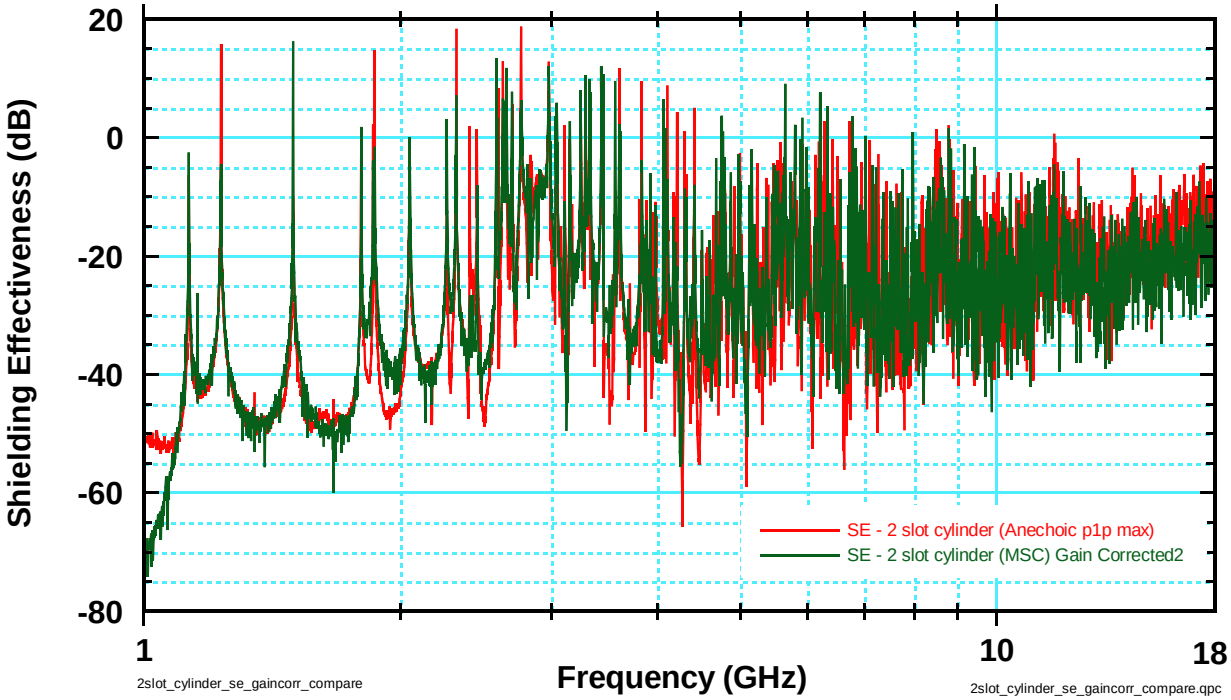

Figure 3-16 Comparison of shielding effectiveness of two slotted cylindrical test object with unintentional emitter correction used for mode-stirred chamber data.

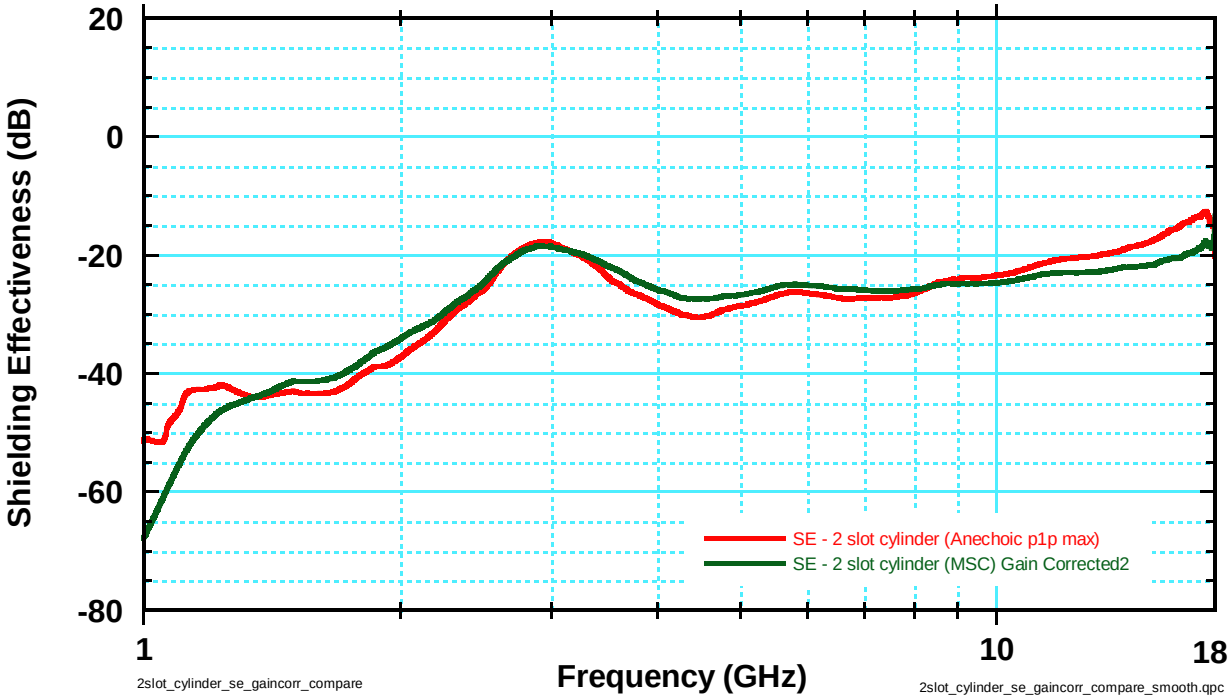

Figure 3-17 Smoothed comparison of shielding effectiveness of two slotted cylindrical test object with unintentional emitter correction used for mode-stirred chamber data.

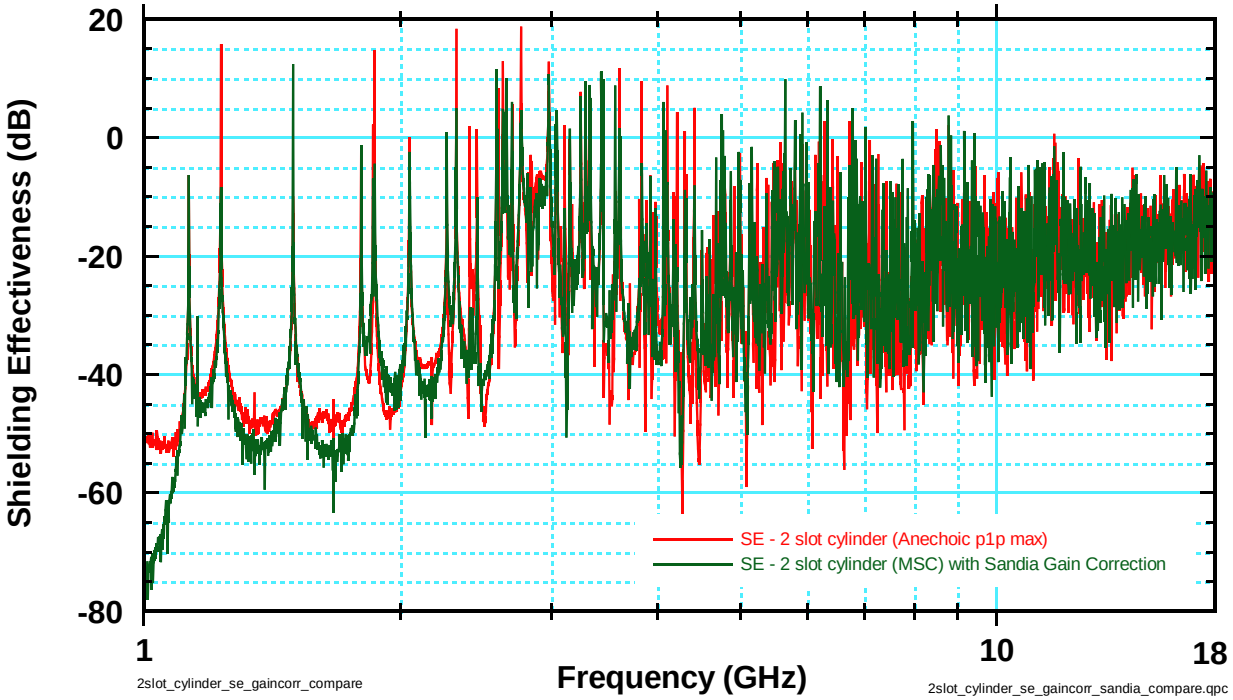

Figure 3-18 Comparison of shielding effectiveness of two slotted cylindrical test object with Sandia correction (4L/λ) used for mode-stirred chamber data.

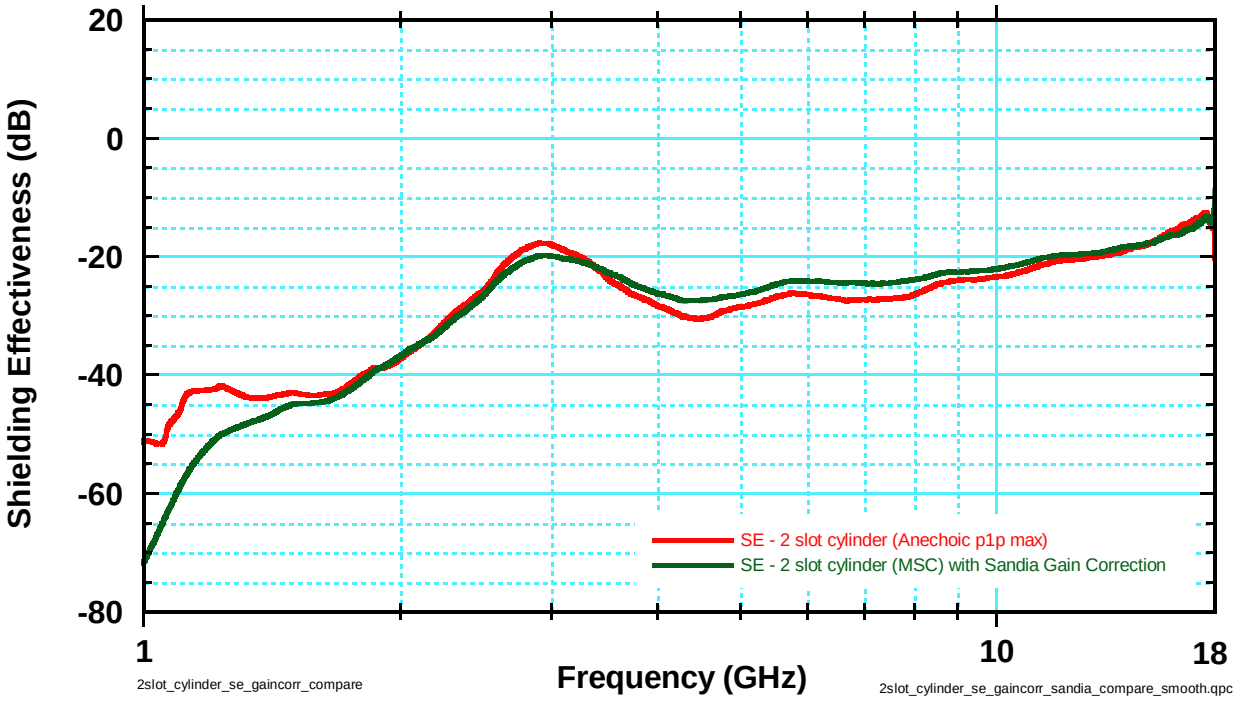

Figure 3-19 Smoothed comparison of shielding effectiveness of two slotted cylindrical test object with Sandia correction (4L/λ) used for mode-stirred chamber data.

3.2.4 Eight Slot

The results from the eight slot cylinder measurements are shown in Figure 3-20. Again, the amplitude of the response in the anechoic chamber is larger than that of the response from the mode-stirred chamber, but not as much as with the single and two slotted cylinders.

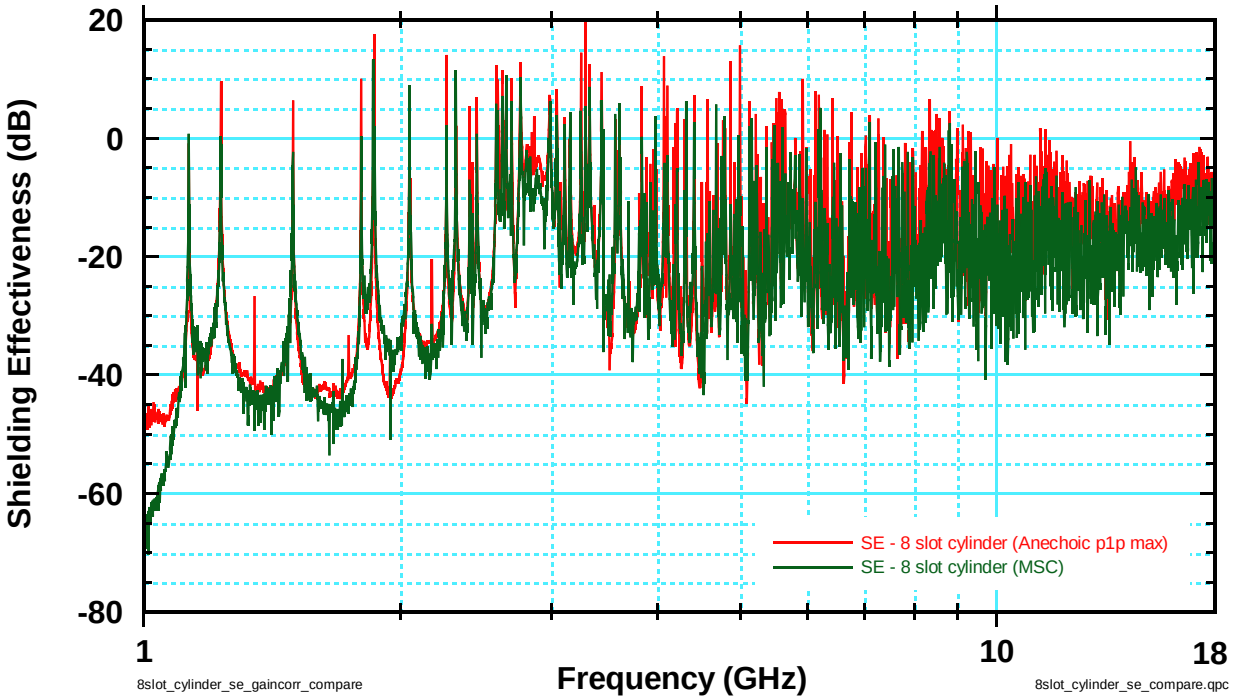

Figure 3-20 Shielding effectiveness of cylindrical test object with eight slots in the mode-stirred chamber and anechoic chamber.

It does not appear that the mode-stirred chamber data needs much correcting at frequencies below the slot resonance. Figure 3-21 and Figure 3-22 compare the anechoic data with the mode-stirred chamber data corrected with the Sandia correction ($2L/\lambda$). Although the raw low frequency data is not corrected with the Sandia correction, the smoothed curves at low frequency match quite well. Overall, from the smoothed curve comparison the Sandia correction matches the anechoic data well, except a slight under correction at slot resonance (3 GHz).

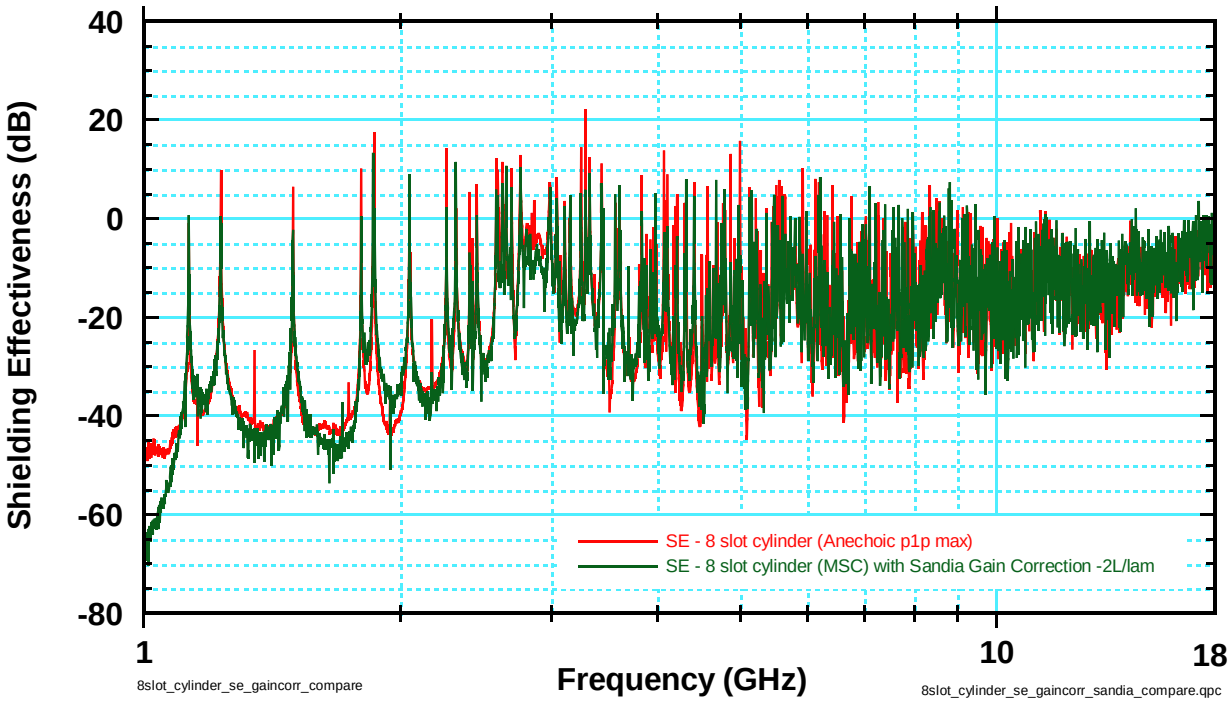

Figure 3-21 Comparison of shielding effectiveness of eight slotted cylindrical test object with Sandia correction (2L/λ) used for mode-stirred chamber data.

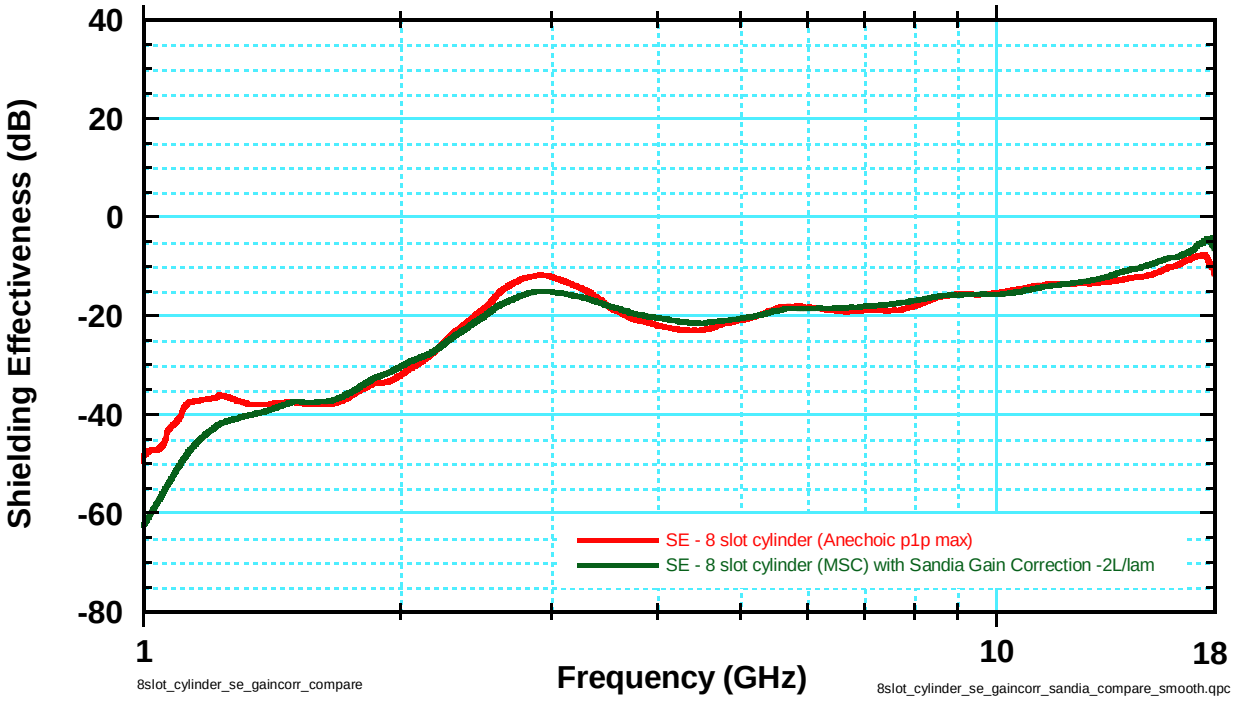

Figure 3-22 Smoothed comparison of shielding effectiveness of eight slotted cylindrical test object with Sandia correction (2L/λ) used for mode-stirred chamber data.

3.2.5 Cylindrical Conclusions

All of the mode-stirred chamber cylinder data was able to be corrected to commensurate levels with that of the anechoic data, using one of the three corrections discussed in Chapter 2. The mode-stirred chamber shielding effectiveness data from the single slotted cylinder was best corrected with the unintentional emitter correction, but also needed an additional 4 dB added to it. The two slotted cylinder mode-stirred chamber data was best corrected with the Sandia correction factor of ($4L/\lambda$). This factor under corrects at slot resonance, as was shown in the smoothed curves. Also, it under corrects slightly in the raw data below slot resonance. Between 4 and 8 GHz the Sandia factor over corrects an average of 4 dB in the smoothed curves. The eight slotted cylinder mode-stirred chamber data was best corrected with the Sandia correction factor of ($2L/\lambda$). This factor under corrects at slot resonance, as was shown in the smoothed curves. Also, it under corrects slightly in the raw data below slot resonance. A summary of the conclusions is shown in Table 3-5.

Table 3-5 Summary of best corrections for the cylindrical test objects

# of slots	Best Correction	Problems
1	Unintentional Emitter +4 dB	Needed +4dB more correction over entire frequency band from the unintentional emitter correction.
2	Sandia ($4L/\lambda$)	Under corrected smoothed curve at slot resonance.
8	Sandia ($2L/\lambda$)	Under corrected smoothed curve at slot resonance.

3.3 Rectangular Test Object Shielding Effectiveness Measurements

The rectangular box test object series of measurements was performed on one box with four interchangeable front cover plates: single slot plate; a two slotted plate; a four slotted plate; and a zero slotted plate (or blank plate) which was used as a noise floor measurement. A brief summary of the data is presented in Section 3.3.1, with a brief summary of modal responses in rectangular cavities. The results of the experiment are presented in increasing number of slots, beginning with the single slot case. The blank plate results are shown with each case to demonstrate the limitations of the data.

3.3.1 Measurement Results - Overview

The rectangular box test object made of aluminum has interior dimensions of 24 inches wide by 15 inches deep by 8.5 inches tall. The 15 by 8 and 15 by 24 inch walls were 0.5 inch thick and welded on the edges. The back plate was a blank plate. All interfaces between plates and the box were treated with a bronze wool gasket and two layers of copper tape, to seal extraneous apertures and reduce unwanted coupling. A drawing of the rectangular box test object with the single slot plate installed is shown in Figure 3-23. A 4.3mm monopole probe was used to measure the perpendicular electric field at the inside surface on the bottom plate. The probe was placed 9.875 inches from the front face of the box and centered on the bottom side of the box as shown in Figure 3-23.

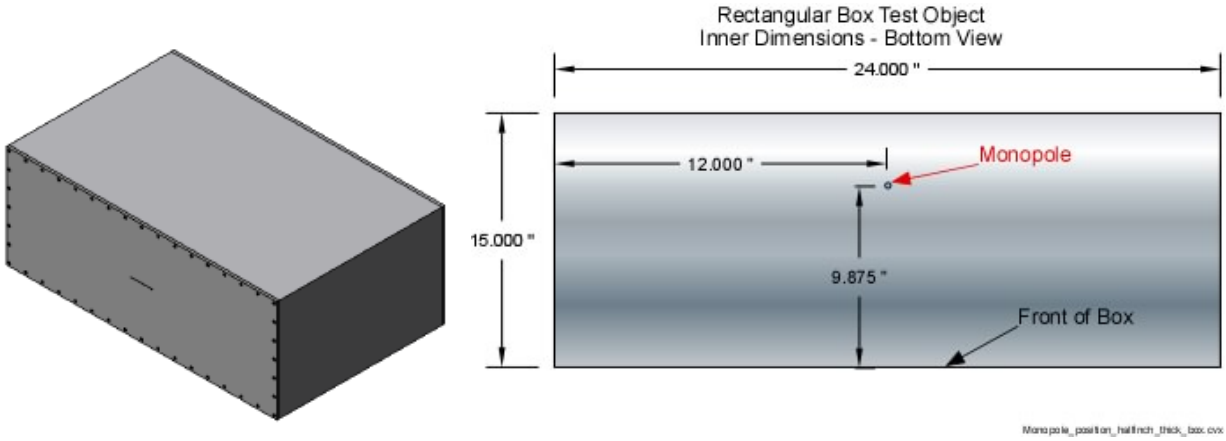

Figure 3-23 Drawing of the rectangular box test object with the single slot plate installed.

For the rectangular cavity geometry shown above only TM and TE modes can exist and only TM^z and TE^z modes shall be discussed. Each mode has a frequency where a particular mode is cutoff, i.e. below that frequency the mode cannot exist. The equations governing the cutoff frequencies are shown in (3.11) and (3.12). The letters m, n, and p represent the mode number. The first 20 TM^z and TE^z modes are shown in increasing order in Table 3-6 and Table 3-7, respectively. The location of the monopole probe shown in Figure 3-23 allows for detection of some of the TE^z modes, but not the TM^z. Table 3-7 also shows the frequencies of the observed TE^z modes seen in the measured data of the box with the single slotted plate installed.

$$\left(f_r\right)_{mnp}^{TM^z} = \frac{1}{2\pi\sqrt{\mu\varepsilon}}\sqrt{\left(\frac{m\pi}{a}\right)^2+\left(\frac{n\pi}{b}\right)^2+\left(\frac{p\pi}{c}\right)^2} \qquad \begin{matrix} m=1,2,3,... \\ n=1,2,3,... \\ p=0,1,2,... \end{matrix} \tag{3.11}$$

Where a, b, and c are the inner dimensions of the rectangular cavity with c > a > b. [4].

Table 3-6 First 20 TM_z modes of rectangular test object

m	n	p	$(f_r)_{mnp}$ TM_z (GHz)
1	1	0	0.7980
1	1	1	0.8350
1	1	2	0.9374
2	1	0	1.0494
2	1	1	1.0778
1	1	3	1.0867
2	1	2	1.1589
1	1	4	1.2666
2	1	3	1.2827
3	1	0	1.3694
3	1	1	1.3913
2	1	4	1.4383
1	2	0	1.4432
3	1	2	1.4550
1	2	1	1.4640
1	1	5	1.4658
1	2	2	1.5247
3	1	3	1.5554
2	2	0	1.5960
2	2	1	1.6149

$$\left(f_r\right)_{mnp}^{TE^z} = \frac{1}{2\pi\sqrt{\mu\varepsilon}}\sqrt{\left(\frac{m\pi}{a}\right)^2+\left(\frac{n\pi}{b}\right)^2+\left(\frac{p\pi}{c}\right)^2} \qquad \left.\begin{matrix} m=0,1,2,... \\ n=0,1,2,... \\ p=1,2,3,... \end{matrix}\right\} \; m=n\neq 0 \tag{3.12}$$

Where a, b, and c are the inner dimensions of the rectangular cavity with c > a > b. [4].

Table 3-7 First 20 TE_z modes of rectangular test object

m	n	p	$(f_r)_{mnp}$ TE_z (GHz)	f (GHz) observed
1	0	1	0.4640	Frequencies below 0.5 GHz not measured in MSC
1	0	2	0.6298	0.6293
0	1	1	0.7366	Not observed
2	0	1	0.8244	0.8242
1	1	1	0.8350	0.8338 (very small)
1	0	3	0.8360	0.8358
0	1	2	0.8508	Not observed
2	0	2	0.9279	Not observed
1	1	2	0.9374	Not observed
0	1	3	1.0130	Not observed
1	0	4	1.0593	Not observed
2	1	1	1.0778	1.0768
2	0	3	1.0786	1.0778
1	1	3	1.0867	Not observed
2	1	2	1.1589	Not observed
0	1	4	1.2039	1.2032
3	0	1	1.2056	1.2044
2	0	4	1.2596	1.2585
1	1	4	1.2666	Not observed
3	0	2	1.2787	1.2774

The data shown in Figure 3-24 are the uncorrected results of all four rectangular box test object configurations measured in the mode-stirred chamber. The very sharp spikes are some of the TE^z modes of the cavity discussed previously. The red curve is the box with the blank plate installed and represents the noise floor of the mode-stirred chamber measurements. There is no problem with noise in the mode-stirred chamber data for this measurement series.

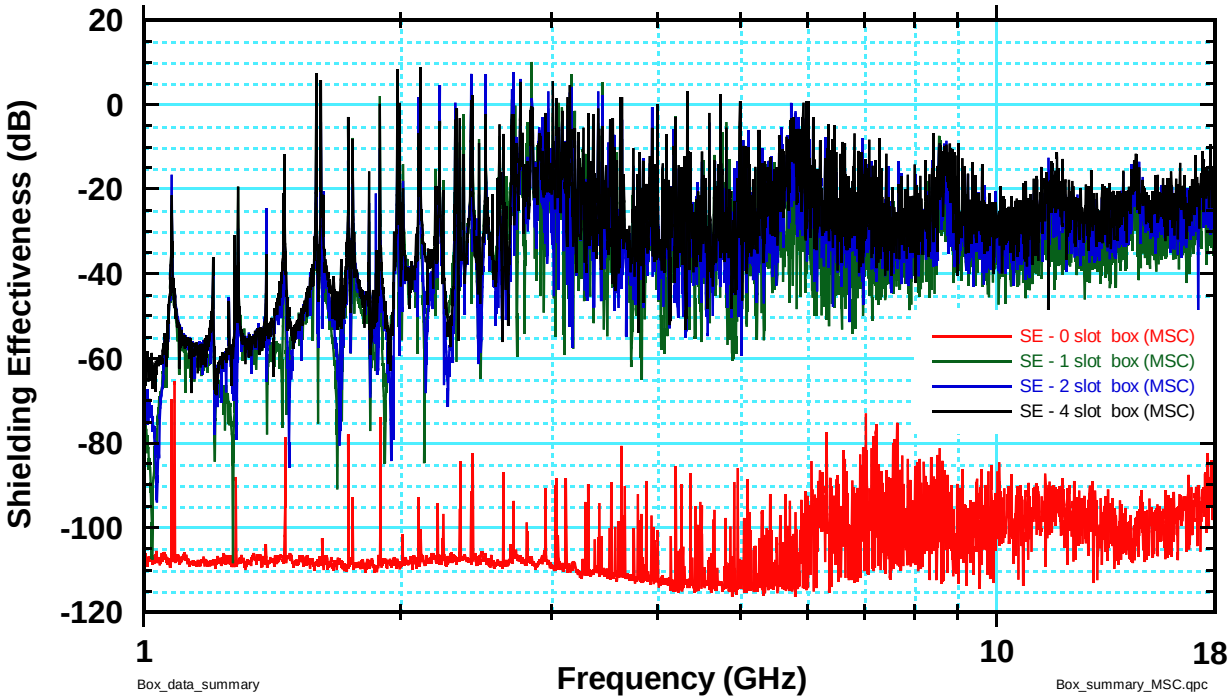

Figure 3-24 Comparison of shielding effectiveness of rectangular test objects in the mode-stirred chamber.

The data shown in Figure 3-25 are the reduced results of all four rectangular box test object configurations measured in the anechoic chamber. Each curve is the maximum amplitude of each position of the azimuthal scan. Again, the very sharp spikes are some of the TE^z modes of the cavity discussed previously. The red curve is the box with the blank plate installed and represents the noise floor of the anechoic measurements. There is no problem with noise in the anechoic data above 1.42 GHz for this measurement series. Below 1.42 GHz the data must be considered suspect, since some of the slotted plate data is at the same level as the noise floor. The peaks below 1.42 GHz that are above the noise floor level are valid, but the average smoothed data below 1.42 GHz is skewed toward the high side.

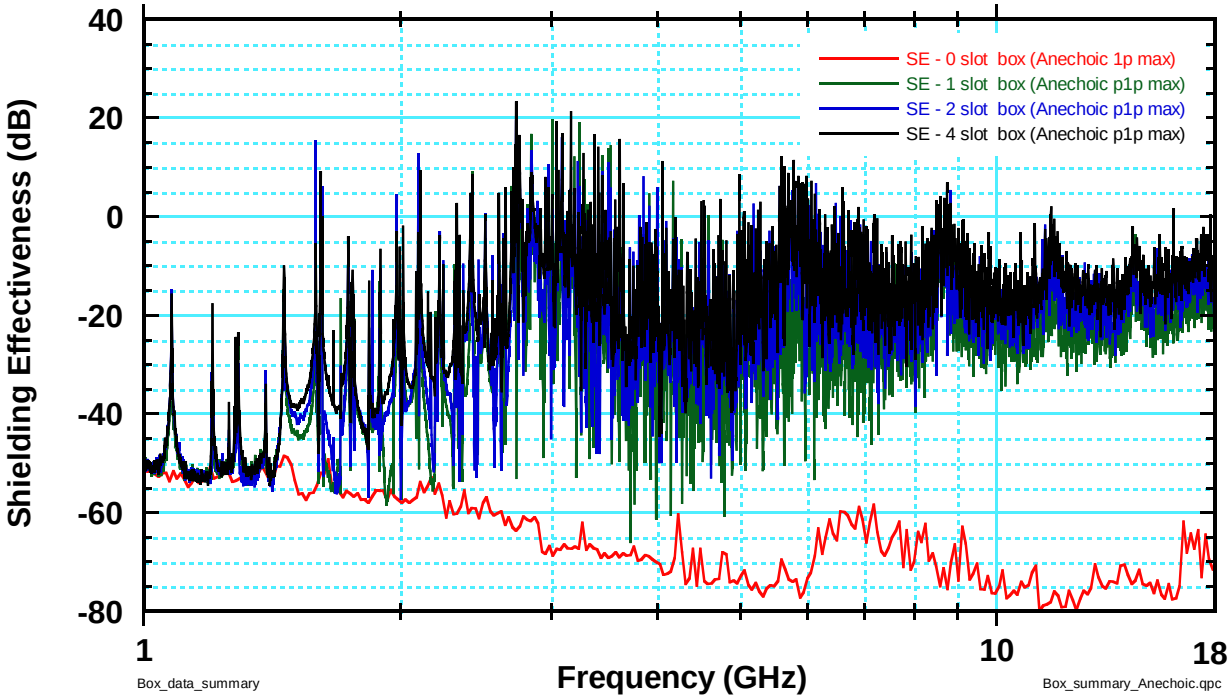

Figure 3-25 Comparison of shielding effectiveness of rectangular test objects in the Anechoic Chamber.

3.3.2 Single Slot

The results from the single slot rectangular box measurements are shown in Figure 3-26. The amplitude of the response in the anechoic chamber is larger than that of the response from the mode-stirred chamber, as expected.

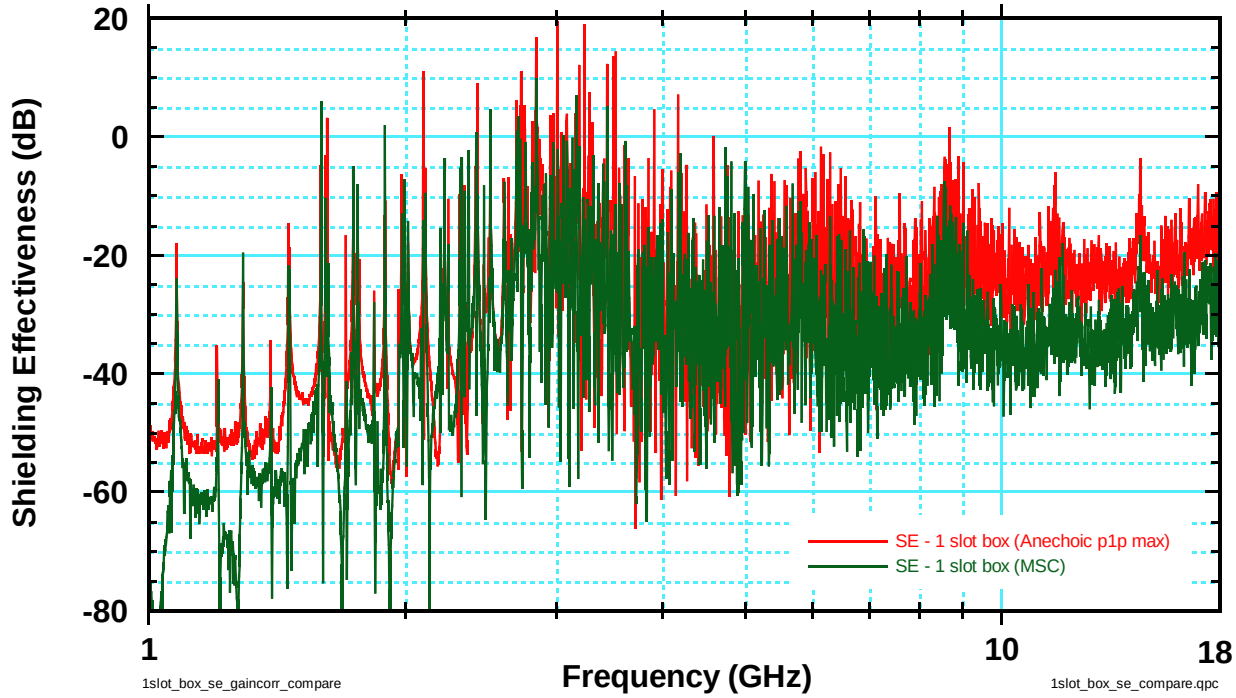

Figure 3-26 Shielding Effectiveness of single slotted rectangular test object in the mode-stirred chamber and anechoic chamber.

Based upon the need for both a low frequency and high frequency correction, the correction for an unintentional emitter was used. The corrected mode-stirred chamber data and anechoic data are compared in Figure 3-27. Again a smoothing function (or moving average box car filter) was used to see the overall trend of the curves by essentially removing the high Q features of the cavity modes. Figure 3-28 compares the smoothed corrected mode-stirred chamber data with the anechoic data. There seems to be an approximately constant deviation of the two curves. If we add 4 dB to the corrected mode-stirred chamber data, the curves appear to overlap for the majority of the frequency band, as seen in Figure 3-29 and smoothed in Figure 3-30. As a comparison study, the Sandia factor of $4L/\lambda$ was used to correct the mode-stirred chamber data as shown in Figure 3-31 and smoothed in Figure 3-32. The Sandia factor does a fair compensation above 4 GHz, but under corrects at frequencies lower than 4 GHz.

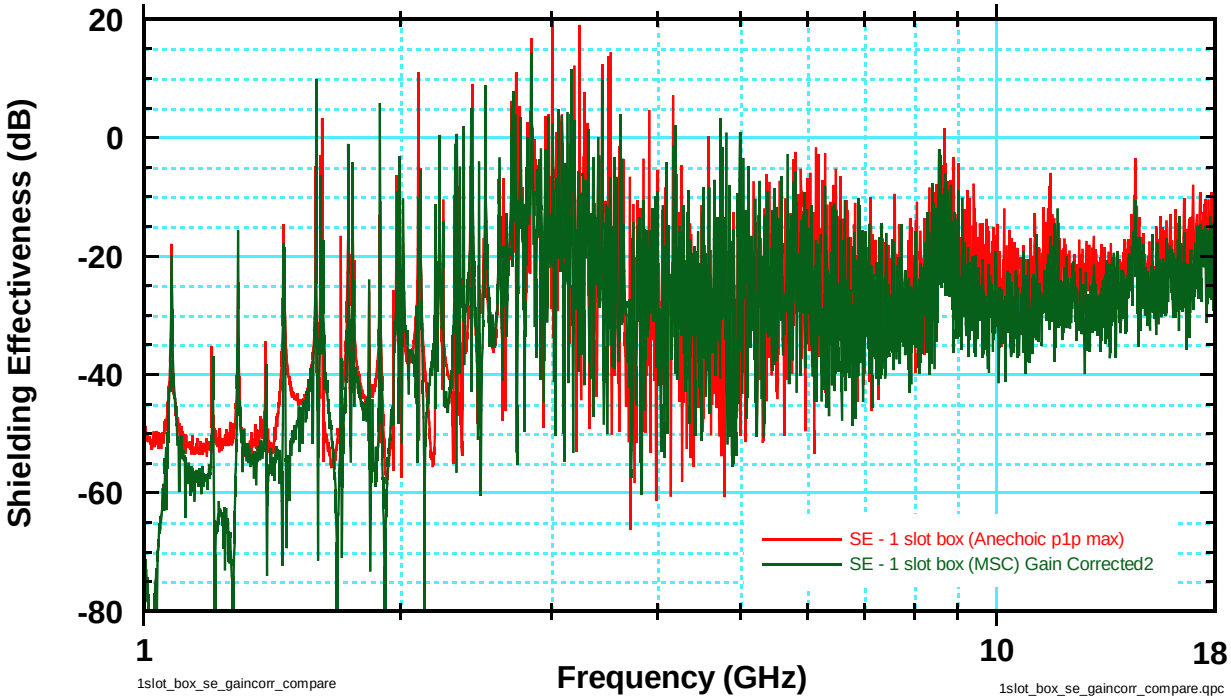

Figure 3-27 Comparison of shielding effectiveness of single slotted rectangular box test object with unintentional emitter correction used for mode-stirred chamber data.

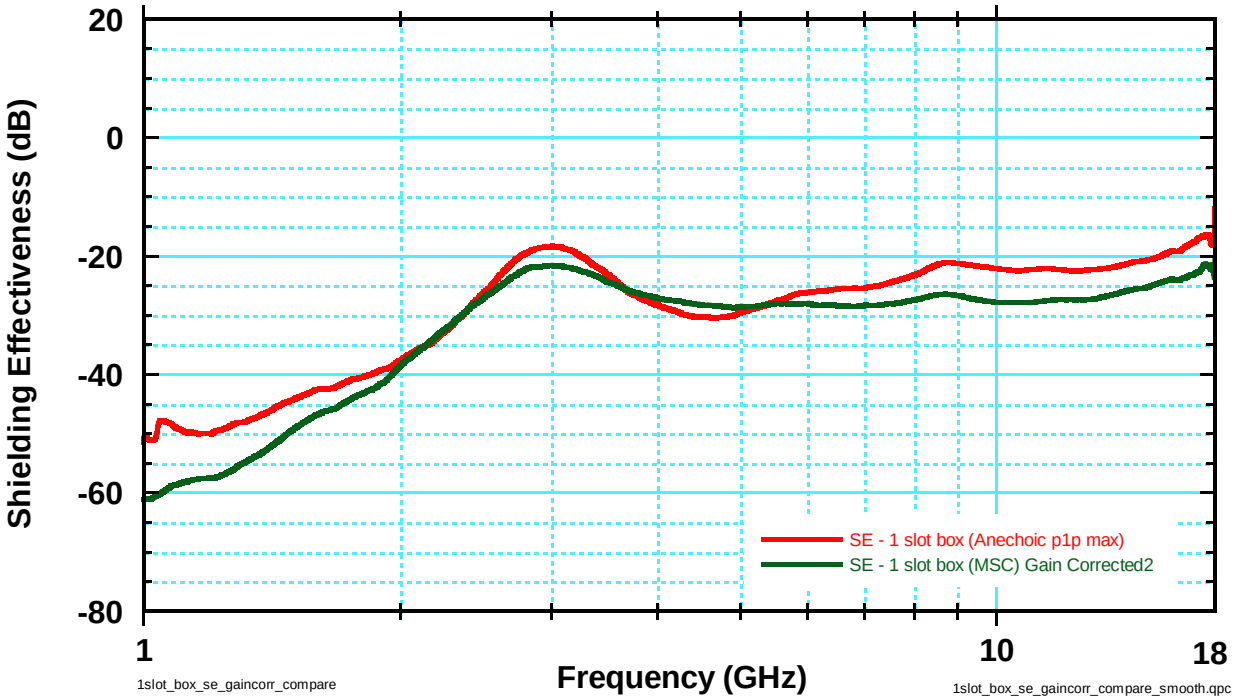

Figure 3-28 Smoothed comparison of shielding effectiveness of single slotted rectangular box test object with unintentional emitter correction used for mode-stirred chamber data.

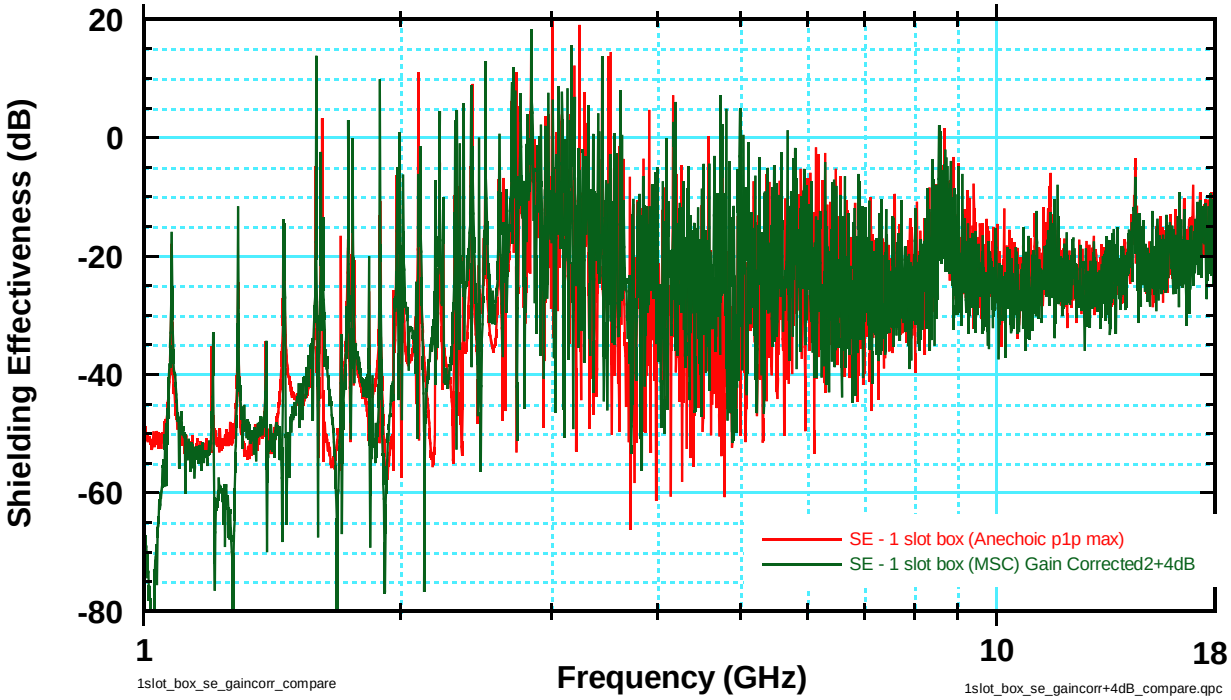

Figure 3-29 Comparison of shielding effectiveness of single slotted rectangular box test object with unintentional emitter correction + 4dB used for mode-stirred chamber data.

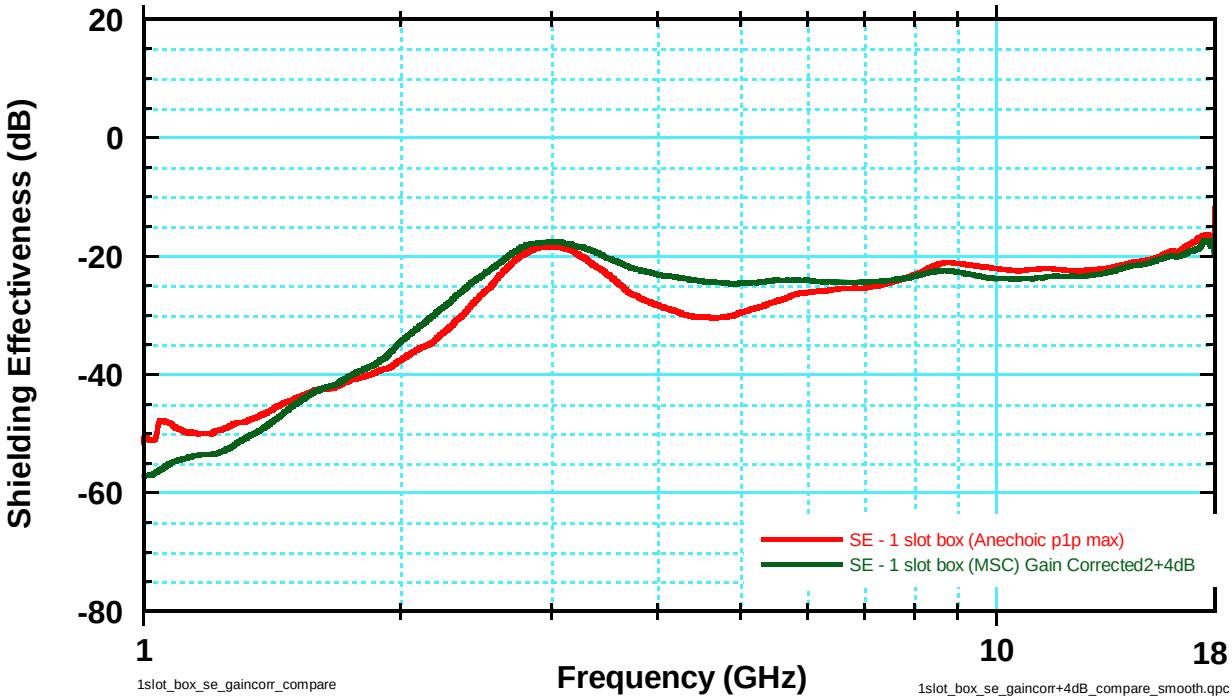

Figure 3-30 Smoothed comparison of shielding effectiveness of single slotted rectangular box test object with unintentional emitter correction + 4dB used for mode-stirred chamber data.

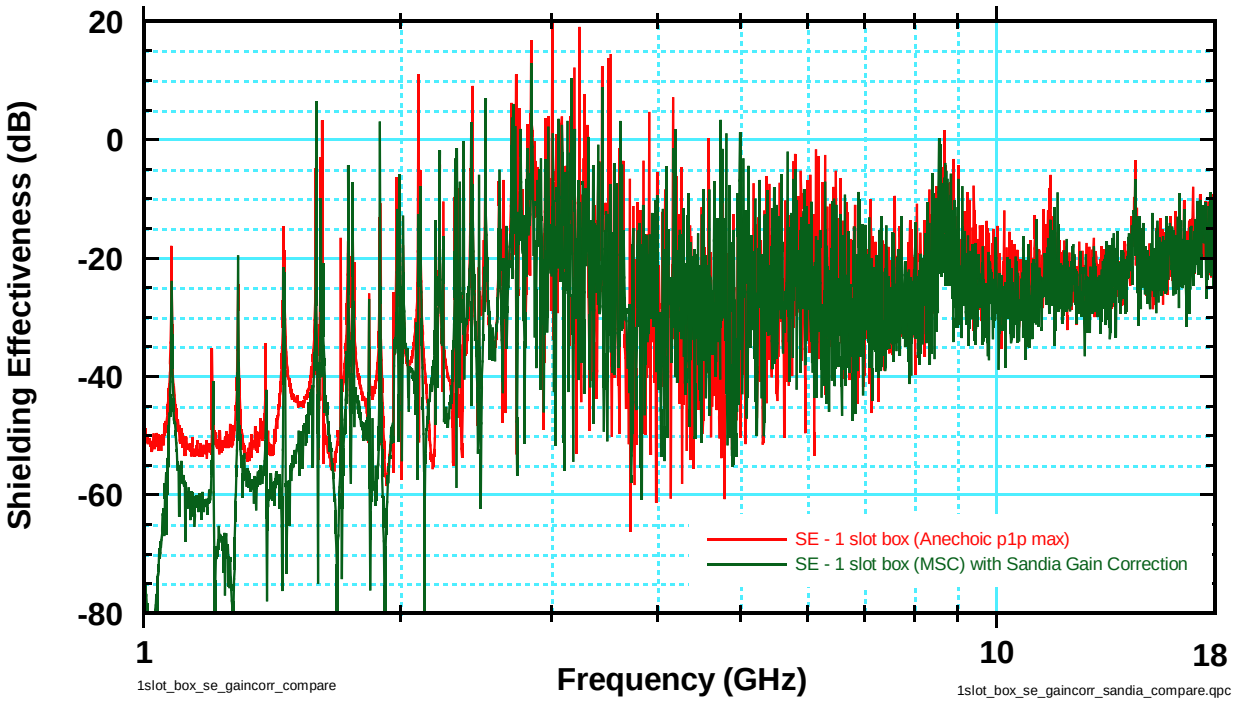

Figure 3-31 Comparison of shielding effectiveness of single slotted rectangular box test object with Sandia (4L/λ) correction used for mode-stirred chamber data.

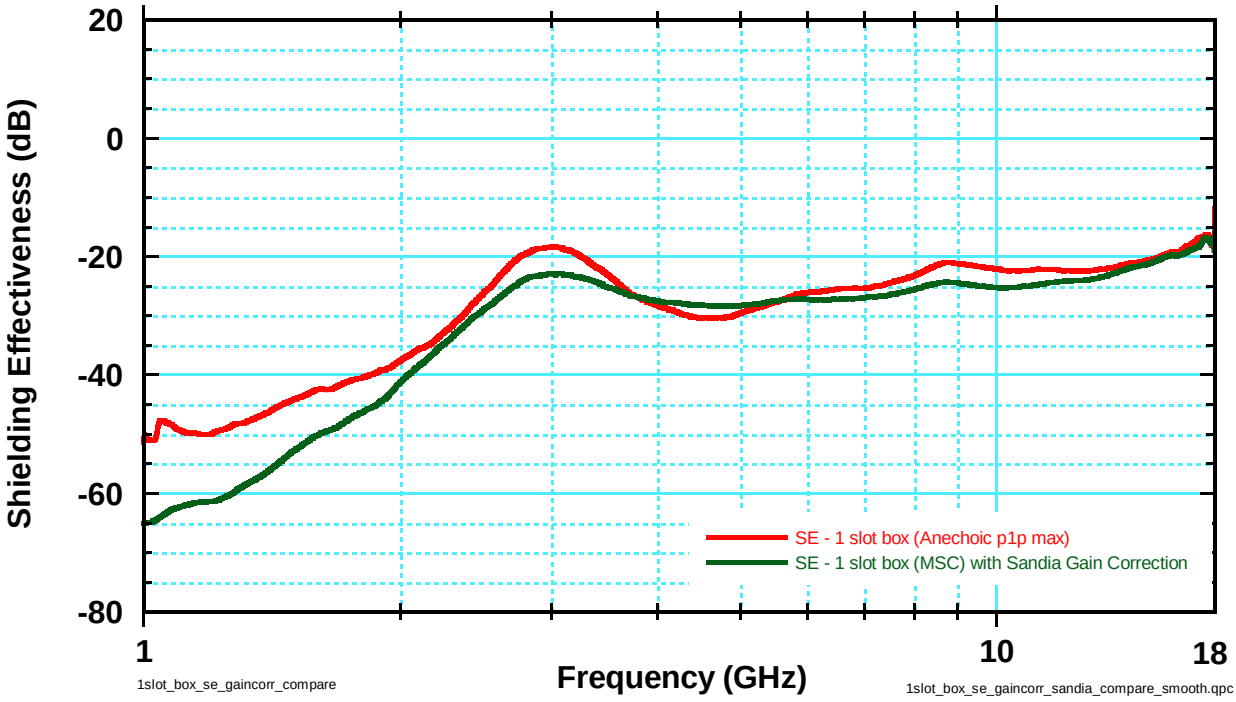

Figure 3-32 Smoothed comparison of shielding effectiveness of single slotted rectangular box test object with Sandia (4L/λ) correction used for mode-stirred chamber data.

3.3.3 Two Slot

The results from the rectangular box with the two slotted plate measurements are shown in Figure 3-33. Again, the amplitude of the response in the anechoic chamber is larger than that of the response from the mode-stirred chamber, as expected.

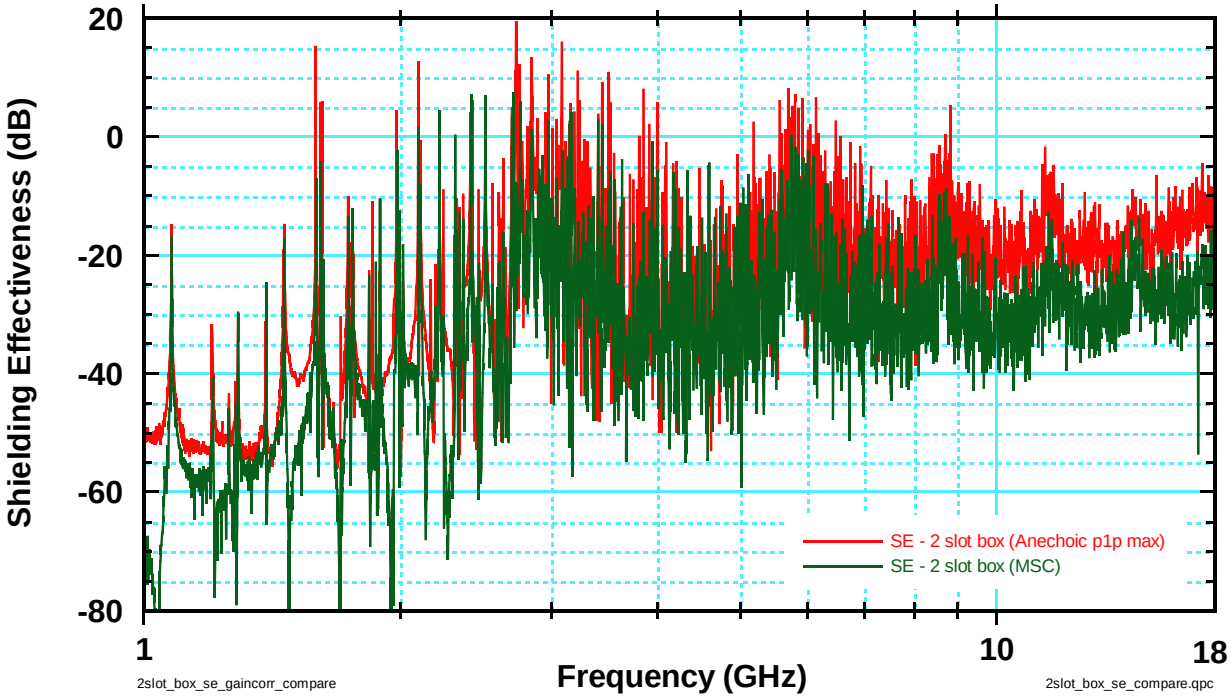

Figure 3-33 Shielding effectiveness of rectangular test object with two slotted plate, in the mode-stirred chamber and anechoic chamber.

Based upon the need for both a low frequency and high frequency correction, the correction for an unintentional emitter was used. The corrected mode-stirred chamber data and anechoic data are compared in Figure 3-34. Figure 3-35 compares the smoothed corrected mode-stirred chamber data with the anechoic data. Again, there seems to be an approximately constant deviation of the two curves. If we add 4 dB to the corrected mode-stirred chamber data, the curves appear to overlap for the majority of the frequency band, as seen in Figure 3-36 and smoothed in Figure 3-37. Overall, from the smoothed curve comparison the unintentional emitter correction plus 4dB matches the anechoic data very well, except for a slight over correction from 4 to 5 GHz.

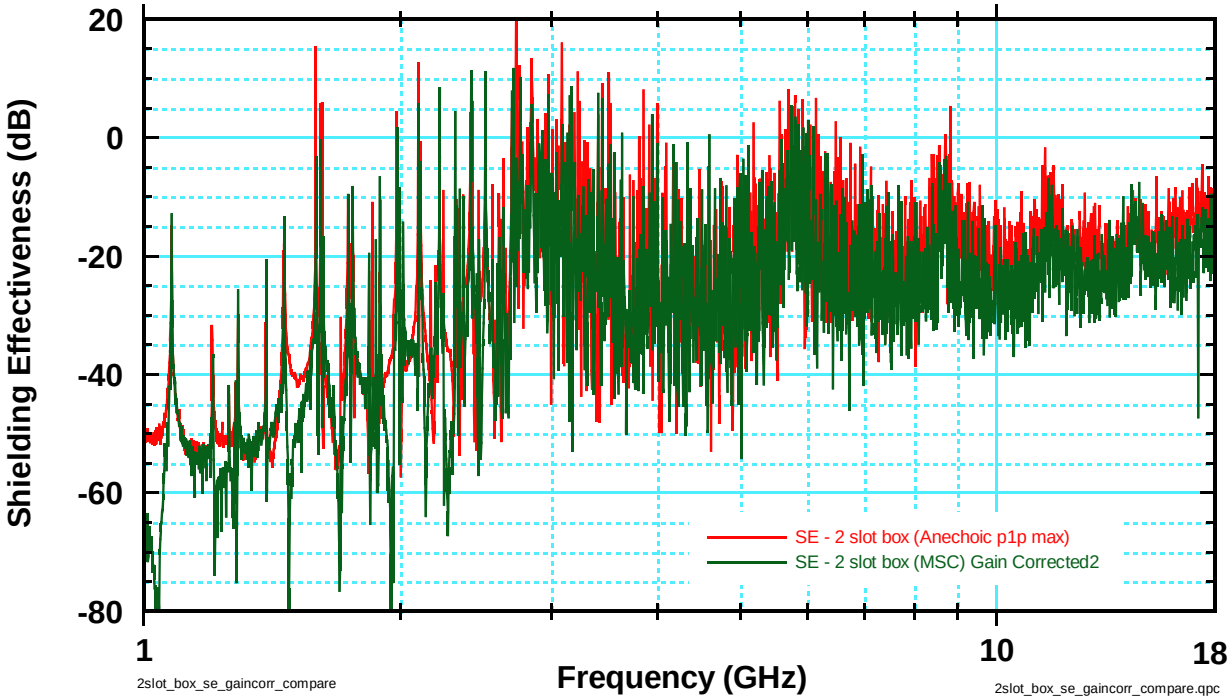

Figure 3-34 Comparison of shielding effectiveness of rectangular box test object with two slotted plate, with unintentional emitter correction used for mode-stirred chamber data.

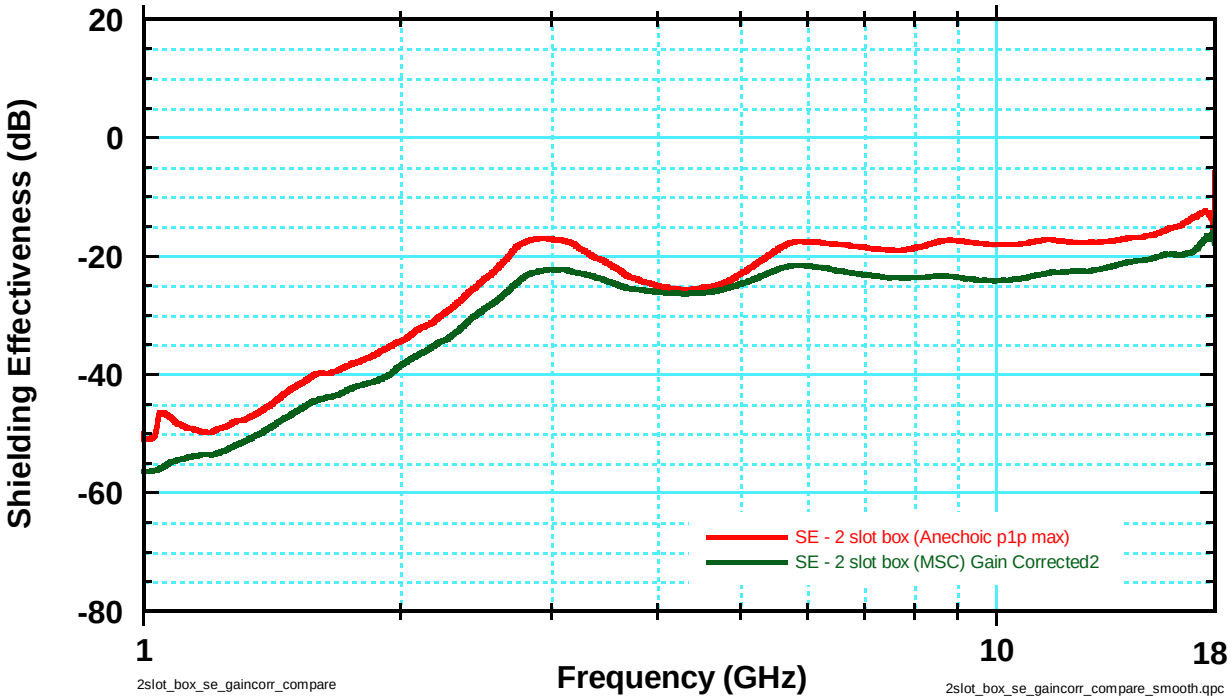

Figure 3-35 Smoothed comparison of shielding effectiveness of rectangular box test object with two slotted plate, with unintentional emitter correction used for mode-stirred chamber data.

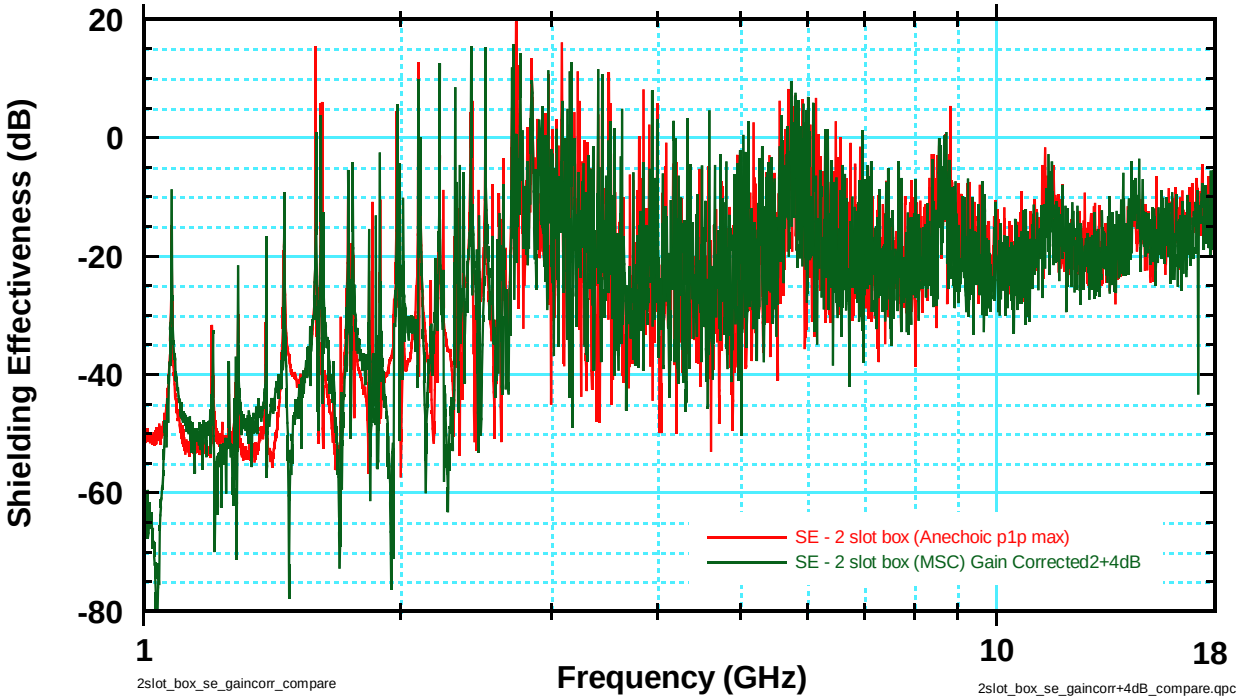

Figure 3-36 Comparison of shielding effectiveness of rectangular box test object with two slotted plate, with unintentional emitter + 4dB correction used for mode-stirred chamber data.

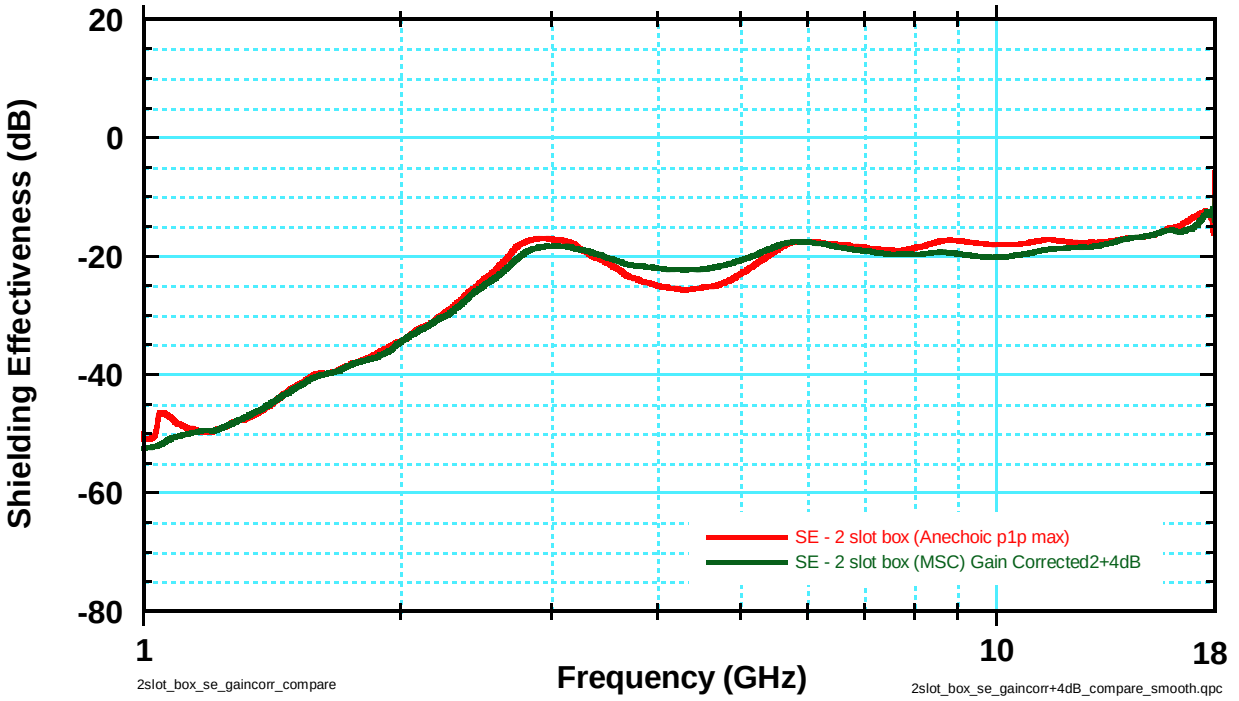

Figure 3-37 Smoothed comparison of shielding effectiveness of rectangular box test object with two slotted plate, with unintentional emitter + 4dB correction used for mode-stirred chamber data.

3.3.4 Four Slot

The results from the rectangular box with the four slotted plate measurements are shown in Figure 3-38. Again, the amplitude of the response in the anechoic chamber is larger than that of the response from the mode-stirred chamber, but not as much as with the single and two slotted plates.

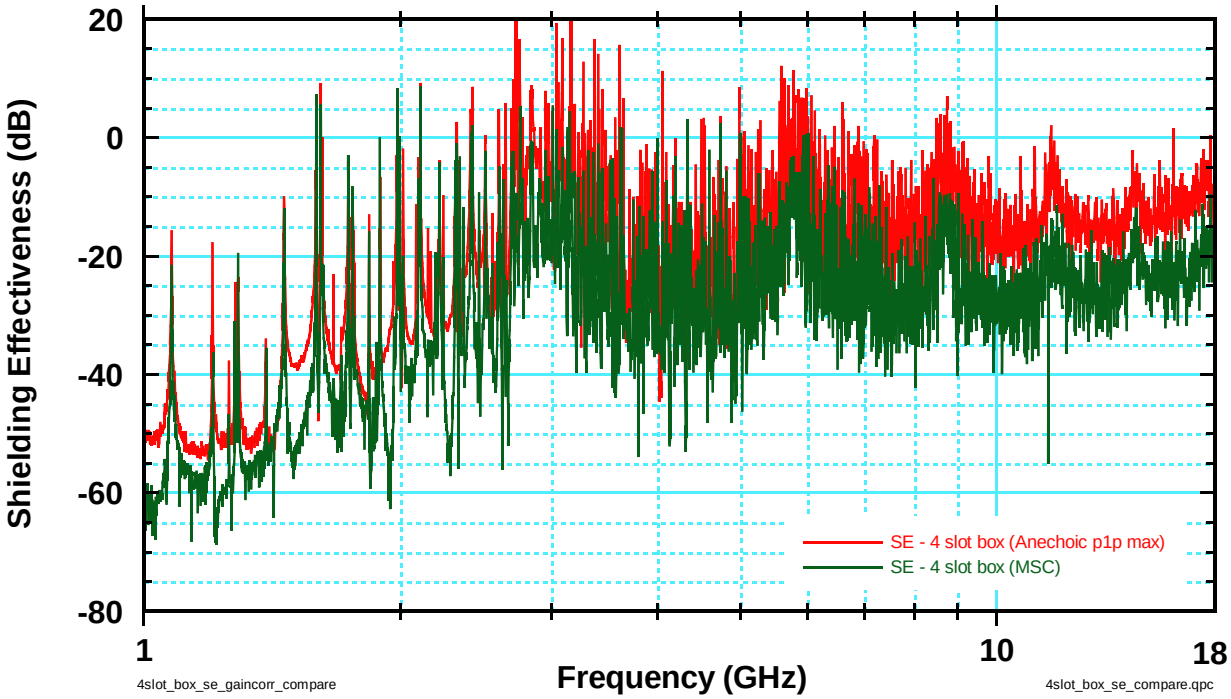

Figure 3-38 Shielding effectiveness of rectangular test object with four slotted plate, in the mode-stirred chamber and anechoic chamber.

Again, based upon the need for both a low frequency and high frequency correction and the previous results, the correction for an unintentional emitter plus 4 dB was used. The corrected mode-stirred chamber data and anechoic data are compared in Figure 3-39. Figure 3-40 compares the smoothed corrected mode-stirred chamber data with the anechoic data. The other corrections were studied, but none corrected as well as the case shown. Overall, from the smoothed curve comparison the unintentional emitter correction plus 4dB matches the anechoic data well, except for a slight under correction at slot resonance and from 6 to 12 GHz where the under correction is approximately 2-3 dB.

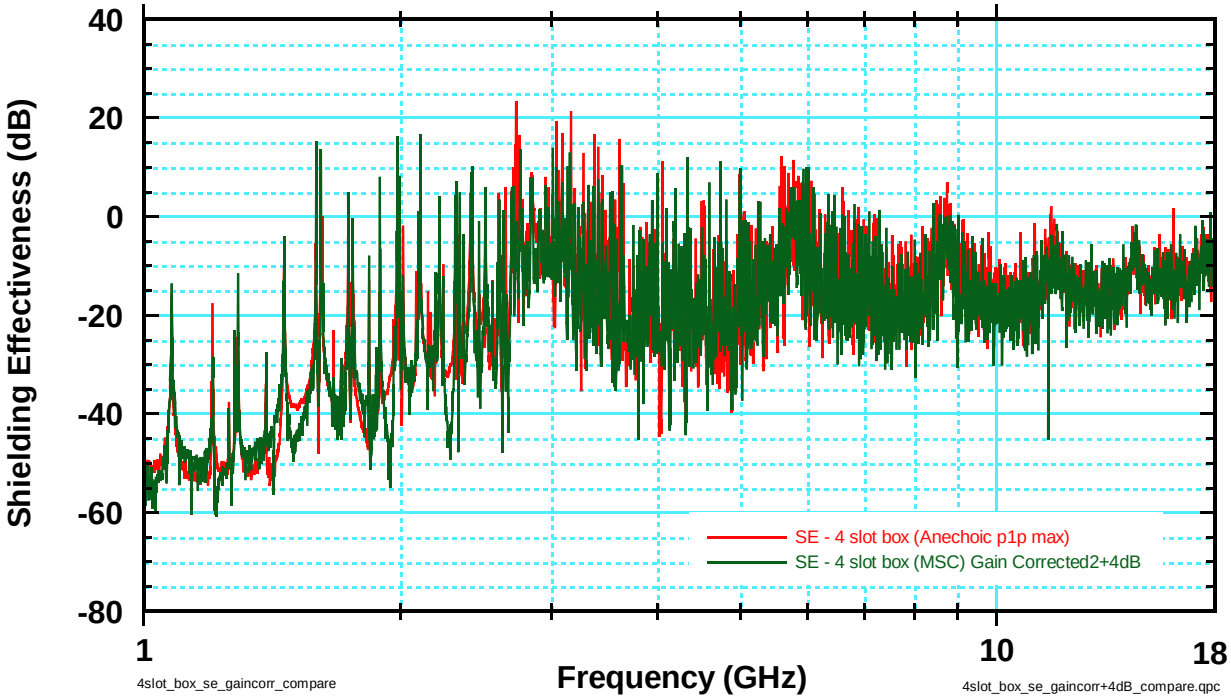

Figure 3-39 Comparison of shielding effectiveness of rectangular box test object with four slotted plate, with unintentional emitter + 4dB correction used for mode-stirred chamber data.

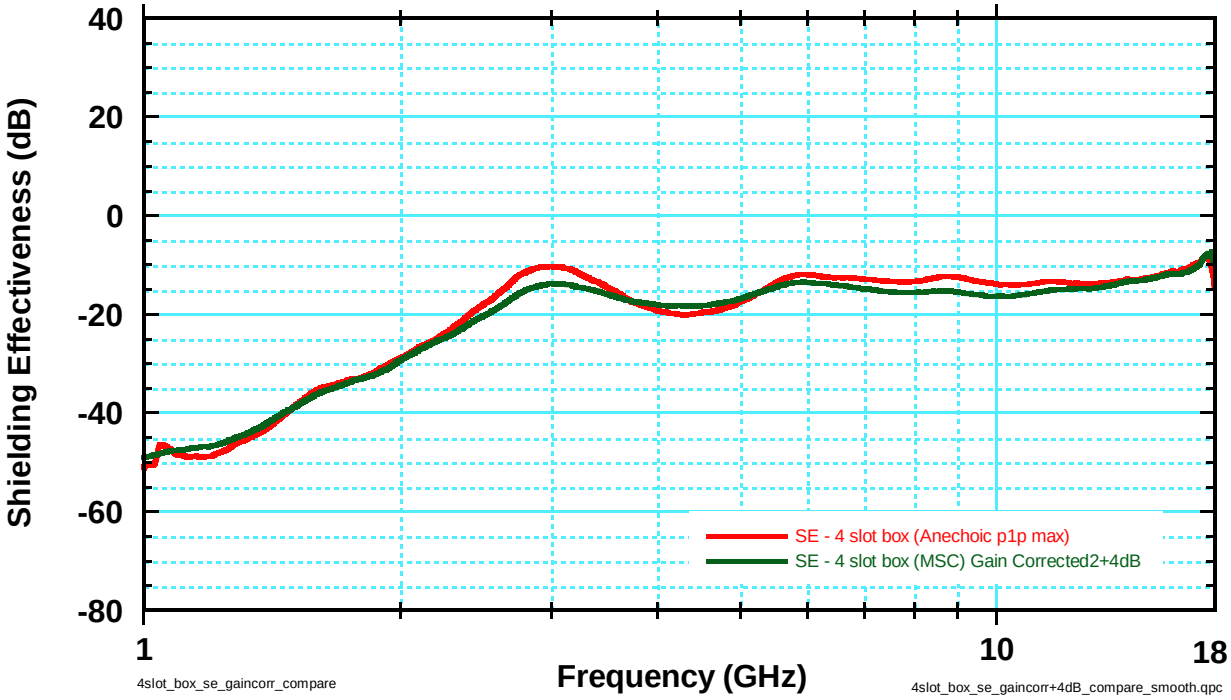

Figure 3-40 Smoothed comparison of shielding effectiveness of rectangular box test object with four slotted plate, with unintentional emitter + 4dB correction used for mode-stirred chamber data.

3.3.5 Rectangular Box Conclusions

All of the mode-stirred chamber rectangular box data was able to be corrected to commensurate levels with that of the anechoic data, using the unintentional emitter correction plus 4 dB. For the single slot plate and the two slotted plate the unintentional emitter correction plus 4 dB over corrected in the 4 to 5 GHz frequency range. Based upon the smoothed data, the four slotted plate mode-stirred chamber data corrected by the unintentional emitter correction plus 4 dB under corrected the shielding effectiveness at resonance by approximately 5 dB and also under corrected the frequency band between 6 and 12 GHz by 2 to 3 dB on average.

A summary of the conclusions is shown in Table 3-5.

Table 3-8 Summary of best corrections for the rectangular box test objects

# of slots	Best Correction	Problems
1	Unintentional Emitter +4 dB	Needed +4dB more correction over entire frequency band from the unintentional emitter correction. Over corrected in the 4 to 5 GHz frequency range.
2	Unintentional Emitter +4 dB	Needed +4dB more correction over entire frequency band from the unintentional emitter correction. Over corrected in the 4 to 5 GHz frequency range.
4	Unintentional Emitter +4 dB	Needed +4dB more correction over entire frequency band from the unintentional emitter correction. Under corrected at slot resonance by ~5 dB. Under corrected in the 6 to 12 GHz frequency range by ~2-3 dB.

3.4 Lossy Cavity Shielding Effectiveness Measurements

A set of coupling measurements were performed on the single slot cylinder and the single slot rectangular box test objects where the Q of the test object was intentionally lowered. A section of Radar Absorbing Material (or absorber) was introduced into the interior of the test object's cavity to simulate a lossy cavity. The main purpose of introducing losses into a cavity is to study the effects the losses have on the mode-stirred chamber correction needed. The lossy cavity is a somewhat more realistic case for weapons, than a high Q or empty cavity. Another reason for this is to suppress the cavity modes so that the shielding effectiveness response from the aperture is clearly dominant.

3.4.1 Cylindrical Test Object Test Results

The results from the low Q single slot cylinder measurements are shown in Figure 3-41. The amplitude of the response in the anechoic chamber is larger than that of the response from the mode-stirred chamber, as expected. Note how the cavity modes are being suppressed by the absorber introduced in the interior of the cylinder.

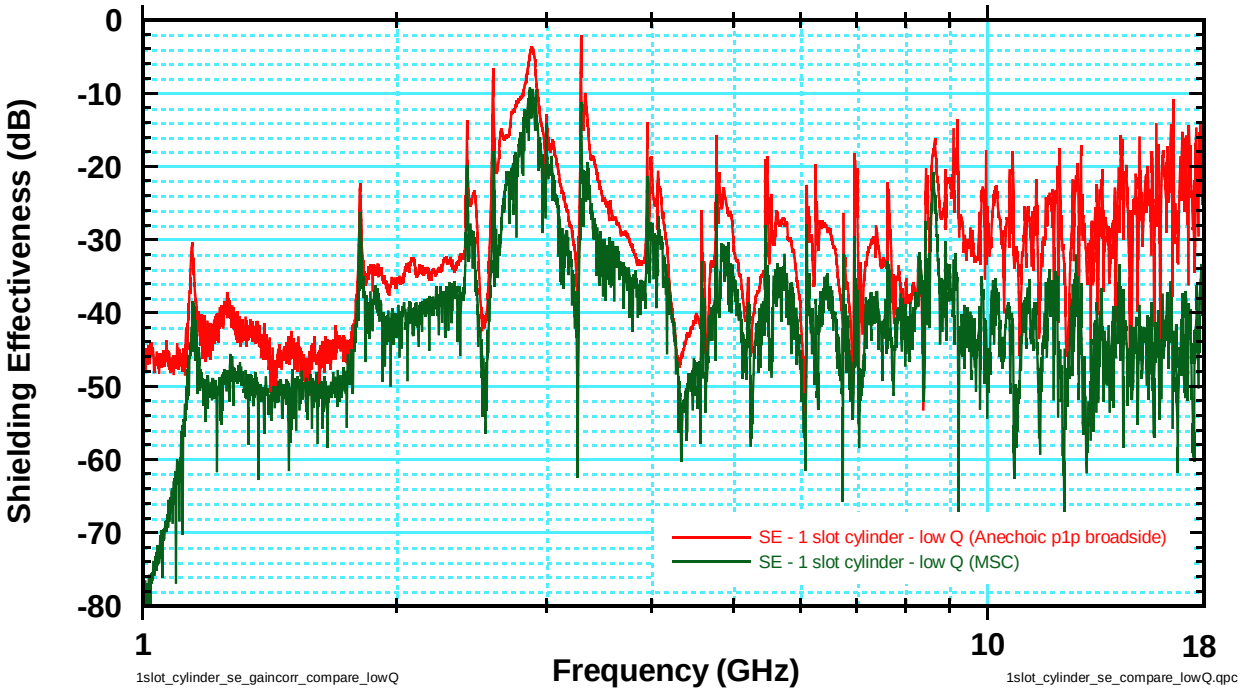

Figure 3-41 Shielding effectiveness of single slotted cylindrical test object with absorber inside, in the mode-stirred chamber and anechoic chamber.

Based upon the need for both a low frequency and high frequency correction and the need for a very large correction at 18 GHz, the correction for an intentional emitter was used. The corrected mode-stirred chamber data and anechoic data are compared in Figure 3-42. The comparison from 1.5 GHz to 18 GHz is very good. Figure 3-43 compares the smoothed corrected mode-stirred chamber data with the anechoic data. The smoothed curves show the intentional emitter factor over corrects, on average, from 4 to 10 GHz by approximately 3 dB. The individual peaks in the raw data match extremely well from 1.5 to 5 GHz.

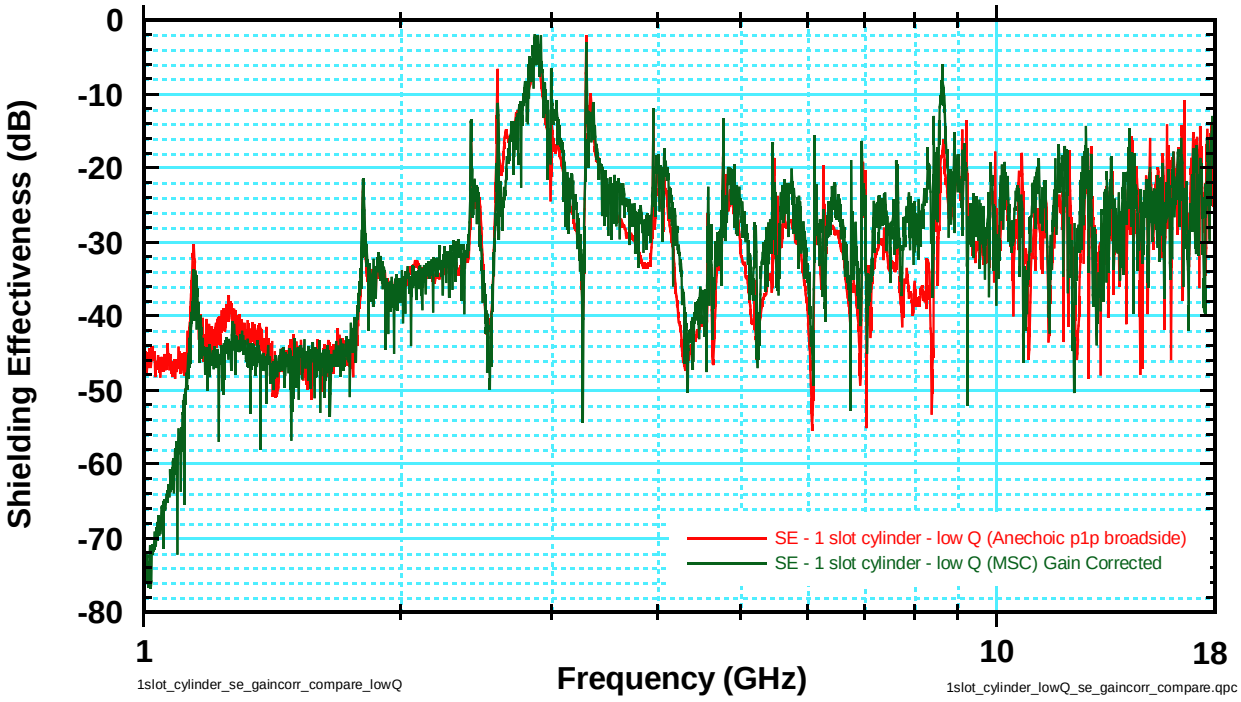

Figure 3-42 Comparison of shielding effectiveness of the low Q single slotted cylindrical test object with intentional emitter correction used for mode-stirred chamber data.

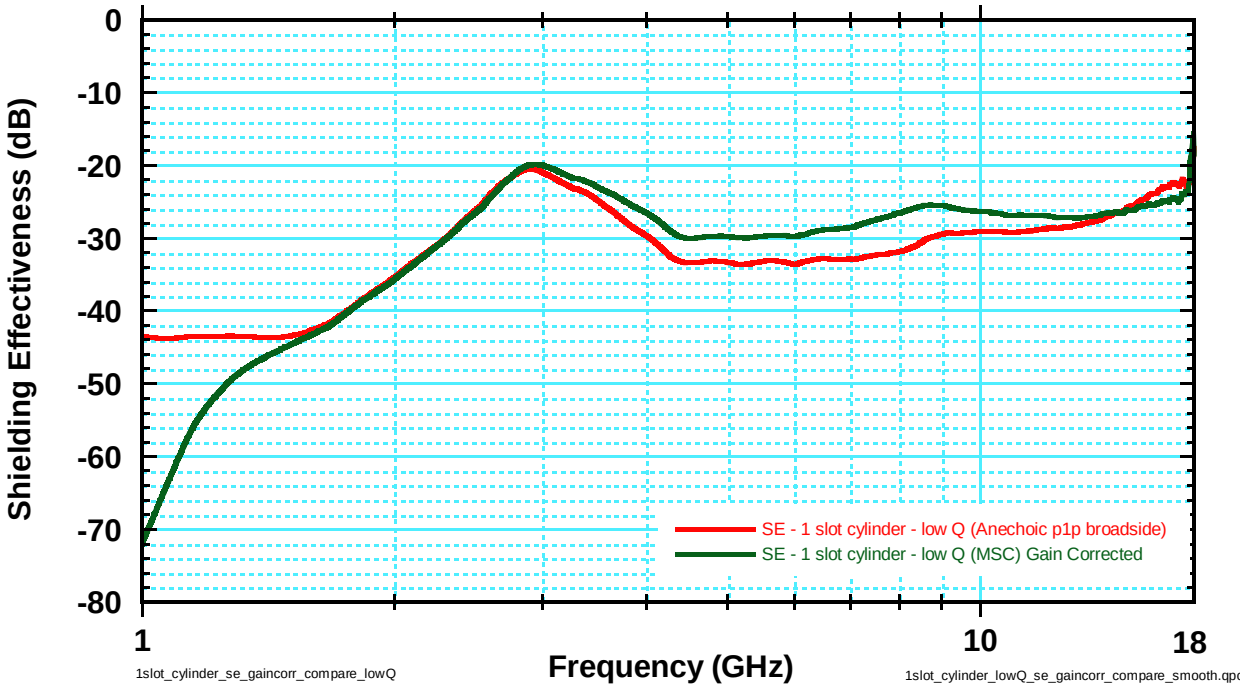

Figure 3-43 Smoothed comparison of shielding effectiveness of the low Q single slotted cylindrical test object with intentional emitter correction used for mode-stirred chamber data.

3.4.2 Rectangular Test Object Test Results

The results from the low Q single slot rectangular box measurements are shown in Figure 3-44. The amplitude of the response in the anechoic chamber is larger than that of the response from the mode-stirred chamber, as expected. Note how the cavity modes are almost completely removed by the absorber introduced in the interior of the box. The anechoic data below 1.5 GHz is at the same level as the noise floor and should be considered suspect, at the least.

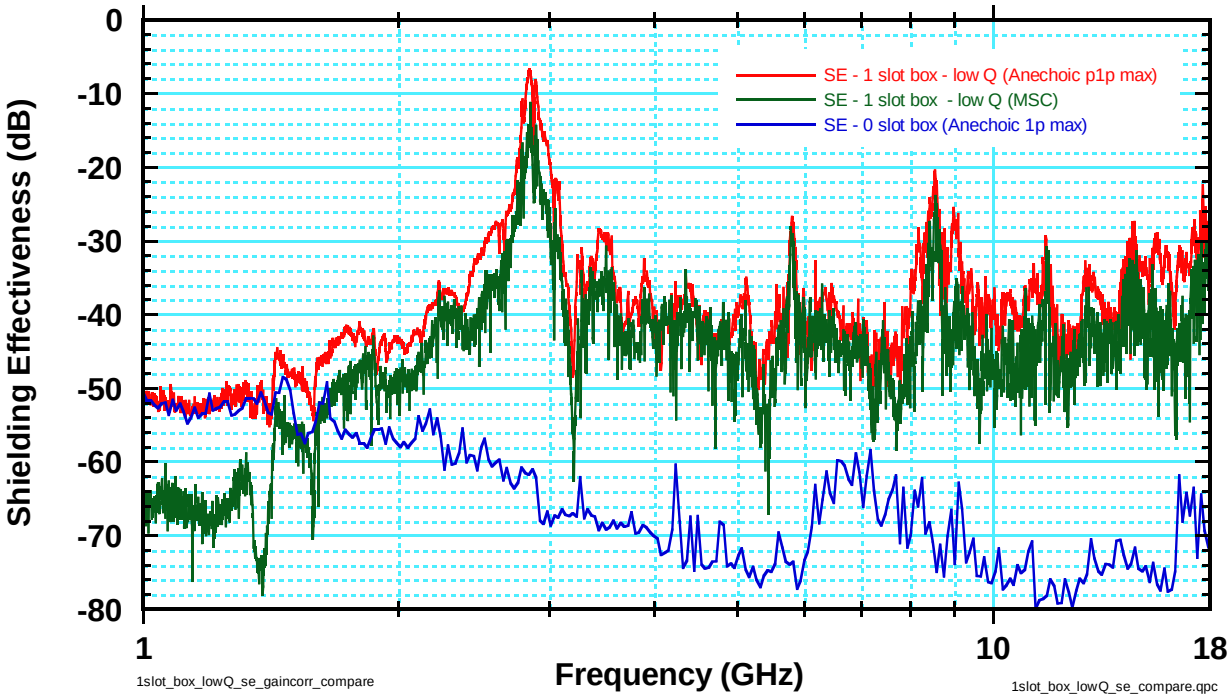

Figure 3-44 Shielding effectiveness of low Q single slotted rectangular test object in the mode-stirred chamber and anechoic chamber.

Based upon the need for both a low frequency and high frequency correction, the correction for an unintentional emitter was used. The corrected mode-stirred chamber data and anechoic data are compared in Figure 3-45. The comparison from 1.5 GHz to 18 GHz is very good. Figure 3-46 compares the smoothed corrected mode-stirred chamber data with the anechoic data. The smoothed curves show the unintentional emitter factor over corrects and under corrects, on average, less than 2 dB across the band.

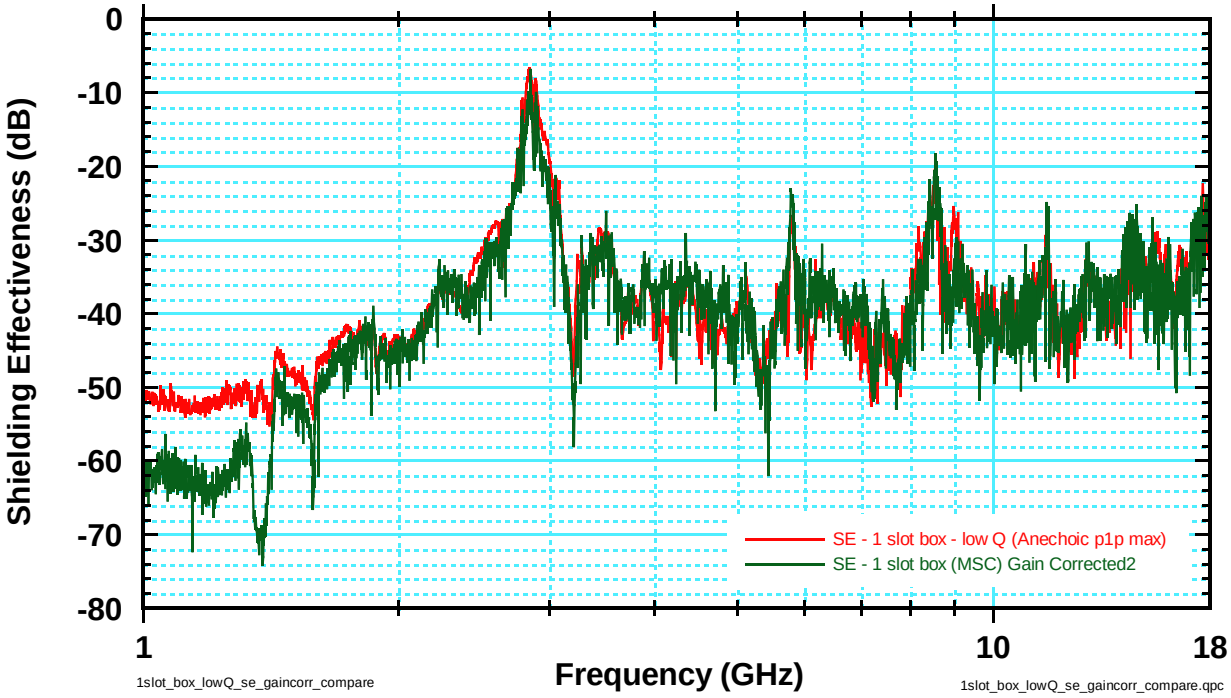

Figure 3-45 Comparison of shielding effectiveness of the low Q single slotted rectangular box test object with unintentional emitter correction used for mode-stirred chamber data.

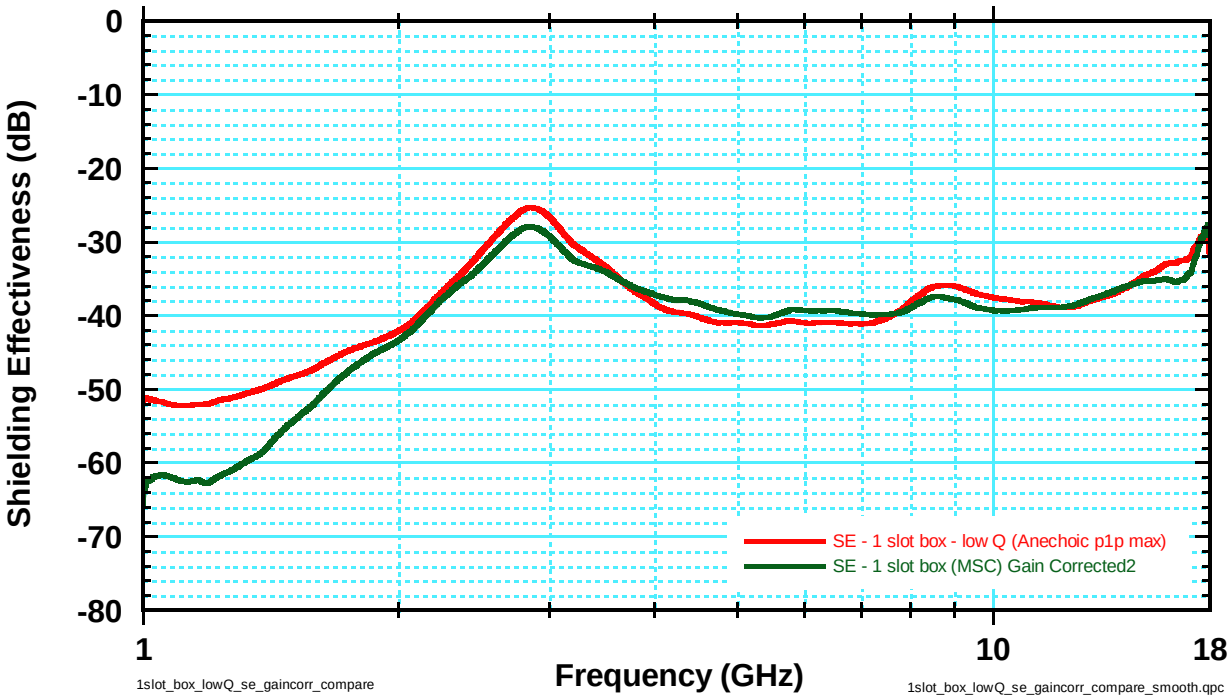

Figure 3-46 Smoothed comparison of shielding effectiveness of the low Q single slotted rectangular box test object with unintentional emitter correction used for mode-stirred chamber data.

3.4.3 Lossy Test Object Conclusions

Both low Q test objects were able to be corrected to commensurate levels with that of the anechoic data, using factors described in Chapter 2. Using the intentional emitter correction on the low Q single slot cylinder mode-stirred chamber data yields very good agreement with the anechoic data. The smoothed curves show an over correction, on average, from 4 to 10 GHz by approximately 3 dB. For the single slot plate with low Q the unintentional emitter correction over corrects and under corrects, on average, less than 2 dB across the band.

A summary of the conclusions is shown in Table 3-9.

Table 3-9 Summary of best corrections for the low Q test objects

Test Object	Best Correction	Problems
1 slot low Q cylinder	Intentional Emitter	Over correction in the 4 to 10 GHz frequency range on average by 3 dB.
1 slot low Q rectangular box	Unintentional Emitter	Deviation from average anechoic data by plus or minus 2 dB across the frequency band.

4.0 Conclusions and Summary

Mode-stirred chamber and anechoic chamber measurements were made on two sets of canonical test objects with varying numbers of thin slot apertures. The shielding effectiveness was compared to determine the level of correction needed to compensate the mode-stirred data to levels commensurate with anechoic data from the same test object.

The cylinders with varying number of slot apertures had very different corrections needed to compensate the mode-stirred chamber data correctly. For a single slot aperture an unintentional emitter correction plus 4 dB was needed, while the two and eight slot cylinders needed the Sandia correction factor to bring the levels up.

The rectangular cavity with varying number of slot apertures had interesting results, in that the same correction factor, namely the unintentional emitter plus 4 dB, worked the best for one, two, and four apertures.

The low Q cylindrical cavity needed less low frequency correction than the high Q cylindrical cavity, but much more correction at higher frequencies. Using the intentional emitter correction factor worked very well to correct the low Q single slot cylindrical mode-stirred chamber data. The introduced losses suppressed the amplitudes of the cavity modes, so that the frequencies below slot resonance (3 GHz) needed less correction, while higher frequencies required more correction.

The low Q rectangular cavity required less correction by a constant amount across the entire frequency band. The low Q cavity only required the unintentional emitter factor for correction, while the high Q cavity required an additional 4 dB. The introduced losses decreased the coupling between the reverberant and free-space environments by 4 dB.

A summary of the best correction factors for each test object measured are shown in Table 4-1.

Table 4-1 Summary of best correction factors by test object

Test Object	Best Correction
1 slot high Q cylinder	Unintentional Emitter +4 dB
2 slot high Q cylinder	Sandia ($4L/\lambda$)
8 slot high Q cylinder	Sandia ($2L/\lambda$)
1 slot low Q cylinder	Intentional Emitter
1 slot high Q rectangular box	Unintentional Emitter +4 dB
2 slot high Q rectangular box	Unintentional Emitter +4 dB
4 slot high Q rectangular box	Unintentional Emitter +4 dB
1 slot low Q rectangular box	Unintentional Emitter

5.0 Recommendations

Excellent progress has been made during this series of experiments to begin to characterize the coupling of electromagnetic environments (both free-space and reverberant) through single and multiple slots into canonical cavities. There is still much work to be done to have validated coupling models to the interior of complex systems, including nuclear weapons.

The objective of the Electromagnetic Radiation (EMR) Cable Coupling project is to characterize electromagnetic leakage into cables and metallic cavities. The ultimate goal of this project is to provide a means of predicting pin-level excitations (voltages or currents) of components within a complex system (weapon) when the exterior of the system is exposed to EMR environments over a very broad range of frequencies. This predictive capability could be used as a tool to define/refine requirements, assess systems in revised environments, optimize new designs, design changes or major upgrades, promote rapid turnaround of prototype designs and troubleshooting, and certify components and systems efficiently.

Looking at the ultimate goal as the three parts of the coupling problem (exterior scattering, aperture-cavity coupling, and cable penetration/wiring propagation), the progress of the goal can be evaluated. The uncertainties associated with the exterior scattering problem (1-2 dB) are within a tolerable range and could be considered completed at this time. The uncertainties associated with the aperture cavity coupling are still believed to be (5-10 dB) higher than acceptable. At this point the aperture cavity problem is estimated to be approximately 25% completed. Finally, the uncertainties associated with the cable penetration / wiring propagation problem are not known. Some data has been taken to characterize the problem. Some comparisons with canonical cables have been made successfully for the internal capacitance and inductance. Efforts of comparing the coupling, either canonical or realistic have not been made. It is recommended that a statistical approach be taken in the modeling of the cable coupling, based upon the capacitance and inductance data from realistic cables.

Some of the tasks to accomplish, from a “high level” perspective, are listed below:

- Adding additional test probe locations for statistical averaging of results
- Further experiments working toward more complex geometries/systems and including cables
- Working with the analysts to refine or redefine the gain correction models
- Comparing modeled results to experimental results
- Refining experiments/models as necessary to help the results come in line with each other and with the theorists' gain correction models
- Determining ways to extrapolate modeling results at higher frequencies or to be able to model at higher frequencies

6.0 References

1. Hill, D.A.; Camell, D.G.; Cavcey, K.H.; and Koepke, G.H., “Radiated emissions and immunity of microstrip transmission lines: theory and reverberation chamber measurements,” *IEEE Trans. Electromag. Compat.*, vol. 38, pp. 165-172, 1996.
2. Koepke, G.H.; Hill, D.A.; and Ladbury, J., “Directivity of the Test Device in EMC Measurements,” *IEEE International Symposium on Electromagnetic Compatibility*, vol. 2, pp. 535-539, Aug. 2000.
3. Hansen, J.E., ***Spherical Near-Field Antenna Measurements.*** London: Peter Peregrinus, 1988.
4. Balanis, C.A., ***Advanced Engineering Electromagnetics***. pp. 390-393 and 495, New York: Wiley, 1989.

7.0 Appendix A – Test Object Drawings

ZONE	REV.	DESCRIPTION	DATE	APPROVED

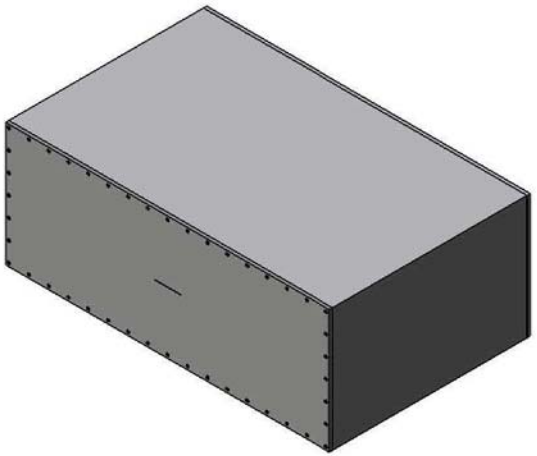

1 - Slot Assembly

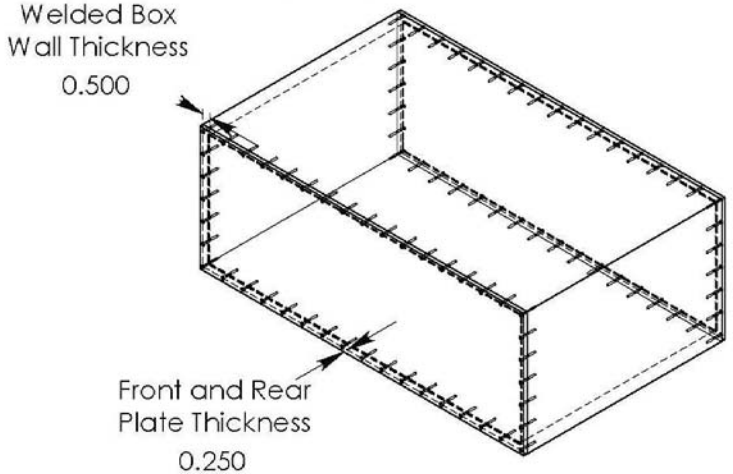

Blank Assembly

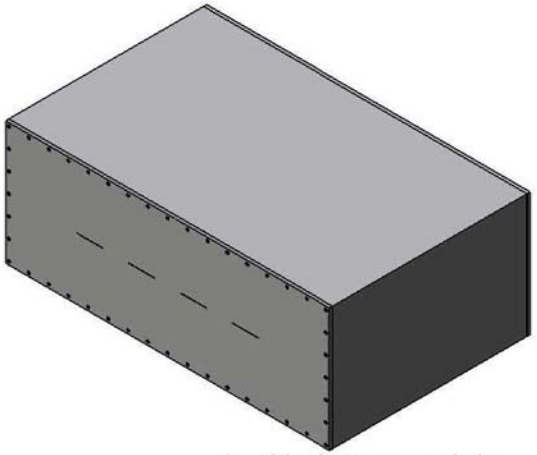

4 - Slot Assembly

SANDIA NATIONAL LABORATORIES, NM

COMMENTS:	TITLE: Box_Assembly2	Rev 2
	Project Name:	
UNLESS OTHERWISE SPECIFIED	Quantity: 1 EA. Part#: CHM50003	
DIMENSIONS ARE IN INCHES TOLERANCES: FRACTIONAL ± ANGULAR: MACH ± BEND ± TWO PLACE DECIMAL ± THREE PLACE DECIMAL ± 0.005	SIZE A MATERIAL 6061 Aluminum FINISH None	Drawn by: Cody Henderson cchend@sandia.gov (505) 845-9865 DATE: 7/13/2005
	SCALE 1:8 WEIGHT: lbs	SHEET 1 OF 5

C B A

5 4 3 2 1

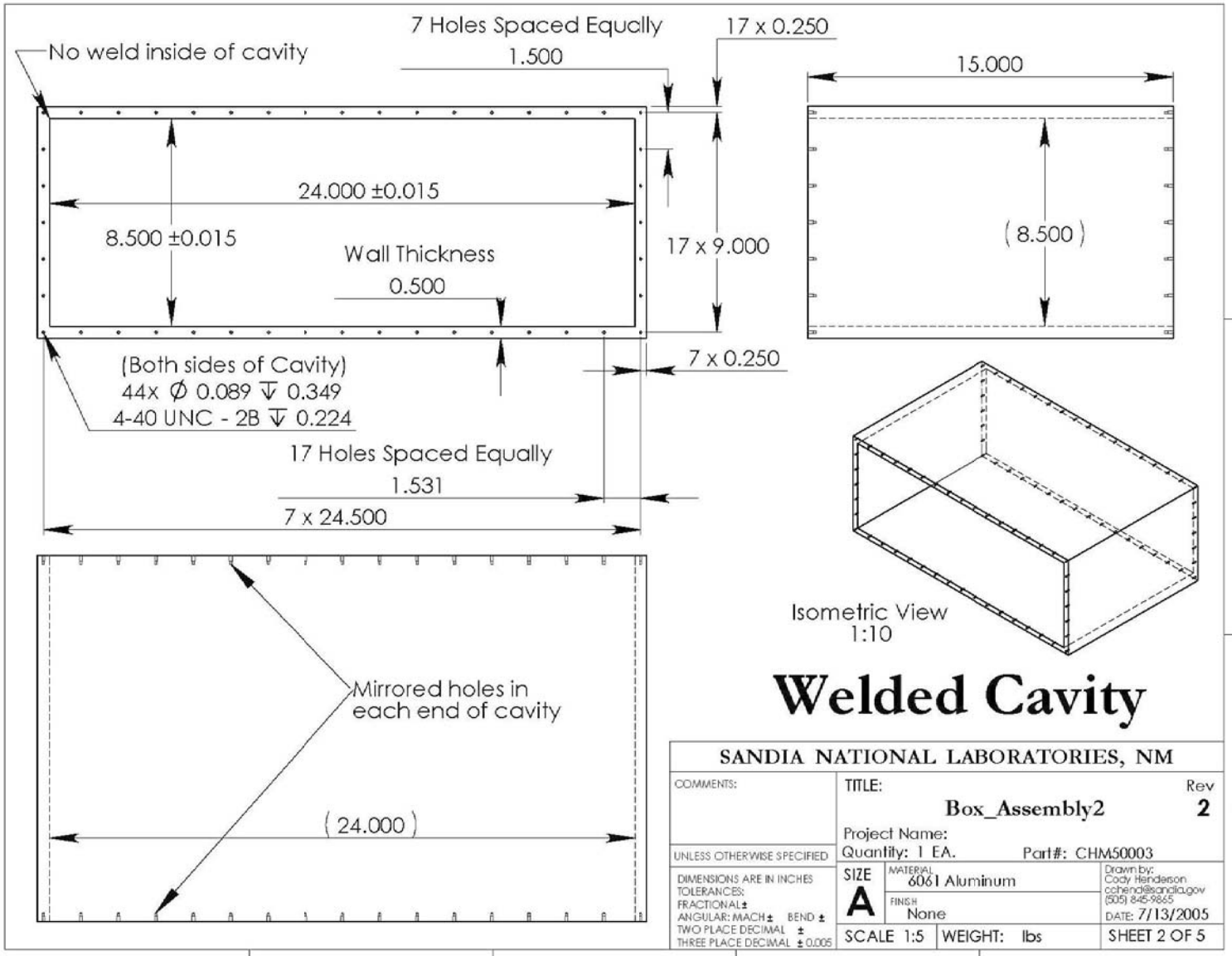
No weld inside of cavity
7 Holes Spaced Equally
1.500
17 x 0.250
15.000
24.000 ±0.015
8.500 ±0.015
Wall Thickness
0.500
17 x 9.000
(8.500)
(Both sides of Cavity)
44x Ø 0.089 ↧ 0.349
4-40 UNC - 2B ↧ 0.224
7 x 0.250
17 Holes Spaced Equally
1.531
7 x 24.500
Isometric View
1:10
Mirrored holes in
each end of cavity
(24.000)
Welded Cavity
SANDIA NATIONAL LABORATORIES, NM
COMMENTS:
TITLE:
Box_Assembly2
Rev
2
Project Name:
Quantity: 1 EA.
Part#: CHM50003
UNLESS OTHERWISE SPECIFIED
DIMENSIONS ARE IN INCHES
TOLERANCES:
FRACTIONAL ±
ANGULAR: MACH ± BEND ±
TWO PLACE DECIMAL ±
THREE PLACE DECIMAL ± 0.005
SIZE
A
MATERIAL
6061 Aluminum
FINISH
None
Drawn by:
Cody Henderson
cahend@sandia.gov
(505) 845-9865
DATE: 7/13/2005
SCALE 1:5
WEIGHT: lbs
SHEET 2 OF 5
C
B
A
5
4
3
2
1

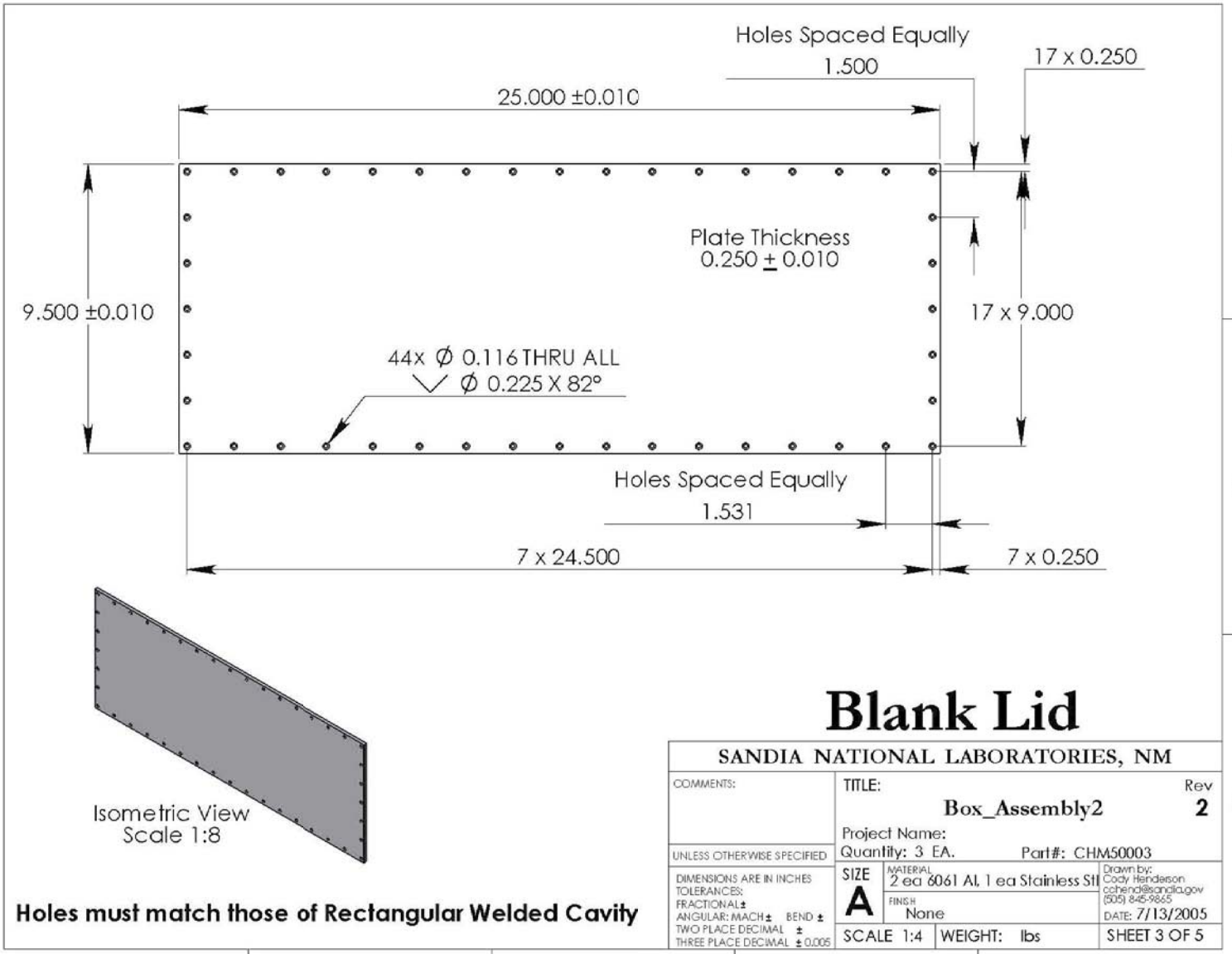
Holes Spaced Equally
1.500
17 x 0.250
25.000 ±0.010
Plate Thickness
0.250 ± 0.010
9.500 ±0.010
17 x 9.000
44x Ø 0.116 THRU ALL
Ø 0.225 X 82°
Holes Spaced Equally
1.531
7 x 24.500
7 x 0.250
Isometric View
Scale 1:8
Blank Lid
SANDIA NATIONAL LABORATORIES, NM
COMMENTS:
TITLE:
Box_Assembly2
Rev
2
Project Name:
Quantity: 3 EA.
Part#: CHM50003
UNLESS OTHERWISE SPECIFIED
DIMENSIONS ARE IN INCHES
TOLERANCES:
FRACTIONAL ±
ANGULAR: MACH ± BEND ±
TWO PLACE DECIMAL ±
THREE PLACE DECIMAL ± 0.005
SIZE
A
MATERIAL
2 ea 6061 Al, 1 ea Stainless Stl
FINISH
None
Drawn by:
Cody Henderson
cahend@sandia.gov
(505) 845-9865
DATE: 7/13/2005
SCALE 1:4
WEIGHT: lbs
SHEET 3 OF 5
Holes must match those of Rectangular Welded Cavity
C
B
A
5
4
3
2
1

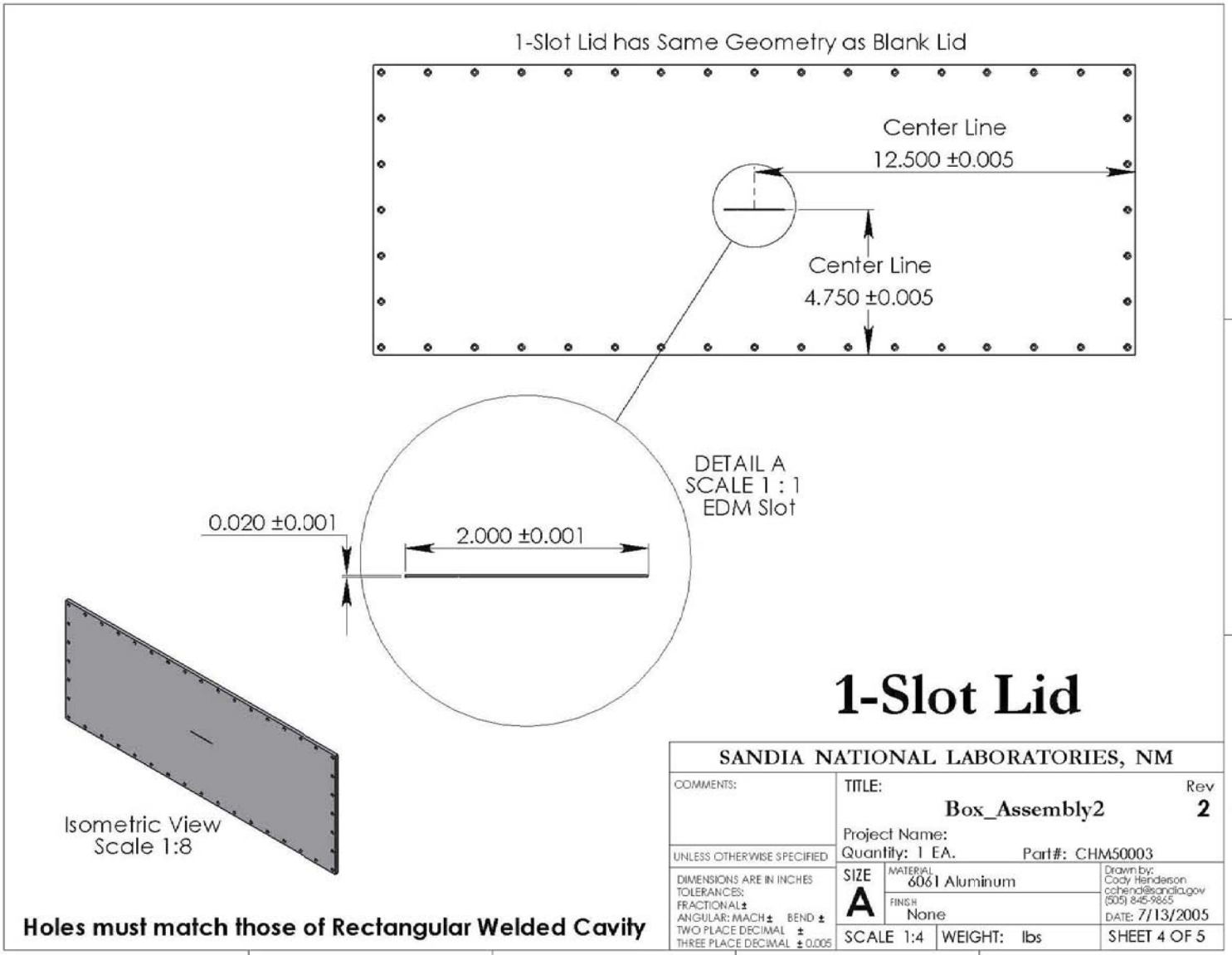
1-Slot Lid has Same Geometry as Blank Lid
Center Line
12.500 ±0.005
Center Line
4.750 ±0.005
DETAIL A
SCALE 1 : 1
EDM Slot
0.020 ±0.001
2.000 ±0.001
Isometric View
Scale 1:8
Holes must match those of Rectangular Welded Cavity
1-Slot Lid
SANDIA NATIONAL LABORATORIES, NM
COMMENTS:
TITLE:
Box_Assembly2
Rev
2
Project Name:
Quantity: 1 EA.
Part#: CHM50003
UNLESS OTHERWISE SPECIFIED
DIMENSIONS ARE IN INCHES
TOLERANCES:
FRACTIONAL ±
ANGULAR: MACH ± BEND ±
TWO PLACE DECIMAL ±
THREE PLACE DECIMAL ± 0.005
SIZE
A
MATERIAL
6061 Aluminum
FINISH
None
Drawn by:
Cody Henderson
cahend@sandia.gov
(505) 845-9865
DATE: 7/13/2005
SCALE 1:4
WEIGHT: lbs
SHEET 4 OF 5
C
B
A
5
4
3
2
1

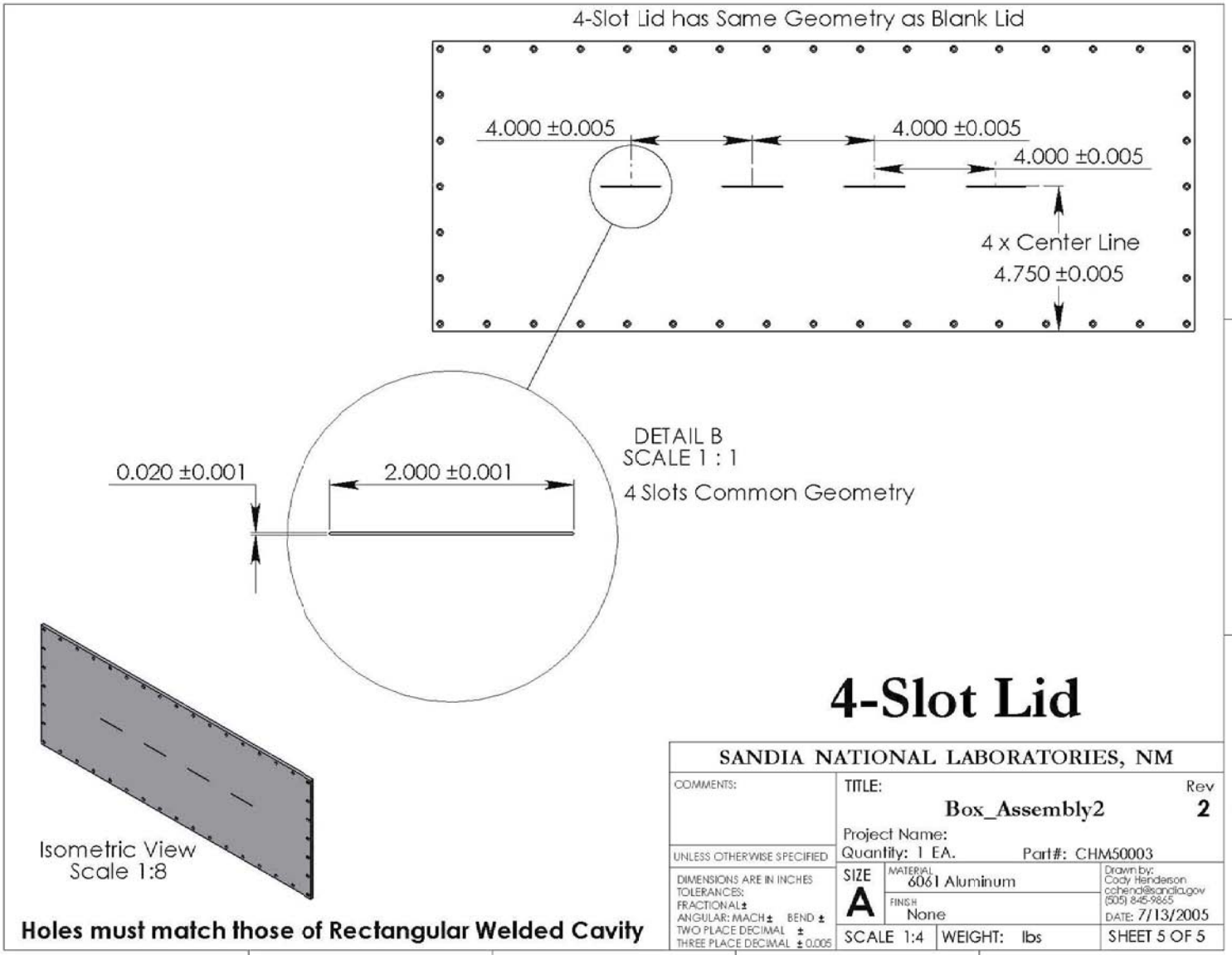
4-Slot Lid has Same Geometry as Blank Lid
4.000 ±0.005
4.000 ±0.005
4.000 ±0.005
4 x Center Line
4.750 ±0.005
DETAIL B
SCALE 1 : 1
4 Slots Common Geometry
0.020 ±0.001
2.000 ±0.001
Isometric View
Scale 1:8
Holes must match those of Rectangular Welded Cavity
4-Slot Lid
SANDIA NATIONAL LABORATORIES, NM
COMMENTS:
TITLE:
Box_Assembly2
Rev
2
Project Name:
Quantity: 1 EA.
Part#: CHM50003
UNLESS OTHERWISE SPECIFIED
DIMENSIONS ARE IN INCHES
TOLERANCES:
FRACTIONAL ±
ANGULAR: MACH ± BEND ±
TWO PLACE DECIMAL ±
THREE PLACE DECIMAL ± 0.005
SIZE
A
MATERIAL
6061 Aluminum
FINISH
None
Drawn by:
Cody Henderson
cahend@sandia.gov
(505) 845-9865
DATE: 7/13/2005
SCALE 1:4
WEIGHT: lbs
SHEET 5 OF 5
C
B
A
5
4
3
2
1

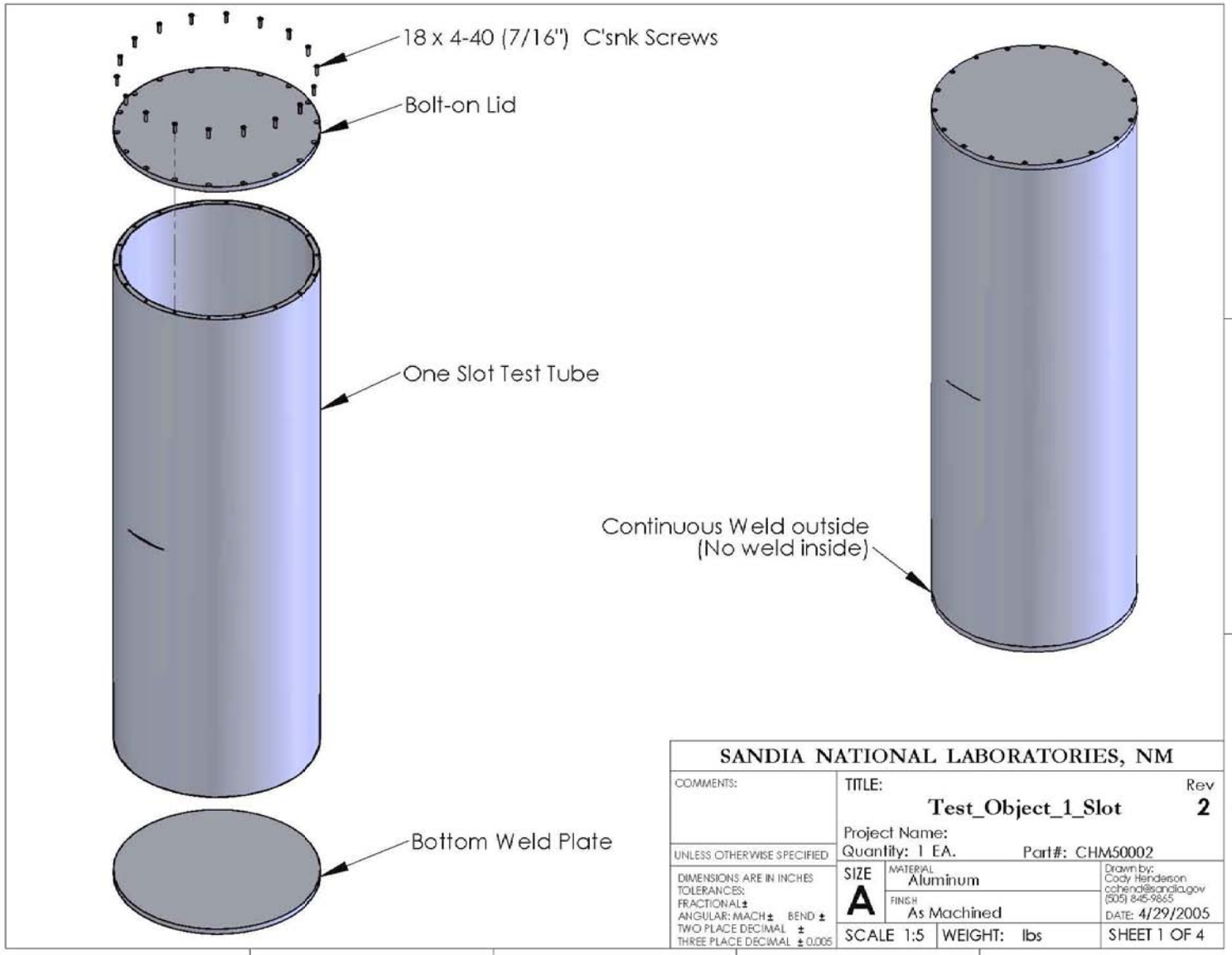

SANDIA NATIONAL LABORATORIES, NM

COMMENTS:	TITLE: Test_Object_1_Slot	Rev 2
	Project Name:	
UNLESS OTHERWISE SPECIFIED	Quantity: 1 EA. Part#: CHM50002	
DIMENSIONS ARE IN INCHES TOLERANCES: FRACTIONAL ± ANGULAR: MACH ± BEND ± TWO PLACE DECIMAL ± THREE PLACE DECIMAL ± 0.005	SIZE A MATERIAL Aluminum FINISH As Machined	Drawn by: Cody Henderson cahend@sandia.gov (505) 845-9865 DATE: 4/29/2005
	SCALE 1:5 WEIGHT: lbs	SHEET 1 OF 4

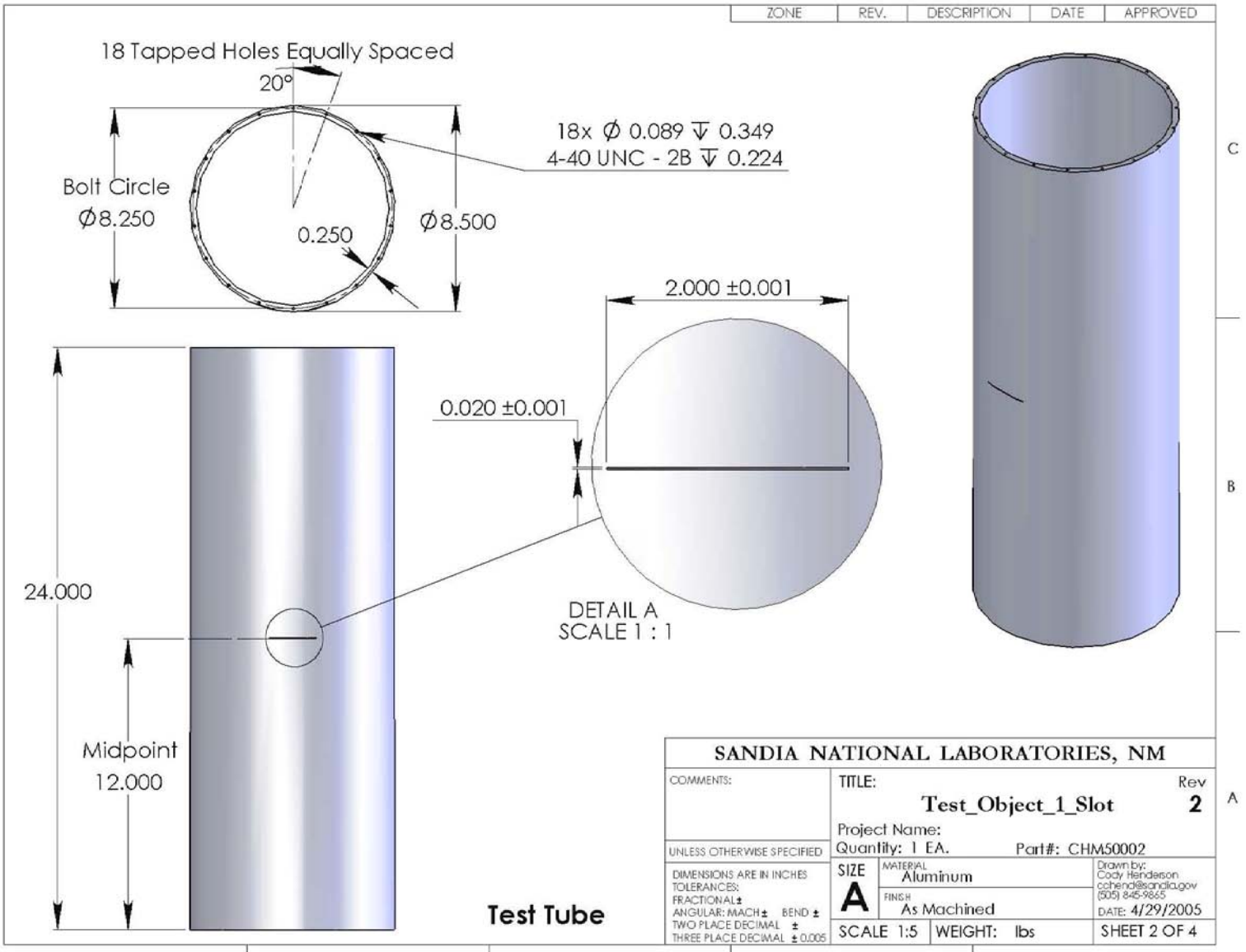
ZONE
REV.
DESCRIPTION
DATE
APPROVED
18 Tapped Holes Equally Spaced
20°
18x Ø 0.089 ↧ 0.349
4-40 UNC - 2B ↧ 0.224
Bolt Circle
Ø8.250
0.250
Ø8.500
2.000 ±0.001
0.020 ±0.001
24.000
Midpoint
12.000
DETAIL A
SCALE 1 : 1
Test Tube
C
B
A
SANDIA NATIONAL LABORATORIES, NM
COMMENTS:
TITLE:
Test_Object_1_Slot
Rev
2
Project Name:
Quantity: 1 EA.
Part#: CHM50002
UNLESS OTHERWISE SPECIFIED
DIMENSIONS ARE IN INCHES
TOLERANCES:
FRACTIONAL ±
ANGULAR: MACH ± BEND ±
TWO PLACE DECIMAL ±
THREE PLACE DECIMAL ± 0.005
SIZE
A
MATERIAL
Aluminum
FINISH
As Machined
Drawn by:
Cody Henderson
cahend@sandia.gov
(505) 845-9865
DATE: 4/29/2005
SCALE 1:5
WEIGHT: lbs
SHEET 2 OF 4
5
4
3
2
1

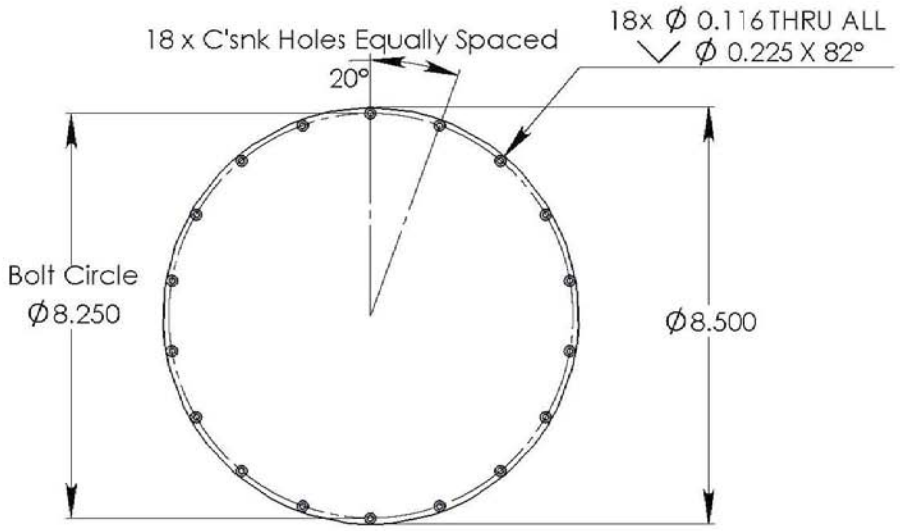

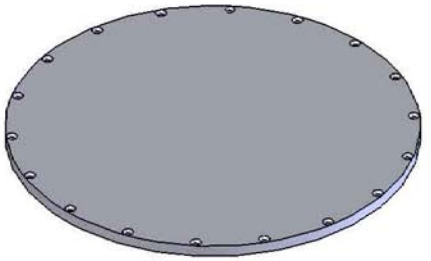

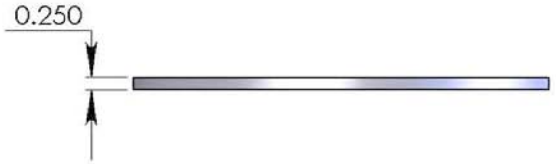

Top Bolt-on Lid

SANDIA NATIONAL LABORATORIES, NM			
COMMENTS:	TITLE: Test_Object_1_Slot		Rev 2
	Project Name:		
UNLESS OTHERWISE SPECIFIED	Quantity: 1 EA.	Part#: CHM50002	
DIMENSIONS ARE IN INCHES TOLERANCES: FRACTIONAL ± ANGULAR: MACH ± BEND ± TWO PLACE DECIMAL ± THREE PLACE DECIMAL ± 0.005	SIZE A	MATERIAL: Aluminum FINISH: As Machined	Drawn by: Cody Henderson cahend@sandia.gov (505) 845-9865 DATE: 4/29/2005
	SCALE 1:3	WEIGHT: 1.378 lbs	SHEET 3 OF 4

5 4 3 2 1

C B A

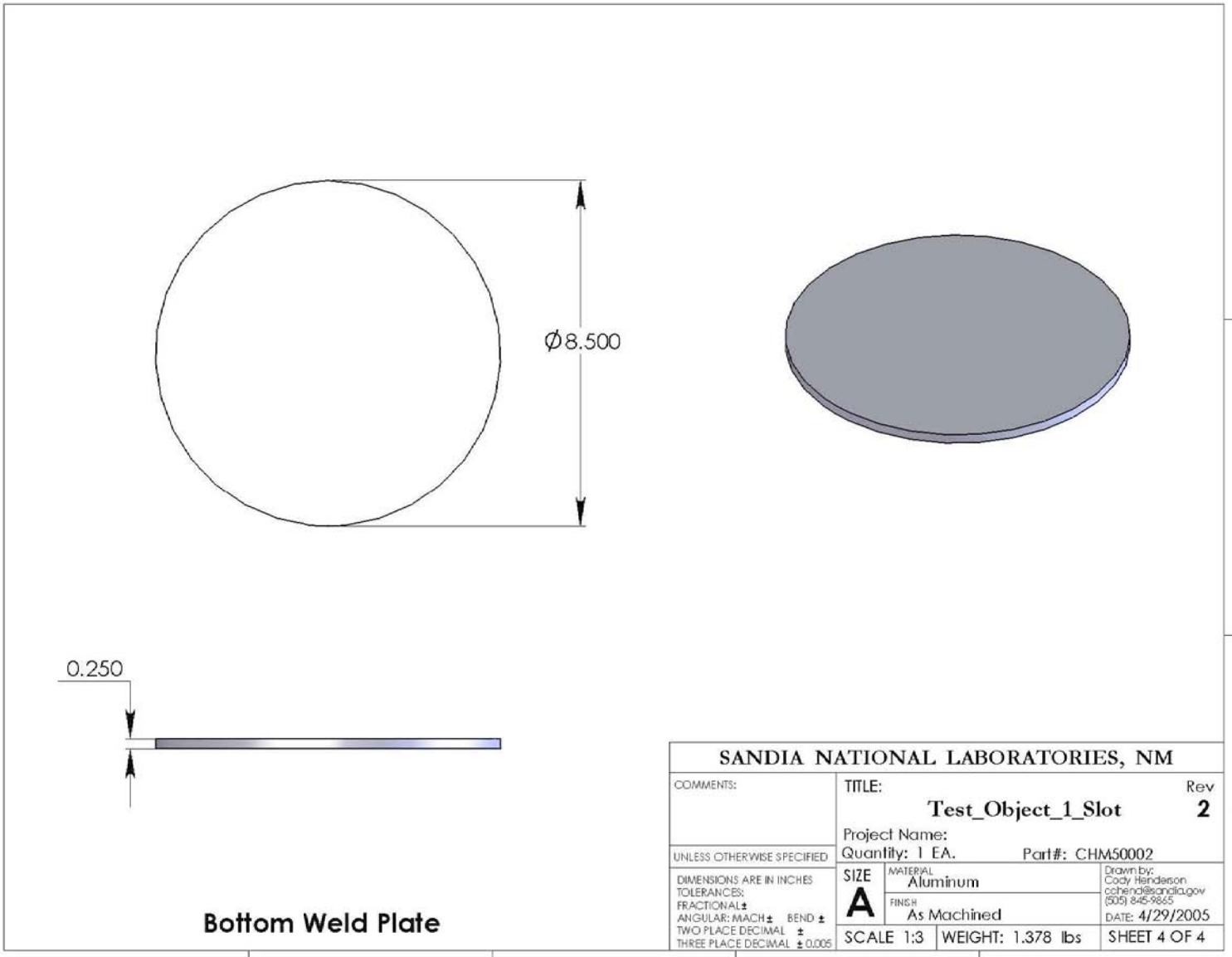
Ø8.500
0.250
Bottom Weld Plate
SANDIA NATIONAL LABORATORIES, NM
COMMENTS:
TITLE:
Test_Object_1_Slot
Rev
2
Project Name:
Quantity: 1 EA.
Part#: CHM50002
UNLESS OTHERWISE SPECIFIED
DIMENSIONS ARE IN INCHES
TOLERANCES:
FRACTIONAL ±
ANGULAR: MACH ± BEND ±
TWO PLACE DECIMAL ±
THREE PLACE DECIMAL ± 0.005
SIZE
A
MATERIAL
Aluminum
FINISH
As Machined
Drawn by:
Cody Henderson
cahend@sandia.gov
(505) 845-9865
DATE: 4/29/2005
SCALE 1:3
WEIGHT: 1.378 lbs
SHEET 4 OF 4
C
B
A
5
4
3
2
1

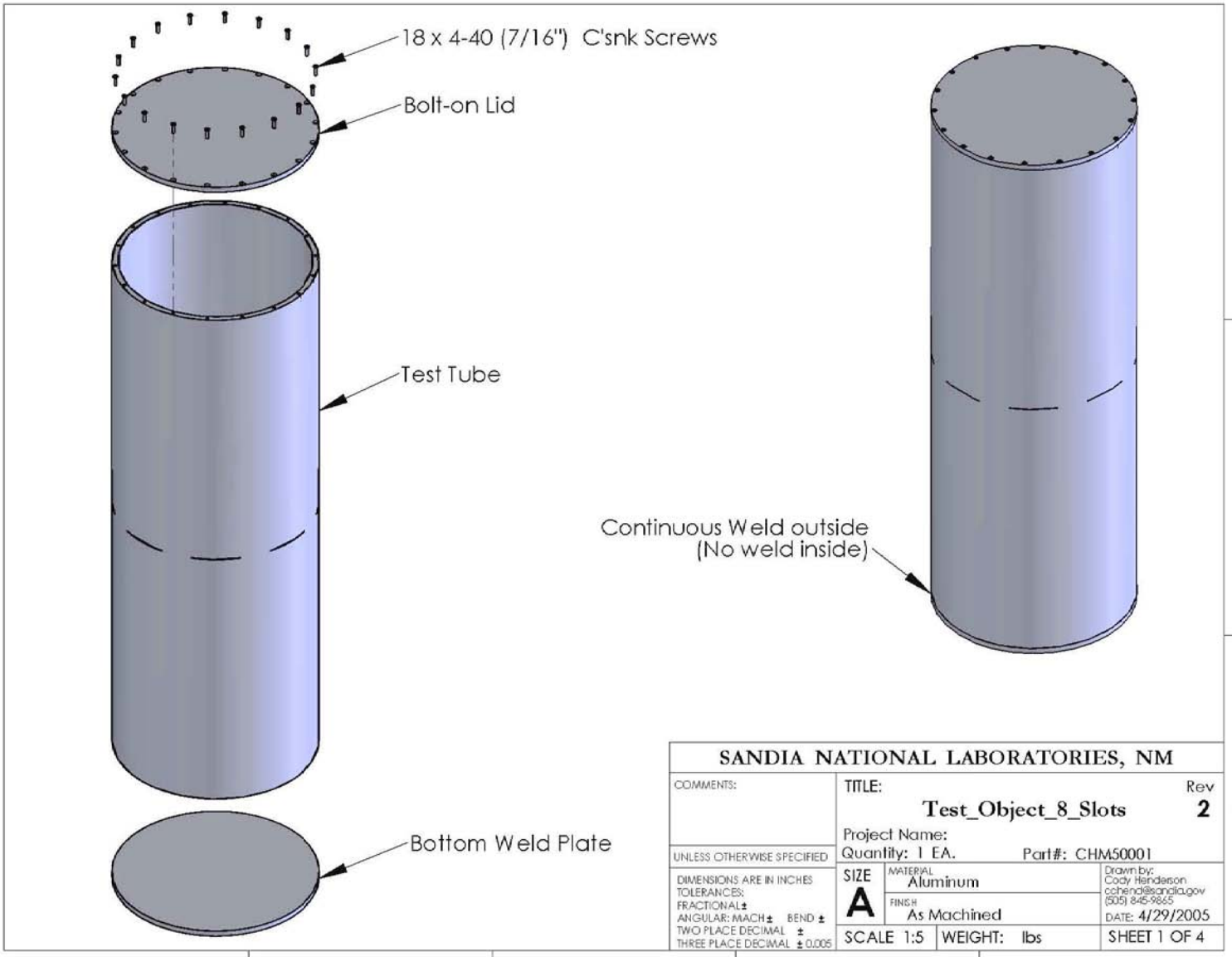
18 x 4-40 (7/16") C'snk Screws
Bolt-on Lid
Test Tube
Bottom Weld Plate
Continuous Weld outside
(No weld inside)
C
B
A
SANDIA NATIONAL LABORATORIES, NM
COMMENTS:
TITLE:
Test_Object_8_Slots
Rev
2
Project Name:
Quantity: 1 EA.
Part#: CHM50001
UNLESS OTHERWISE SPECIFIED
DIMENSIONS ARE IN INCHES
TOLERANCES:
FRACTIONAL ±
ANGULAR: MACH ± BEND ±
TWO PLACE DECIMAL ±
THREE PLACE DECIMAL ± 0.005
SIZE
A
MATERIAL
Aluminum
FINISH
As Machined
Drawn by:
Cody Henderson
cahend@sandia.gov
(505) 845-9865
DATE: 4/29/2005
SCALE 1:5
WEIGHT: lbs
SHEET 1 OF 4
5
4
3
2
1

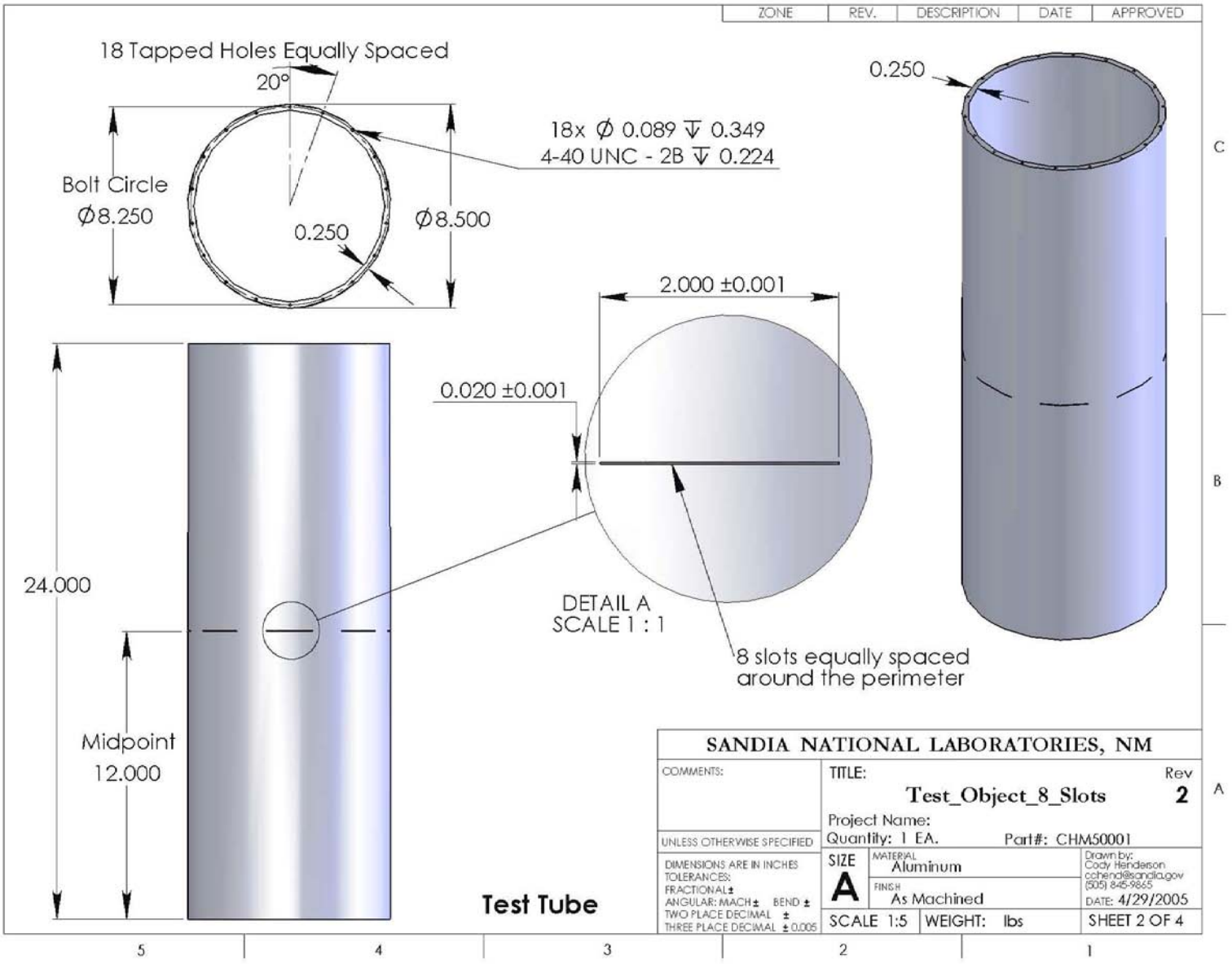
ZONE
REV.
DESCRIPTION
DATE
APPROVED
18 Tapped Holes Equally Spaced
20°
18x Ø 0.089 ↧ 0.349
4-40 UNC - 2B ↧ 0.224
Bolt Circle
Ø8.250
0.250
Ø8.500
0.250
2.000 ±0.001
0.020 ±0.001
24.000
Midpoint
12.000
DETAIL A
SCALE 1 : 1
8 slots equally spaced
around the perimeter
Test Tube
SANDIA NATIONAL LABORATORIES, NM
COMMENTS:
TITLE:
Test_Object_8_Slots
Rev
2
Project Name:
Quantity: 1 EA.
Part#: CHM50001
UNLESS OTHERWISE SPECIFIED
DIMENSIONS ARE IN INCHES
TOLERANCES:
FRACTIONAL ±
ANGULAR: MACH ± BEND ±
TWO PLACE DECIMAL ±
THREE PLACE DECIMAL ± 0.005
SIZE
A
MATERIAL
Aluminum
FINISH
As Machined
Drawn by:
Cody Henderson
cahend@sandia.gov
(505) 845-9865
DATE: 4/29/2005
SCALE 1:5
WEIGHT: lbs
SHEET 2 OF 4
C
B
A
5
4
3
2
1

Distribution

Internal:

5	MS1152	M. B. Higgins, 1653
1	MS1152	M. Caldwell, 1653
1	MS1152	H. G. Hudson, 1653
1	MS1152	D. R. Charley, 1653
2	MS9018	Central Technical Files, 08944
2	MS0899	Technical Library, 04536


Sandia National Laboratories